

FP7-IST-60918
1 March 2013 (36months)

DR 4.3:

Methodologies for grasp acquisition and planning

H. Marino, C.J. Rosales, M. Kopicki, G. Santaera, E. Lumberto, Y. Wu, A. Artoni, G. Pannocchia, M. Gabiccini, and J.L. Wyatt

University of Birmingham, UK
(jlw@cs.bham.ac.uk)

Due date of deliverable: 2016-02-29
Actual submission date: 2016-02-29
Lead partner: University of Birmingham, UK
Revision: final
Dissemination level: PU

This report describes the activities related to *planning and control of grasping actions* given the complete or partial detection of an object. It includes work on: modelling underactuated and adaptive robotic hands, learning grasps for underactuated hands and transferring them robustly to different initial hand-object poses, adjusting hand pose via infrared sensor readings to grasp objects in an uncertain configuration with the respect to that perceived by vision, planning complex grasping and manipulation tasks either under uncertainty using discrete search methods or via direct trajectory optimization methods for systems with unspecified contact sequences.

1 Tasks, objectives, results	4
1.1 Planned work	4
1.2 Actual work performed	4
1.3 Learning	6
1.3.1 Learning and Inference of Dexterous Grasps for Novel Objects with Underactuated Hands	6
1.3.2 Data-Driven Human Grasp Movement Analysis	6
1.4 Planning	7
1.4.1 Planning of Grasp Acquisition under Uncertainty and Incompleteness	7

1.4.2	On the Problem of Moving Objects with Autonomous Robots: a Unifying High-Level Planning Approach	8
1.4.3	Infrared Sensor-based Grasp Planning	9
1.5	Optimisation	9
1.5.1	A Computational Framework for Environment-Aware Robotic Manipulation Planning	9
1.5.2	Offset-free MPC Explained: novelties, subtleties, and applications	11
A	Annexes	13
A.1	Article: On the Problem of Moving Objects with Autonomous Robots: a Unifying High-Level Planning Approach	13
A.2	Article: IR Sensor-based Grasp Planner for the Pisa/IIT SoftHand Under Uncertainty	22
A.3	Article: Learning and Inference of Dexterous Grasps for Novel Objects with Underactuated Hands	31
A.4	Article: Data-Driven Human Grasp Movement Analysis	40
A.5	Article: A computational framework for environment-aware robotic manipulation planning	49
A.6	Article: Offset-free MPC explained: novelties, subtleties, and applications	68
A.7	Article: Active Touch for Grasping	80

Executive Summary

This report describes the activities within the PaCMan consortium to define methodologies for *grasp acquisition and planning*. The material included in this report describes the results that fall under Task 4.3 (M 7-30), and Task 4.4 (M 1-36) at M 36.

Role of grasp acquisition and planning in PaCMan

This deliverable documents the effort of the consortium in devising new strategies to define *practical* approaches to tackle the problem of *grasping under uncertainty and novelty*, either caused by sensor noise, clutter, visual occlusions, or new object shapes. To this end, the ability to move through the different stages of the grasping process, from novel shape to grasp formulation, planning reach to grasp, making first contact, updating the belief state, and planning robust or information gathering trajectories are all phases we have tackled during the project.

Contribution to the PaCMan scenario

In our view, grasp methodologies that try to cope with pose uncertainty, object shape estimation inaccuracies, object novelty, clutter and partial occlusions are central to PacMan's overall goals. We tackle these by a variety of methods. The grasping methodologies here have all been evaluated on datasets drawn from the PaCMan scenario.

1 Tasks, objectives, results

1.1 Planned work

The selection of correct grasp strategies when the object to be grasped in unknown or only partially visible environments is a trivial task for humans. Although robotics has made significant progress in autonomous grasping, the problem of grasping novel objects in under uncertainty and partial information is still an open area. In this report, we document our work to tackle these problems.

The planned work for the final year involved Tasks 4.3 and Tasks 4.4. These aimed to demonstrate grasp acquisition using our methods for learning and planning under uncertainty, in particular the goal was to demonstrate these on real robot hands, and in particular to show ability to plan grasps under pose and shape uncertainty and incompleteness. We also promised methods to achieve optimal choice of contact forces during grasp acquisition. We describe all of these here.

1.2 Actual work performed

The work we have performed can be divided into work on learning, planning, and optimisation. We quickly summarise our achievements in each area, before describing the specific contributions in detail. Each of these approaches directly address our Task 4.3 and 4.4 goals of grasp acquisition and grasp planning and learning under uncertainty and incompleteness.

Learning: in previous years we presented our method for learning grasps from small numbers of examples, using a probabilistic approach, which employs a product of experts to provide generalisation of final grasp configurations. This year we have extended this in two ways. First, we present the adaptation to underactuated robotic hands of the grasp planning algorithm previously devised only for fully actuated hands — the DLR-HIT Hand II was used last year by the University of Birmingham. Our approach, by using a product of experts, learns now not only the desired final grasp, but also good grasping trajectories from rigid body simulations of the Pisa/IIT SoftHand. The new method shows that it is possible to use just a few example grasps in order to be able to transfer this knowledge to unknown, even partially visible objects. This has resulted in a paper to be submitted to IROS. More details can be found in [A.3](#). In a second contribution, reported in DR2.2, we have extended our learning method to work with the compositional hierarchy. In a third piece of work we have extended our approach based on multiple eigenspaces to learning a data-driven taxonomy of grasps. This has been trained on 4500 postures. We describe this in Sec. [1.3.2](#).

Planning: with regard to planning under uncertainty and incomplete information we have two strands of work. One is grasping under uncertainty, taking into account the value of tactile information. At a choice point at the end of year 1 we chose to pursue this using a planning method that performed belief space planning by embedding information gains in the physical space. This year we have completed an implementation on the Boris platform, and present the results of this and simulation studies in a draft paper to be submitted to autonomous robots. The work is described in more detail in Sec. 1.4.1. In a second strand we completed our work on high level planning to move objects between locations. Sec. 1.4.2 presents our approach to solve this problem, possibly by using handoffs, table support, and regrasping. This work constituted the theoretical foundation for the high-level planning needed to perform Task 5.3 at M24. The planner has now been tested (in simulation) also in more complex scenarios, with respect to bimanual object passing, with promising results. The good level of maturity reached by the work is testified by the journal publication in A.2. We have also developed sensing and planning to guide grasp acquisition prior to the moment of contact. In Sec. 1.4.3, we describe this work, in which we plan and control the approach trajectory using IR sensors.

Optimisation: We have developed our framework for optimisation of contacts and contact forces. Originally we promised to do this only for grasp acquisition. In fact we have gone far beyond this, developing a framework which tackles general manipulation problems. In Sec. 1.5.1, we describe a planning strategy based on direct trajectory optimization that does not require a-priori specification of the contact sequence and presents, from the outset, the benefits of providing dynamically consistent plans and allowing for opportunistic exploitation of environmental constraints. This work has now reached a good level of maturity, as testified by the conference publication in A.5. In Sec. 1.5.2, we focus on the description of model predictive control algorithms for nonlinear (and linear) discrete-time systems, with the intended objective of clarifying the main concepts needed to guarantee offset-free performances. A strong accent is put on the role played by the disturbance and the observer models, which are paramount to ensure the stability of MPC-based manipulation controllers derived from manipulation planners described in Sec. 1.5.1. More details can be found in the conference publication in A.6.

We now detail the work for each of these areas in turn.

1.3 Learning

1.3.1 Learning and Inference of Dexterous Grasps for Novel Objects with Underactuated Hands

While we promised to be able to grasp novel objects in Task 5.5 at month 36, we were able to demonstrate such capabilities for fully actuated hands at month 24 [1].

In this section, we show our work towards the extension of our approach to underactuated hands: on the one hand, they have the advantage of adapting to the object and partly accommodating the uncertainty in object’s shape and position via mechanical compliance, but on the other they present challenging aspects at the planning level.

In fact, most of the reliability they can offer is obtained through a close, daring interaction of the hand with the object and the environment during grasping. In a majority of cases, the grasp involves interactions with the object, moving it to the stable grasp pose. This is a natural property of underactuated hands, but it poses relevant challenges to the learning method.

To move forward in this direction, our previously proposed algorithm has been extended to be able to use more than a single training example for the same grasp category, and to moreover include multiple trajectories as part of the learning process. Furthermore, it does not rely on an explicit representation of the contact sequence. The core learning method uses a product of experts.

Nine training examples, three per grasp type (rim, pinch, and handle) were executed in simulation with a human in control. Only two objects were used in this training phase. Tests were conducted on fifteen different, previously unseen objects, whose models consisted only of a point cloud taken from just one view. Reconstructions were thus partial, typically less than 25% of the object’s surface area. Automatic selection of the grasp which was most-likely to succeed led to 12 good grasps out of the 15 tests, giving a generalization success rate of 80%.

Extensions of this work where also object-environment interactions are considered are under development, as recognized to be of utmost relevance.

A more in depth picture of this approach and what has been so far achieved can be seen in Sec. A.3.

1.3.2 Data-Driven Human Grasp Movement Analysis

As the description of human hand motions is very complex, methods to reduce this complexity have attracted much attention in the motor control literature. Early studies prevalently used direct analysis methods such as visual inspection to define grasp taxonomies (e.g. [2]). More recently, analytical methods have been employed to perform grasping data dimensionality reduction (e.g. [3]). In this section, a methodology is presented which al-

lows to obtain a data-generated grasp taxonomy along with low-dimensional representations: these could be used for human grasping data classification and posture reconstruction, as well as design specification for underactuated hands design.

The technique used here is an adaptation of the Multiple Eigenspaces technique, originally proposed in computer vision ([4]). Here, an *Eigenspace* is an affine sub-space (i.e. has a *mean* datapoint (DP), and a certain number of linear directions) of the full hand configuration space representing a subset of the data. The generation of eigenspaces needs to consider, at the same time, which are the DPs belonging together, and what the dimension (i.e. the number of linear directions to incorporate) should be.

Applying the technique to more than 4500 postures has led to a number of low dimensional affine sub-spaces similar to grasp categories which can be found in a classical grasp taxonomy ([2]).

An interesting application of this methodology is represented by the possibility of using such sub-spaces to have a simplified, task-driven hand design approach; this in order to be able to capture the nature of some duties that the hand must fulfill, without over-complicating the actuation method, and possibly the overall hand design. This is against the idea of considering the single linear direction which best interpolates all the samples like in Principal Component Analysis, as this is affected by the data population itself.

A more detailed view on this method and on the achieved results can be seen in Sec. A.4.

1.4 Planning

1.4.1 Planning of Grasp Acquisition under Uncertainty and Incompleteness

In this work we have now ported our framework for reach to grasp planning under uncertainty to a real robot. We have also carried out extensive simulation analysis. The approach requires the robot to find collision-free trajectories that are robust in the face of such uncertainty. There are two fundamentally different approaches. First, a trajectory may be formulated that is robust to current uncertainty, but does not reason about how future information may reduce that uncertainty. Second, the robot may plan a trajectory to gather information that will reduce the uncertainty, so as to make a final grasping trajectory more reliable. Previous work typically separates these two aspects, separately planning information gathering trajectories and grasping trajectories. The two can be theoretically joined in a continuous state and action POMDP, but this leads to an infinite dimensional belief space planning problem that is hard to solve. We instead pursued a more tractable approach to combine information gathering and

reach-to-grasp trajectories. Our main insight is we can embed the value of information in the much lower dimensional physical space to avoid the full complexity of belief state planning. This gives a well posed and tractable problem for reach-to-grasp planning under uncertainty. The specific contributions of our work are to: (i) plan information gain whilst simultaneously attempting to grasp the target object; (ii) encode expected information gain by warping distances in the workspace, creating a non-Euclidean metric that is information-sensitive; (iii) employ a hierarchical planning approach to reduce planning complexity in this space; (iv) update the belief about the objects pose using a tactile observation model for a multi-finger hand palpating the object; (v) evaluate different methods, proving that our approach improves reach-to-grasp planning for a dexterous robot. We also use the grasp learning algorithm to generate the final target grasp. We assume a possibly incomplete shape model of the object is previously obtained from sensing. The work has been demonstrated in trials in simulation and on Boris. Empirical results confirm that sequential re-planning achieves a greater success rate than single grasp attempts, and that the information gain approach requires fewer iterations before a grasp is achieved. This is now written up into a journal paper for submission which is attached.

1.4.2 On the Problem of Moving Objects with Autonomous Robots: a Unifying High-Level Planning Approach

In this work we propose a high-level planner that unifies different object moving strategies such as pick-and-place and handoff, and exploits support surfaces if required to achieve the goal. Both a real and simulated examples with different objects and multiple manipulators show the efficacy and scalability of this approach.

Our main contribution with this paper is a graph-based modelization of the problem, associated to a novel planning algorithm, that effectively unifies previously described strategies. In this graph, each node represents the state of the object to be moved, while the arcs correspond to feasible change of state (more details on this are given in Sec. IV in the annex (Sec. A.2)). In a hierarchical planning layered architecture, our planner needs to be placed below a symbolic reasoning planner. The experimental validation of the proposed approach has been carried out on the Vito robot of Centro di Ricerca “E. Piaggio”. In order to test the planner on a more complex setup with multiple end-effectors, a simulation with five Kuka LWR and one conveyor belt has been also performed.

More details on this new approach and on the achieved results can be found in Sec. A.2.

1.4.3 Infrared Sensor-based Grasp Planning

In this work we present an approach to refine grasps for soft robotic hands which allows to cope with situations where uncertainty is so large that the intrinsic adaptability of the hand is not enough to overcome it.

Once a pre-planned grasp, e.g. from a database, has been selected for execution to an object detected in a scene, an infrared sensor-informed grasp planner is run online that essentially reduces uncertainties related to object shape, and its pose in the environment and with respect to the hand. The proposed method implements a pre-grasp hand pose optimization algorithm that allows to minimize the distances between hand fingertips and the object to be grasped by continuously controlling the wrist pose and the amount of hand closing along the hand synergy.

Experimental studies with the Kuka-LWR arm and the Pisa/IIT Soft-hand demonstrate the benefit of the developed technique and the improvement in the grasping performance with respect to the open-loop execution of grasps planned on the basis of prior visual cues only.

Our contributions with this work are both theoretical and technological. On the theoretical side, the centering of the hand while it wraps around the object is posed as a nonlinear optimization problem, where the cost function is directly related to the distances between the hand fingertips (where the IR sensors are located) and the object. Since the cost function is intrinsically numerical and evaluated at run time, we propose a Gauss-Newton-like strategy to obtain an approximation of the residual distance and its Jacobian with respect to the possible hand moves, i.e. its pose and the amount of closing.

On the technological side, our contribution is represented by the design of thimbles with embedded IR sensors, which can cohabit with the IMU-glove on the Pisa/IIT SoftHand.

More details on this new approach and on the achieved results can be found in Sec. A.2.

1.5 Optimisation

1.5.1 A Computational Framework for Environment-Aware Robotic Manipulation Planning

Moving beyond with respect to what we committed to investigate in Tasks 4.2 and 4.3, we introduce, in this section, a computational framework for direct trajectory optimization of general manipulation systems without *a priori* specified contact sequences, possibly exploiting *environmental constraints* as a tool to accomplish a task.

Originally, we planned to approach the problem of robust grasping by dividing it into three main stages: (i) move from hand pre-shape to first

object contact (Task 4.1), (ii) perform an incipient grasp and assess the first-order properties of the surface of the object, possibly changing candidate contact locations so that the quality of the incipient grasp is maximized (Task 4.2), and (iii) perform the actual grasp acquisition by optimizing the distribution of the applied contact forces (Task 4.3).

In this section, we report on our efforts to devise a framework to be employed not only for grasp planning, but also for manipulation planning, that should be able to merge all three previous phases in a systematic and coherent way. The user should be focused on providing high-level objectives, e.g. “move object A from pose 1 to pose 2 in a given amount of time”, and the framework should be able to provide a manipulation plan that should take care of all the rest, e.g. should specify low-level actions and their correct sequence for the manipulation system at hand (single-arm configuration, dual-arm configuration), defining the whole contact sequence (where and when to make and to break contacts), should provide trajectories consistent with the dynamics of the manipulation system, unilateral contacts, friction constraints and actuation limits.

Related work to which we compare ours indeed include those using: (i) *traditional grasp planners*, such as [5] and [6]; (ii) *general purpose planning algorithms*, such as [7] and [8]; (iii) *machine learning approaches*, as [9] and [10]; (iv) *optimization-based trajectory planners*, such as [11], [12], and [13]. In particular, with respect to [13], which is the closest to ours, we can affirm that, besides a much more efficient computational pipeline, by explicitly instantiating environmental contact forces, we fabricate a strategy such that, if the task may be more efficiently and/or more robustly performed with the aid of constraints provided by the environment, the proposed approach can devise manipulation strategies that cleverly and opportunistically exploit environmental constraints.

Moreover, two approaches are presented to model the dynamics of systems with intermittent contacts: the first one, in which continuous contact reaction forces are generated by nonlinear virtual springs, is convenient to tackle scenarios where we try to avoid *sliding* contacts; the second one, which is based on a velocity-based time stepping scheme, is suitable in scenarios where *sliding* interaction primitives may lead to convenient interactions among the hand, the manipulandum and the environment.

In both cases, beside system’s state and applied torques, object and environment contact forces are included among the free optimization variables, and they are rendered consistent via suitably devised sets of *complementarity* conditions. To maximize computational efficiency, sparsity patterns in the linear algebra expressions generated during the solution of the optimization problem are exploited, and Algorithmic Differentiation (also known as Automatic Differentiation) is leveraged to calculate derivatives. These aspects appear completely unexplored in the literature of high-level planning for systems with intermittent contacts.

The approach is evaluated in three simulated planar manipulation tasks: (i) moving a circular object from an initial pose to a final pose in the workspace with two independent fingers, (ii) rotating a capsule-shaped object with an underactuated two-fingered gripper, and (iii) rotating a circular object in hand with three independent fingers. Tasks (i) and (ii) show that our algorithm quickly converges to locally optimal solutions that opportunistically exploit environmental constraints. Task (iii) demonstrates that even dexterous fingertip gaits can be obtained as a special solution in the very same framework.

More details on this new approach and on the achieved results can be found in Sec. A.5.

1.5.2 Offset-free MPC Explained: novelties, subtleties, and applications

This section presents an updated and comprehensive description of offset-free MPC algorithms for nonlinear (and linear) discrete-time systems, with the intended objectives of clarifying the main concepts, showing new results, highlighting subtleties by means of challenging applications. First, the offset-free tracking problem for nonlinear systems is presented, putting a strong accent on the role of the disturbance model and observer, and then novel and stronger offset-free estimation results are presented. Next, recent advances in linear offset-free MPC are described, which show the equivalence of the velocity form algorithm (so far considered an alternative method) to a particular disturbance model and observer. Then, the concepts of offset-free estimation are exploited to design an offset-free economic MPC algorithm, which can asymptotically achieve the highest economic performance despite persistent model errors and disturbances. Extensive application results are presented to show the benefits of offset-free MPC algorithms over standard ones, and to clarify misconceptions and design errors that can prevent constraint satisfaction, closed-loop stability, and offset-free performance.

More details on this new approach and on the achieved results can be found in Sec. A.6.

References

- [1] M. Kopicki, R. Detry, M. Adjigble, R. Stolkin, A. Leonardis, and J. L. Wyatt, “One-shot learning and generation of dexterous grasps for novel objects,” *The International Journal of Robotics Research*, 2015.
- [2] M. Cutkosky, “On grasp choice, grasp models, and the design of hands for manufacturing tasks,” *Robotics and Automation, IEEE Transactions on*, vol. 5, no. 3, pp. 269–279, 1989.
- [3] M. Santello, M. Flanders, and J. F. Soechting, “Postural hand synergies for tool use,” *The Journal of Neuroscience*, vol. 18, no. 23, pp. 10105–10115, 1998.
- [4] A. Leonardis, H. Bischof, and J. Maver, “Multiple eigenspaces,” *Pattern Recognition*, vol. 35, no. 11, pp. 2613–2627, 2002.
- [5] C. Rosales, “Grasp planning under task-specific contact constraints,” Ph.D. dissertation, Universitat Politècnica de Catalunya, 2013.
- [6] A. Miller and P. Allen, “Graspit! a versatile simulator for robotic grasping,” *IEEE Robotics and Automation Magazine*, vol. 11, no. 4, pp. 110–122, 2004.
- [7] Y. Koga and J.-C. Latombe, “On multi-arm manipulation planning,” in *IEEE Int. Conf. on Robotics and Automation (ICRA)*, 1994.
- [8] B. Cohen, M. Phillips, and M. Likhachev, “Planning single-arm manipulations with n-arm robots,” in *Robotics: Science and Systems (RSS)*, 2014.
- [9] S. Levine and P. Abbeel, “Learning neural network policies with guided policy search under unknown dynamics,” in *Neural Information Processing Systems (NIPS)*, 2014.
- [10] S. Levine, N. Wagener, and P. Abbeel, “Learning contact-rich manipulation skills with guided policy search,” 2015, under review.
- [11] I. Mordatch, Z. Popović, and E. Todorov, “Contact-invariant optimization for hand manipulation,” in *Eurographics/ACM Symposium on Computer Animation*, 2012.
- [12] I. Mordatch and E. Todorov, “Combining the benefits of function approximation and trajectory optimization,” in *Proceedings of Robotics: Science and Systems*, Berkeley, USA, July 2014.
- [13] M. Posa, C. Cantu, and R. Tedrake, “A direct method for trajectory optimization of rigid bodies through contact,” *Int. Journal of Robotics Research (IJRR)*, vol. 33, no. 1, pp. 69–81, 2014.

A Annexes

A.1 Article: On the Problem of Moving Objects with Autonomous Robots: a Unifying High-Level Planning Approach

Authors H. Marino, M. Ferrati, A. Settimi, C. Rosales, M. Gabiccini

Info Published in: Robotics and Automation Letters, IEEE. Date of Publication: January 18 2016. ISSN: 2377-3766;
DOI: 10.1109/LRA.2016.2519149

Abstract Moving objects with autonomous robots is a wide topic that includes single-arm pick-and-place tasks, object regrasping, object passing between two or more arms in the air or using support surfaces such as tables and similar. Each task has been extensively studied and many planning solutions are already present in the literature. In this paper we present a planning scheme which, based on the use of pre-defined elementary manipulation skills, aims to unify solutions which are usually obtained by means of different planning strategies rooted on hard-coded behaviors. Both robotic manipulators and environment fixed support surfaces are treated as end-effectors of movable and non-movable types, respectively. The task of the robot can thus be broken down into elementary building blocks, which are end-effector manipulation skills, that are then planned at the kinematic level. Feasibility is ensured by propagating unforeseen low-level failures at the higher level and by synthesizing different behaviors. The validity of the proposed solution is shown via experiments on a bimanual robot setup and in simulations involving a more complex setup similar to an assembly line.

Relation with the deliverable this work is concerned with the problem of planning a grasp sequence to move one object from an initial configuration to a final one. Since the initial configuration is not known a priori, but has to be estimated using vision, nor the sequence of handoffs is pre-specified (but automatically synthesized), the present work contributes to the goals of Task 4.4.

Attachment (following pages until next annex)

On the Problem of Moving Objects with Autonomous Robots: a Unifying High-Level Planning Approach

Hamal Marino^{1,2}, Mirko Ferrati¹, Alessandro Settimi^{1,2}, Carlos Rosales¹, and Marco Gabiccini^{1,2,3}

Abstract—Moving objects with autonomous robots is a wide topic that includes single-arm pick-and-place tasks, object regrasping, object passing between two or more arms in the air or using support surfaces such as tables and similar. Each task has been extensively studied and many planning solutions are already present in the literature.

In this paper we present a planning scheme which, based on the use of pre-defined elementary manipulation skills, aims to unify solutions which are usually obtained by means of different planning strategies rooted on hard-coded behaviors. Both robotic manipulators and environment fixed support surfaces are treated as end-effectors of movable and non-movable types, respectively. The task of the robot can thus be broken down into elementary building blocks, which are end-effector manipulation skills, that are then planned at the kinematic level. Feasibility is ensured by propagating unforeseen low-level failures at the higher level and by synthesizing different behaviors. The validity of the proposed solution is shown via experiments on a bimanual robot setup and in simulations involving a more complex setup similar to an assembly line.

Index Terms—Manipulation Planning; Cooperative Manipulators; Dual Arm Manipulation

I. INTRODUCTION

INDUSTRIAL and service robots are often used to perform object moving tasks, using different strategies depending on the specific application. Behaviors shaped on the objects characteristics, typical of an industrial environment, are not suitable for a generic approach. As a matter of fact, exploiting all the robot capabilities like using one or more arms, passing the object between them, or using the environment to place the object and re-grasp it, is necessary to adapt to the large variety of possible situations.

Our work focuses on multi-robot coordinated manipulation as defined in [1]. Multiple end-effectors may interact with the same object during the task, either subsequently or at the same time. In this paper, a novel approach to perform object moving that can handle multi-arm robots is reported.

Manuscript received: August, 30, 2015; Revised November, 2, 2015; Accepted January, 6, 2016.

This paper was recommended for publication by Editor Antonio Bicchi upon evaluation of the Associate Editor and Reviewers' comments. This work is supported by the European commission projects PaCMan EU FP7-ICT 600918 and by the grant no. 645599 "SoMa" -Soft-bodied intelligence for Manipulation- within the H2020-ICT-2014-1 program.

¹ Centro di Ricerca "E. Piaggio", University of Pisa, 56122 Pisa, Italy.

Corr. auth.: hamal.marino@centropiaggio.unipi.it

² Dep. of Advanced Robotics, Istituto Italiano di Tecnologia, via Morego, 30, 16163 Genova

³ DICI, University of Pisa, 56122 Pisa, Italy

Digital Object Identifier (DOI): see top of this page.



Fig. 1: Vito, the robot used to perform the reported experiments. Two KUKA Light-Weight Robots (LWR) are mounted on a fixed torso and are equipped with a left and a right Pisa-IIT Soft-Hands. An Asus Xtion Pro-Live is used for vision.

A vision software recognizes the object present in the scene, then an operator selects the final goal for the object through a user interface. A high-level plan is generated on a suitable graph representation built using information stored in a database (DB), and it is then translated into a Cartesian plan that will be executed by the robot. The planning phase is capable of finding different strategies (pick-and-place with one or multiple arms, handoff, regrasp) and, exploiting the environment (e.g. using support surfaces), to move the object from the starting to the final position.

It is worth remarking that we do not use any *a priori* fixed strategies: instead, the strategy emerges from scratch as the outcome of the high level planning phase.

Manipulating objects usually involves a series of action in which objects are recognized, grasped, moved, and released. The simplest robot configuration that can perform these actions is a single arm in a single support surface setup, where an object is grasped, moved, and released in a different position. In such single arm setups, grasp planning, object recognition in a cluttered environment, optimization of the low-level planning, and optimization of the order of objects displacements have been the focus of recent research: [2], [3], [4], [5]. As described in [6], the exploration of a graph whose nodes represent a combination of grasp type and object position produces a sequence of multiple grasp-move-release actions, so that the same end-effector can move an object in a constrained environment, where a single pick-and-place strategy would fail.

Dual arm robot platforms gained an increasing interest because of their larger workspace and number of DoFs, but also

because of their similarity with humans, thus their capability of replacing them in already established assembly lines. These platforms are capable of performing handoff-based manipulations: a sequence of grasp, move, handoff to the second arm, move, and release.

Planning algorithms that use handoff can be found in [7], [8], or even devising the grasp trajectories online in [9], [10]. An alternative to handoff is using a common support surface for passing an object: this approach can be interpreted as a connection between two single arms pick-move-release strategies, but it also poses some additional constraints on the kinematics and the collisions between the robots, the object and the surface. Approaches mainly focused on solving these motion planning issues are [11], [12], [13], [14].

As more robots or objects are added, a coordinated planning becomes the main requirement for such platforms.

An effort to handle this increased complexity is the integration of a semantic/symbolic reasoning into a manipulation planning, in order to perform a single task, such as making a pancake [15], moving cylinders on a cluttered table [16], solving a Tower of Hanoi [17].

Other works like [18], [19] focus mostly on reasoning, using formal languages, to plan a task by using spatial and temporal knowledge, assuming that the motion planning and grasping are handled in a perfect way.

A two-level approach similar to ours has already been presented in [20] and more recently extended in [21]: however, even if the approach in [21] may cope with the specific problem in our context, most of the experimental results reported there in manipulation do not include grasping capabilities of the robot (the robot can only push the object on a table). In order to include such capabilities, some challenges regarding the continuous modelling of grasping would arise, which we decided to handle by discretizing object grasps and, similarly, object passing poses; moreover, exploitation of support surfaces would require an adequate formalism in order to find feasible poses for an object lying on a support surface. We believe that the ability to cope with full grasping sequences with an anthropomorphic underactuated robotic hand and the backtracking ability of our method represent non trivial features of our work with respect to existing approaches.

Since our algorithm's main inputs are the starting and desired positions of an object, an autonomous procedure can be considered to provide such inputs instead of a human operator. For example, [2] and [18] deal with reordering a set of objects in order to access one of them obstructed by others, automatically resulting in a sequence of single object pick-move-place actions equivalent to multiple selections of target by the user in our framework.

Our main contribution with this paper is a graph-based modeling of the problem, associated to a novel planning algorithm, that effectively unifies previously described strategies. In this graph, each node represents the *state* of the object to be moved, while the arcs correspond to feasible *change of state* (more details on this are given in Sec. IV). In a hierarchical planning layered architecture, our planner needs to be placed below a symbolic reasoning planner as the ones cited above.

The experimental validation of the proposed approach has been carried out on the Vito robot of Centro di Ricerca “E. Piaggio” (see Fig. 1). In order to test the planner on a more complex setup with multiple end-effectors, a simulation with five Kuka LWR and one conveyor belt has been also performed.

II. PROBLEM STATEMENT

The problem we are tackling deals with providing a robot the ability to autonomously answer the request: “move that object from the initial pose to a desired target pose”, given any number of end-effectors (e.e.) and support surfaces.

Instead of pre-specifying a particular strategy to achieve this result, we only build a set of correspondences between end-effectors, objects, and grasps. Given this set, a task planning is executed that results in a feasible sequence of actions (*move*, *grasp*, and *ungrasp*) in Cartesian space to be performed in order to reach the goal.

A sample-based, low-level planner then finds collision-free joint space trajectories for the robot in order to obtain the desired motions.

In case of low-level planning failures, a recover procedure takes place in order to activate a new task planning, trying to find a different feasible sequence of actions.

Our working assumptions are that:

- a vision system provides all necessary information about the current state of the environment to the planner, handling object recognition and pose estimation with sufficient accuracy¹;
- all objects appearing in the scene can either be grasped or considered as fixed obstacles;
- a grasp database, to be provided to the algorithm, encodes information related on how each object can be grasped by each end-effector;
- information about the desired target configuration is provided by the user. Specifically, the final position and orientation of the object in Cartesian space and the desired final end-effector supporting it (any robot e.e. or support surface) have to be specified using the GUI (see Fig. 2).

III. DEFINITIONS AND DATABASE GENERATION

To perform the high-level task planning, the devised algorithm relies on fundamental information stored in a database.

We will now define the concepts used by the planner and how the information related to those concepts is generated and stored in the database. A very simple, exemplary database is shown in Fig. 3. We store geometric information about the support surfaces, approximations of each arm reachable region, the grasps associated between an object and an end-effector, and the feasible grasps that can be used simultaneously by two end-effectors during an hand-off.

In particular, grasp information about the end-effector poses

¹We will not describe the pose estimation vision system here, as the implementation can be found in [22].

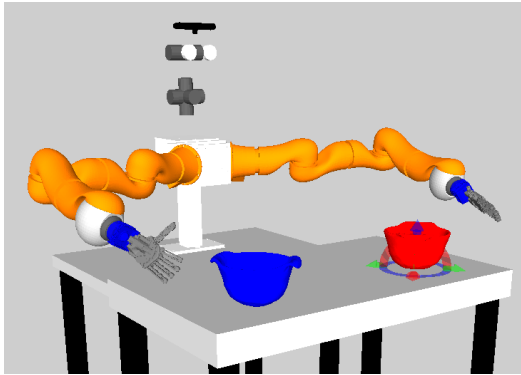


Fig. 2: RViz visualization. The blue object (left) represents the initial object configuration given by the vision system; the red object (right) represents the goal configuration selected by the user. For a picture of the whole User Interface see attached multimedia file.

w.r.t. the objects can be generated automatically for fully actuated hands (as in e.g. [23], [24]) or manually, like we did, using a motion capture system.

Objects			
Obj_id	3D views	Name	
o1	PointClouds	Cylinder	
End-Effectors			
EE_id	Reachable Workspaces	Movable	Name
e1	w1,w2,w3	FALSE	Table
e2	w1,w2	TRUE	LeftArm
e3	w2,w3	TRUE	RightArm
Workspaces			
Workspace_id	Adjacency	Geometry	Name
w1	w2	box1	Left
w2	w1,w3	box2	Middle
w3	w2	box3	Right
Grasp_id	EE_id	Name	Allowed_transitions
g1	e1	TopTable	g5 , g6 , g8 , g9
g2	e1	SideTable	g5 , g8
g3	e1	BottomTable	g4 , g5 , g7 , g8
g4	e2	TopLeftArm	g3 , g8 , g9
g5	e2	SideLeftArm	g1 , g2 , g3 , g7 , g9
g6	e2	BottomLeftArm	g1 , g7 , g8
g7	e3	TopRightArm	g3 , g5 , g6
g8	e3	SideRightArm	g1 , g2 , g3 , g4 , g6
g9	e3	BottomRightArm	g1 , g4 , g5

Fig. 3: Example of a database overall structure. Objects, End-Effectors, Workspaces, and Grasps tables are reported.

A. Objects

All (known) objects in a given set are included in the database; for each of them, we store multiple 3D views that are used for object recognition and pose estimation using a 3D vision library ([22]) to gather the necessary start state information before the planning starts.

B. End-Effectors

An *end-effector* is an entity which can act/apply a grasp/support on an object: there are both “movable” end-effectors (such as robot hands connected to arms) and “non-movable” ones (such as a fixed surface in the environment which can be exploited for statically stable object support). From a task planning perspective, there is no distinction between movable and non-movable end-effectors, as both types can interact with an object in specific ways, and can exchange the object with specific interaction transitions.

C. Workspaces

Our *environment* is the union of all the points reachable by all the end-effectors (movable and non-movable). For fixed surfaces (which are non-movable end-effectors), reachable points are represented by thin normal extrusions of the surfaces themselves.

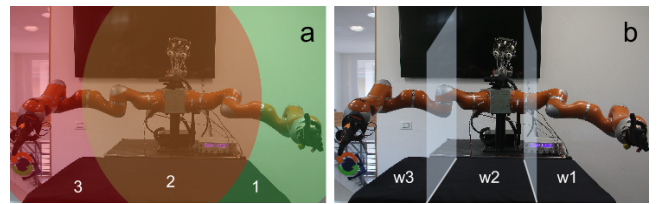


Fig. 4: (a) The reachable regions of the left and right arm are respectively reported in green and red, while the one of the table is represented by the table itself. (b) Using the intersection between simple approximations of these regions (cuboids), we defined for this scenario $w1$, $w2$, and $w3$.

In order to split the environment into regions useful for the high level planning, we approximate the reachable region of each end-effector with simpler convex models. We use cuboids because they are a natural 3D extension of support surfaces. We then check for intersections in order to find regions where multiple end-effectors can interact with each other. These intersections are called *workspaces*.

Workspaces are candidates for object *passing*, since they may be reached by more than one end effector simultaneously. Workspaces enjoy the additional property of *adjacency* if they can be reached by the same movable end-effector. Thus, adjacent ones are candidates for object *moving*.

With reference to Fig. 3 (tables) and Fig. 4(b), since workspaces $w1$ (left workspace) and $w2$ (middle workspace) are adjacent (check Workspaces table, rows 1 and 2), and also reachable by the movable e.e. $e2$ (left arm), (check End-Effectors table, row 2), object $o1$ (Cylinder) can be moved between these two workspaces. This allows to affirm that the Cylinder can be moved between the left and the middle workspace using the left arm with the grasps from $g4$ to $g6$ (check Grasps table, rows with $e2$ in EE_id column).

Reachability information between end-effectors and workspaces is stored in End-Effectors table.

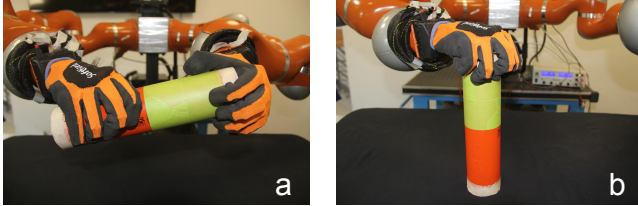


Fig. 5: (a) transition between Top-LeftArm and Side-RightArm grasps (g4-g8). (b) transition between Bottom-Table and Top-RightArm grasps (g3-g7).

D. Grasps

In this work, a *grasp* is defined as the relative configuration of the end-effector and a specific object once it is grasped. This Cartesian information is not shown in Fig. 3 for better readability. We associate to each object of our database one or more grasps.

If an object has to be handed off from an end-effector to another, there will be an instant in time where both e.e. are grasping the object.

A *transition* between two grasps is an interaction primitive that has no kinematic overlap between the two different end-effectors performing the grasps at the same time, i.e. there is no collision between the e.e.'s when they both are in their final grasp configuration with respect to the object.

The transitions we consider in this work are used by the high-level planner without any further distinction, but we can interpret them in the following way:

- pick and place actions when a non-movable end-effector is involved together with a movable one,
- a sequence of grasp-ungrasp actions when both end-effectors are movable.

No transition is allowed between any two non-movable end-effectors.

As an example, with reference to Fig. 3, End-Effectors table, *e1* (Table) and *e3* (RightArm) can both reach *w2* (Middle workspace) (check End-Effectors table). *e1* can support *o1* (Cylinder) with *g3* (Bottom-Table grasp), while *e3* can grasp *o1* with *g7* (Top-RightArm). Since a transition between *g3* and *g7* exists (check Grasps table, row 3), the cylinder can be safely grasped with the right arm from the table, as shown in Fig. 5, right panel.

The Cartesian product between reachable workspaces, adjacency, and grasp transitions, allows to create a graph as the one depicted in Fig. 6.

IV. ALGORITHM DESCRIPTION

An object is in a certain state $S_{e,g,w}$ when: (i) it is being grasped by a particular end-effector *e*, with (ii) a specific grasp *g*, and (iii) it is inside a specific workspace *w*. Moving an object means making a transition from its current state to a different one. In this work, a high-level plan is a sequence of states and transitions.

We show in Algorithm 1 the complete proposed algorithm, denoting with:

- C_{Init} , C_{Current} , and C_{Final} the initial, current and final object configurations in Cartesian space,
- G the graph,
- P_C the Cartesian plan,
- $S_{\text{Init}} = S_{e_i, g_i, w_i}$ and $S_{\text{Final}} = S_{e_t, g_t, w_t}$ the initial and final object configurations in high-level space,
- P_{HL} the high-level plan,
- Arc_{Id} the id of the arc that makes the planning fail,
- p_i a single item of the Cartesian plan,
- M a joint space motion plan.

Algorithm 1: MoveObject

```
(states,transitions) = GetInformationFromDB();
G= GenerateGraph(states,transitions);
CCurrent= GetInitialStateFromVision();
CFinal= GetFinalStateFromUser();
repeat
    GHL= G;
    CInit= CCurrent;
    SInit= ConvertCartesianToHighLevel(CInit);
    SFinal= ConvertCartesianToHighLevel(CFinal);
repeat
    PHL= ComputeShortestPath(GHL,SInit,SFinal);
    if PHL is empty then
        | GlobalFailure;
    end
    PC= ConvertHighLevelToCartesian(PHL);
    if PC is empty then
        | ArcId= GetFailedConversion();
        | GHL= Backtracking(GHL,ArcId);
    end
    until PC is not empty;
    /* Executing the cartesian plan */
    for pi ∈ PC do
        M=MotionPlanning(pi);
        if M is valid then
            Execute(M);
            CCurrent= CurrentObjectPosition();
        else if CCurrent == CInit then
            | GlobalFailure;
        else
            | break for;
        end
    end
until CFinal == CCurrent;
```

A. Graph Generation

Using the full DB structure as illustrated in Sec. III, a graph *G* is generated by intersecting transitions between grasps, reachability from end-effectors to workspaces and workspaces adjacency information. For the exemplary database content illustrated in Fig. 3, the generated graph is depicted in Fig. 6. Note that this is a simplified example: a real experiment graph could have hundreds of nodes and thousands of arcs, as reported in TABLE I. For a picture of a real generated

graph see attached multimedia file.

Each node of the graph represents a state $S_{e,g,w}$ of the object. Each arc represents one of the two different kinds of transition (akin to “transit” and “transfer” concepts of [6]):

- 1) from S_{e,g,w_i} to S_{e,g,w_j} : change of workspace with the same grasp (thus the same end-effector), where e must be movable and w_i and w_j must be adjacent (in the sense of Sec. III-C) and reachable by e . This is represented by the dashed lines in Fig. 6.
- 2) from $S_{e_i,g_k,w}$ to $S_{e_l,g_l,w}$: change of end effector inside a certain workspace, where a transition between grasp g_k and g_l must exist (as described in Sec. III-D). This is represented by the solid lines in Fig. 6.

The weight of any arc could be chosen based on the failure probability of the associated transition or on the stability of the grasps involved. In this work we make the simple consideration that a change of end effector (transition from $S_{e_i,g_k,w}$ to $S_{e_l,g_l,w}$) has a higher failure rate w.r.t. a change of workspace (transition from S_{e,g,w_i} to S_{e,g,w_j}), thus we use weights with different order of magnitude, e.g. 1.0 and 0.1, respectively.

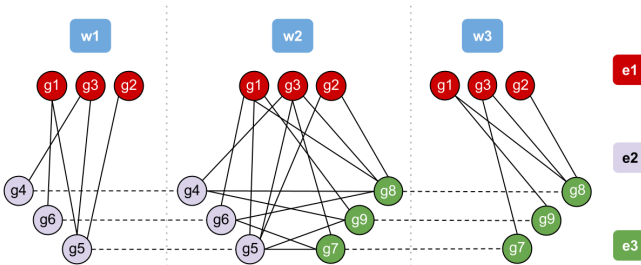


Fig. 6: Graph generated from the exemplary DB in Fig. 3: each node represents a state of the object being grasped by the end effector e_i ($i = 1, \dots, 3$) with the grasp g_k ($k = 1, \dots, 9$), in workspace w_m ($m = 1, \dots, 3$). Solid lines represent grasp transitions within the same workspace; dashed lines represent object displacements between workspaces with the same grasp. Simultaneous changes in workspace and grasp being applied to the object are not allowed in the current framework.

Note that the built graph no longer distinguishes between the type of end effectors or transitions.

B. Cartesian-to-High-Level Pose Conversion

In order to provide the initial and final states $S_{\text{Init}} = S_{e_i,g_i,w_i}$ and $S_{\text{Final}} = S_{e_t,g_t,w_t}$ our algorithm uses the information gathered from the vision system and the input by the user, respectively.

Workspaces w_i and w_t are found by using the database geometry, searching for those containing the required initial and target poses (note that workspaces do not overlap because they are the cells of a grid).

Initial end-effector e_i is assumed to be known, while target end-effector e_t is assumed to be known and non-movable in order to avoid ambiguous situations where multiple end effectors could simultaneously hold the object in the target position (see Fig. 7).

Finally, a search for grasps (g_i, g_t) that fulfill the initial and final pose is performed; this involves searching through all possible grasps associated to the end-effectors (e_i, e_t) , which are checked for similarity with respect to the initial and target poses of the object.



Fig. 7: The object in its final position can be grasped by three different end-effector (table, left hand, right hand)

C. Computation of the shortest path

We want to find a sequence of states from S_{Init} to S_{Final} , while minimizing the number of grasp transitions between end-effectors. To this sake any shortest path algorithm can be used: we choose Dijkstra [25] as one of the most widely known and easiest to implement.

In Fig. 8 we show the solution (path) for given initial and final states, which uses a direct handoff between the two end-effectors, while in Fig. 9 we show a plan with different initial and target states that automatically uses the table as intermediate end-effector in order to minimize path length. Each path represents a set of workspace/grasp transitions, which need to be converted into a discrete sequence of Cartesian position of the object and its grasping end-effector.

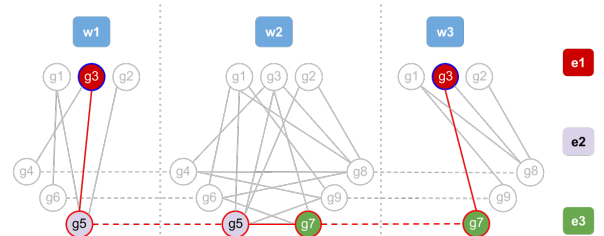


Fig. 8: Planning given by Dijkstra, the transition on the table is avoided because it would require more grasp transitions for the task.

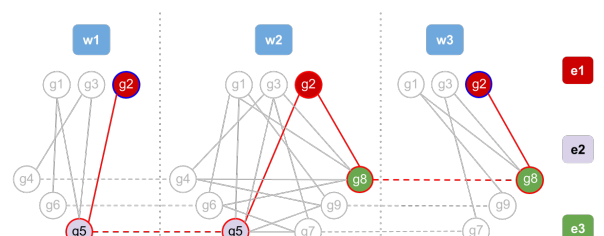


Fig. 9: Planning given by Dijkstra, the transition on the table is used because it is the shortest one for these initial and final states.

D. High-Level-to-Cartesian Conversion

The aforementioned conversion from the high-level plan P_{HL} to a Cartesian sequence P_C is a critical aspect of our approach, since it allows the decoupling between high-level object passing/moving and low-level motion planning. Each arc in the high-level plan is associated to low-level commands: in particular, a change of workspace generates a *move* command for an end-effector, while a change of grasp generates a pair of *grasp-ungrasp* commands for the end-effectors involved.

The discrete high-level plan is first simplified by removing unnecessary intermediate transitions, so that an end-effector \hat{e} moving an object through multiple workspaces $S_{\hat{e},g,w_1} \dots S_{\hat{e},g,w_n}$ generates a single *move* command for the end effector to reach the final workspace w_n .

After reaching that workspace, the object is either in its final target position, or needs to be passed to another end-effector by a sequence of *grasp-ungrasp* commands. In order to find a valid position for the object to be grasped by the next end-effector while still being grasped by the previous one, the following procedure has been applied.

- Create a virtual serial chain connecting the initial and final end-effectors together as if they were rigidly attached to each other by a constant $SE(3)$ matrix M . This represents the poses the end-effectors have to maintain in order to exchange the object.
- Consider as a virtual base-link the base-link of the initial arm, and as a virtual end-effector the base-link of the final arm.
- Solve the IK for the virtual chain with any jacobian-based approach avoiding self-collisions and collisions with environment. The target of this IK corresponds to the base-link of the final arm: in this way the closed-loop kinematic chain given by the two-arms connected through the object is respected.

E. Backtracking procedure

In case the conversion between high-level and Cartesian plans fails due to the inability of finding a collision-free configuration for performing a particular transition, a backtracking procedure is performed; this removes the arc associated to the failing transition and goes back to computing a shortest path on the updated graph.

The loop between phases in sub-sections IV-C, IV-D and backtracking is iterated until no backtracking is necessary (i.e. all states and transitions of a high-level plan are found to be feasible) or no valid high-level plan is found, in which case the target state is not kinematically reachable from the initial state with a collision free set of transitions.

F. Execution of the Plan

The execution of the *move*, *grasp*, *ungrasp* commands requires the use of a low level motion planning. If more than a single end-effector *move* command has to be performed, they are performed simultaneously, computing collision-free trajectories

that involve the various end-effectors. This can be efficiently done using, e.g. a sample-based random planner.

In our implementation we used RRT* [26] with RRT-Connect [27] as a backup, both implemented in MoveIt! [28]. Even though the initial and final joint configurations have been tested to be collision-free, a collision-free motion plan is not granted to be found. In this unlikely case, the current object position is considered: if it is different from the starting one, a new high-level action plan is initialized with the current object position as the new starting one; otherwise, the algorithm ends with a failure to avoid an infinite loop.

V. EXPERIMENTAL RESULTS

In this section the experiments to validate our approach are reported. Experiments have been performed without specifying any preferred strategy. The algorithm elaborates a plan and, depending on the situation, it produces a strategy with either a single or dual arm, with or without handoffs. We will now describe the different emerging behaviors obtained during the experiments. A video of these experiments is available in [29].

A. Experiments

Moving an object using handoff: In the reported examples (see Fig. 10) the robot uses two movable end effectors to move the object to the target position: this behavior is preferred since less e.e. switches are needed to perform it.

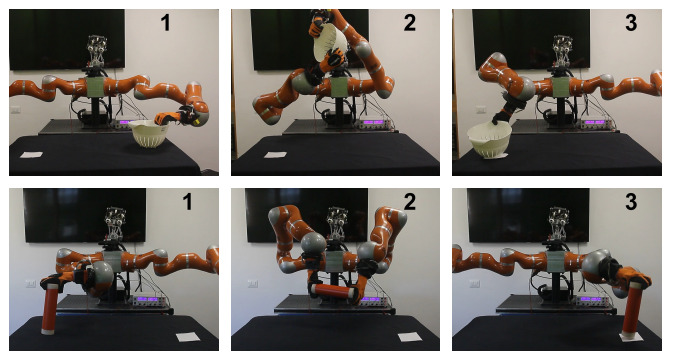


Fig. 10: Handoff experiments with a colander (on the top) and a cylinder (on the bottom).

Using support surfaces: Support surfaces are exploited in the case one single handoff is not possible. In this way the robot can re-grasp the object and then achieve the goal. In Fig. 11 single arm regrasping are reported, while in Fig. 12 the robot uses both arms to perform the task.

Pick-and-place: In the experiments reported in Fig. 13 the robot can execute the moving task using only one arm without any re-grasping. The particular case of trashing an object is shown in Fig. 14: the trash bin is being considered as a non-movable e.e. as well.

Assembly Line Simulation: To validate the generality and scalability of our approach with respect to the number and type of robots, we simulated kinematically the scenario depicted in Fig. 15. Here, five Kuka LWR arms are placed in front

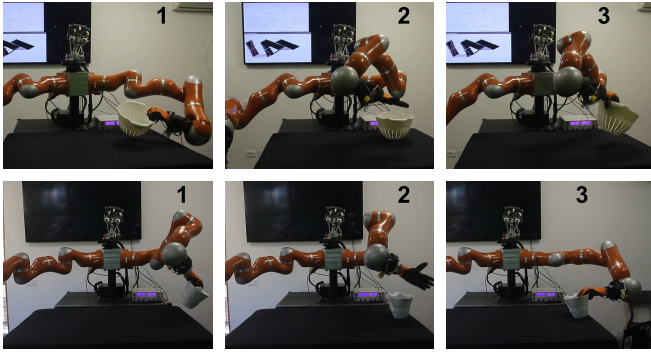


Fig. 11: Single arm object regrasping with a colander (on the top) and a pitcher (on the bottom).

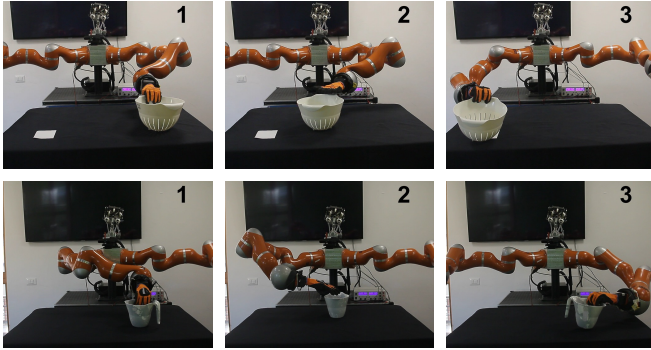


Fig. 12: Dual arm object regrasping with a colander (on the top) and a pitcher (on the bottom).

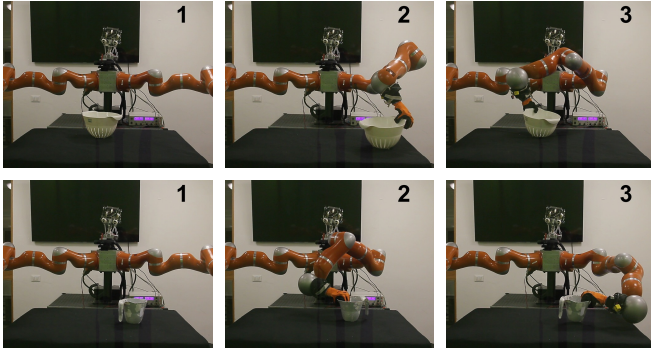


Fig. 13: Single arm pick-and-place experiments with a colander (on the top) and a pitcher (on the bottom). On the left the desired position is reported, then the initial and the final one are respectively in the middle and on the right.

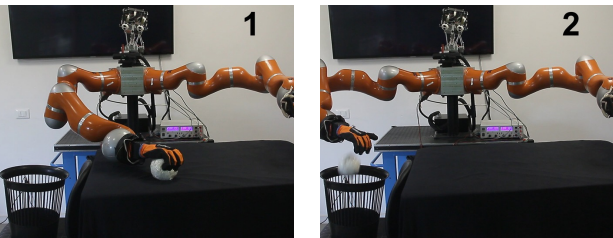


Fig. 14: Trashing a ball experiment.

of four workbenches, one of which contains a conveyor belt, which is modeled as a 1 DoF prismatic robot which can move horizontally objects that are placed on its surface. Using the procedure described in Sec. III-C a high-level description with 9 workspaces was obtained. The cylindrical object, initially resting on the first bench below a shelf (blue cylinder), has to

find itself in the final configuration resting on top of the last bench (red cylinder). The outcome of the planning algorithm is a sequence consisting of the following actions: pick from the source location with first arm, handoff between first and second arm, place on the table, pick with third arm, handoff between third arm and fourth arm, handoff between fourth arm and conveyor belt, handoff between conveyor belt and fifth arm, place in the final location. Please refer also to the video attachment for more details.

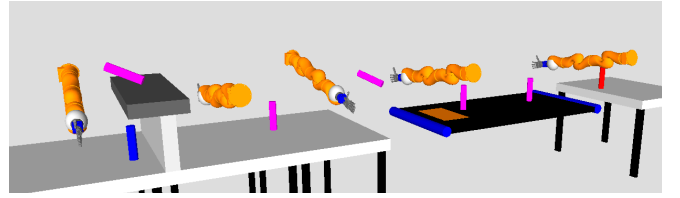


Fig. 15: An assembly line simulation with 5 KUKA LWR and a conveyor belt. The cylinder is moved from the initial position on the left (blue) to the final one on the right (red). The intermediate positions in which the object is exchanged between two e.e.'s are depicted in magenta.

B. Computational Costs

All experiments have been performed on a Intel Core i7-4770K machine with 16GB RAM using a single thread. The algorithm implementation could be highly parallelized thanks to its many parts based on randomized approaches, thus we expect a 3x speed-up to be a realistic value using 4 threads. Please consider this in comparison with other similar works.

In TABLE I we report computation times (in seconds) for the planning procedure described in Algorithm 1, both for the Vito robot and the assembly line scenarios, averaged on 100 trials with 5 different initial and target configurations for each task (table column).

GRAPH	Vito Robot				Assembly Line
	Pitcher	Colander	Ball	Cylinder	Cylinder
Nodes	108	144	80	224	736
Arcs	1609	3426	1056	5248	14016
HL-TIME					
avg	3.2	5.4	1.9	2.6	8.5
max	4.6	9.4	2.4	3.2	21.3
min	1.8	2.5	1.1	2.1	3.1
TOT-TIME					
avg	24.2	28.5	17.6	21.5	53.0

TABLE I: High level planning and total computation times (s).

While a high number of nodes and arcs should intuitively increase the computational time, indeed most of the CPU is used for the collision checking inside HighLevel_to_Cartesian conversion. Objects characterized by a simple geometry such as a ball or a cylinder are usually easier to handle and move, thus less arcs are tested in the loop of Algorithm 1.

The assembly line experiment requires more handoffs and surface supports (transitions), thus it is more likely to fail and cause a replan, as we can see from the greater max-min range. Obviously, the number of transitions depends on the strategy chosen by the high level planner, e.g. 2 for a Pick-and-Place and 3 for an handoff.

For each transition, the motion planning uses five seconds for

RRT* and, as a backup solution, ten attempts of RRT-Connect (up to a total of three more seconds). In our experience, and given the time allotted for the first phase, RRT* fails in about 40% of the transitions, mostly during planning approach trajectories to the object in a pose difficult for the robot to reach.

VI. CONCLUSIONS

In this work we proposed a high-level planner that unifies different object moving strategies such as pick-and-place and handoff, and exploits support surfaces if required to achieve the goal. Both a real and simulated examples with different objects and multiple manipulators show the efficacy and scalability of this approach.

Ongoing work is focused on extending the approach to planning for simultaneously moving more than a single object, on parallelizing planning and execution phases, and on considering more complex interactions between possibly multiple end-effectors and the object to be moved.

All the code of this framework is available at <http://dualmanipulation.bitbucket.org>.

ACKNOWLEDGMENTS

Authors thank Gian Maria Gasparri and Federico Spinelli for fruitful discussions on the preliminary version of this work.

REFERENCES

- [1] C. Smith, Y. Karayannidis, L. Nalpantidis, X. Gratal, P. Qi, D. V. Dimarogonas, and D. Kragic, “Dual arm manipulation a survey,” *Robotics and Autonomous Systems*, vol. 60, no. 10, p. 1340, 2012.
- [2] G. Havar, G. Ozbilgin, E. Erdem, and V. Patoglu, “Geometric rearrangement of multiple movable objects on cluttered surfaces: A hybrid reasoning approach,” in *Robotics and Automation (ICRA), 2014 IEEE International Conference on*. IEEE, 2014, pp. 445–452.
- [3] M. Dogar and S. Srinivasa, “A framework for push-grasping in clutter,” *Robotics: Science and Systems VII*, 2011.
- [4] J. Wolfe, B. Marthi, and S. J. Russell, “Combined task and motion planning for mobile manipulation.” in *ICAPS*, 2010, pp. 254–258.
- [5] J. A. Bagnell, F. Cavalcanti, L. Cui, T. Galluzzo, M. Hebert, M. Kazemi, M. Klingensmith, J. Libby, T. Y. Liu, N. Pollard, et al., “An integrated system for autonomous robotics manipulation,” in *Intelligent Robots and Systems (IROS), 2012 IEEE/RSJ International Conference on*. IEEE, 2012, pp. 2955–2962.
- [6] T. Siméon, J.-P. Laumond, J. Cortés, and A. Sahbani, “Manipulation planning with probabilistic roadmaps,” *The International Journal of Robotics Research*, vol. 23, no. 7-8, pp. 729–746, 2004.
- [7] B. Cohen, M. Phillips, and M. Likhachev, “Planning single-arm manipulations with n-arm robots,” in *Eighth Annual Symposium on Combinatorial Search*, 2015.
- [8] N. Vahrenkamp, D. Berenson, T. Asfour, J. Kuffner, and R. Dillmann, “Humanoid motion planning for dual-arm manipulation and re-grasping tasks,” in *Intelligent Robots and Systems. IROS 2009. IEEE/RSJ International Conference on*, pp. 2464–2470.
- [9] J.-P. Saut, M. Gharbi, J. Cortés, D. Sidobre, and T. Siméon, “Planning pick-and-place tasks with two-hand regrasping,” in *Intelligent Robots and Systems (IROS), 2010 IEEE/RSJ International Conference on*. IEEE, 2010, pp. 4528–4533.
- [10] N. Vahrenkamp, T. Asfour, and R. Dillmann, “Simultaneous grasp and motion planning: Humanoid robot armar-iii,” *Robotics & Automation Magazine, IEEE*, vol. 19, no. 2, pp. 43–57, 2012.
- [11] L. Karlsson, J. Bidot, F. Lagriffoul, A. Saffiotti, U. Hillenbrand, and F. Schmidt, “Combining task and path planning for a humanoid two-arm robotic system,” in *Proceedings of TAMRA: Combining Task and Motion Planning for Real-World Applications (ICAPS workshop)*. Citeseer, 2012, pp. 13–20.
- [12] B. Cohen, S. Chitta, and M. Likhachev, “Search-based planning for dual-arm manipulation with upright orientation constraints,” in *Robotics and Automation (ICRA), 2012 IEEE International Conference on*. IEEE, 2012, pp. 3784–3790.
- [13] F. Zacharias, D. Leidner, F. Schmidt, C. Borst, and G. Hirzinger, “Exploiting structure in two-armed manipulation tasks for humanoid robots,” in *Intelligent Robots and Systems (IROS), 2010 IEEE/RSJ International Conference on*. IEEE, 2010, pp. 5446–5452.
- [14] B. Cohen, S. Chitta, and M. Likhachev, “Single-and dual-arm motion planning with heuristic search,” *The International Journal of Robotics Research*, p. 0278364913507983, 2013.
- [15] M. Beetz, U. Klank, I. Kresse, A. Maldonado, L. Mosenlechner, D. Pangercic, T. Ruhr, and M. Tenorth, “Robotic roommates making pancakes,” in *Humanoid Robots (Humanoids), 2011 11th IEEE-RAS International Conference on*. IEEE, 2011, pp. 529–536.
- [16] S. Srivastava, E. Fang, L. Riano, R. Chitnis, S. Russell, and P. Abbeel, “Combined task and motion planning through an extensible planner-independent interface layer,” in *Robotics and Automation (ICRA), 2014 IEEE International Conference on*. IEEE, 2014, pp. 639–646.
- [17] G. Havar, K. Haspalamutgil, C. Palaz, E. Erdem, and V. Patoglu, “A case study on the tower of hanoi challenge: Representation, reasoning and execution,” in *Robotics and Automation (ICRA), 2013 IEEE International Conference on*. IEEE, 2013, pp. 4552–4559.
- [18] L. P. Kaelbling and T. Lozano-Pérez, “Hierarchical task and motion planning in the now,” in *Robotics and Automation (ICRA), 2011 IEEE International Conference on*. IEEE, 2011, pp. 1470–1477.
- [19] L. Lindzey, R. A. Knepper, H. Choset, and S. S. Srinivasa, “The feasible transition graph: Encoding topology and manipulation constraints for multirobot push-planning,” in *Algorithmic Foundations of Robotics XI*. Springer, 2015, pp. 301–318.
- [20] K. Hauser, T. Bretl, J. Latombe, and B. Wilcox, “Motion planning for a six-legged lunar robot,” *Algorithmic Foundation of Robotics*, 2008.
- [21] K. Hauser and V. Ng-Thow-Hing, “Randomized multi-modal motion planning for a humanoid robot manipulation task,” *The International Journal of Robotics Research*, 2011.
- [22] F. Spinelli, “Pose estimation library,” <https://bitbucket.org/Tabjones/pose-estimation-library>.
- [23] A. T. Miller and P. K. Allen, “Graspit! a versatile simulator for robotic grasping,” *Robotics & Automation Magazine, IEEE*, vol. 11, no. 4, pp. 110–122, 2004.
- [24] D. Berenson and S. S. Srinivasa, “Grasp synthesis in cluttered environments for dexterous hands,” in *Humanoid Robots. Humanoids 2008. 8th IEEE-RAS International Conference on*, pp. 189–196.
- [25] E. W. Dijkstra, “A note on two problems in connexion with graphs,” *Numerische mathematik*, vol. 1, no. 1, pp. 269–271, 1959.
- [26] S. Karaman, M. R. Walter, A. Perez, E. Frazzoli, and S. Teller, “Anytime motion planning using the rrt*,” in *Robotics and Automation (ICRA), 2011 IEEE International Conference on*, p. 1478.
- [27] J. J. Kuffner and S. M. LaValle, “Rrt-connect: An efficient approach to single-query path planning,” in *Robotics and Automation. Proceedings. ICRA '00. IEEE International Conference on*, vol. 2, pp. 995–1001.
- [28] I. A. Sucan and S. Chitta, “Moveit!” <http://moveit.ros.org>.
- [29] H. Marino, M. Ferrati, A. Settimi, C. Rosales, and M. Gabiccini, ‘RA-L submission accompanying video,’ <https://youtu.be/vIHg6gzIemQ>, Sept. 2015.

A.2 Article: IR Sensor-based Grasp Planner for the Pisa/IIT SoftHand Under Uncertainty

Authors E. Luberto, G. Santaera, Y. Wu, M. Gabiccini

Info Submitted to: 2016 IEEE/RSJ International Conference on Intelligent Robots and Systems

Abstract This paper presents an approach to refine grasps for soft robotic hands in the presence of uncertainty. Once a pre-planned grasp, e.g. from a database, has been selected for execution to an object detected in a scene, an infrared sensor-informed grasp planner is run online that essentially reduces uncertainties related to object shape and its pose in the environment. The proposed method implements a grasp location optimization algorithm that allows to minimize the distances between hand fingertips and the object by continuously controlling the wrist pose and the amount of hand closing. Experimental studies with the Kuka-LWR arm and the Pisa/IIT SoftHand illustrate the benefit of the developed technique and the improvement in the grasping performance with respect to the open-loop execution of grasps planned on the basis of prior visual cues only.

Relation with the deliverable this work is concerned with the problem of dealing with uncertainty when performing a grasp with a compliant hand. The present work contributes to the goals of Tasks 4.3 and 4.4.

Attachment (following pages until next annex)

IR Sensor-based Grasp Planner for the Pisa/IIT SoftHand Under Uncertainty

E. Luberto, G. Santaera, Y. Wu, M. Gabiccini

Abstract—This paper presents an approach to refine grasps for soft robotic hands in the presence of uncertainty. Once a pre-planned grasp, e.g. from a database, has been selected for execution to an object detected in a scene, an infrared sensor-informed grasp planner is run that essentially reduces uncertainties related to object shape and its pose in the environment. The proposed method implements a grasp location optimization algorithm that allows to minimize the distances between hand fingertips and the object by continuously controlling the wrist pose and the amount of hand closing. Experimental studies with Kuka-lwr arm and Pisa/IIT SoftHand illustrate the benefit of the developed technique and the improvement in the grasping performance with respect to the open-loop execution of grasps planned on the basis of prior visual cues only.

I. INTRODUCTION

The problem of autonomous robotic grasping has been in the focus of robotic research community for the past several decades [1], [2], [3]. Intelligent, proficient grasp planners have been developed that allow robotic hand to perform grasping tasks closely to humans. For ideal scenarios, where the object shape and location are perfectly known, and precise control of robotic hand can be achieved, pre-programmed autonomous grasping may be possible. To this end, most of the proposed planners [4], [5] rely on finding optimal fingertip placement on the object, while the surrounding environments are considered to be avoided as obstacles. However, these approaches are limited by their hand rigidity and fragility, and the manipulation strategies are very far from those a human would execute in real scenarios.

A real-world grasps are often associated to some uncertainties, the most typical ones being related to object recognition and localization. Usually, robots are equipped with vision sensors [6], [7], [8] to help reducing this uncertainty. However, a certain amount of uncertainty is usually unavoidable due to poor vision results, or incomplete view coverage of the sensor, etc. Other uncertainty may correspond to unexpected location of the object, where in this case, tactile/torque sensors are required to gain some additional information and to refine the object location from contacts [9], [10], [11]. Therefore, dexterous grasping of objects under uncertainty remains a difficult and unsolved problem in robotics.

E. Luberto, G. Santaera, Y. Wu are with Centro di Ricerca E. Piaggio, Universit di Pisa, Largo L. Lazzarino 1, 56122 Pisa, Italy. santaeragaspore@inwind.it, ema.1bt@hotmail.it, yier.wu@for.unipi.it

M. Gabiccini is with Dipartimento di Ingegneria Civile e Industriale (DICI), Largo Lucio Lazzarino 1, 56122 Pisa, with Centro di Ricerca E. Piaggio, Universit di Pisa, Largo L. Lazzarino 1, 56122 Pisa, and with Department of Advanced Robotics (ADVR), Italian Institute of Technology, Via Morego 30, 16163 Genova, Italy. m.gabiccini@ing.unipi.it



Fig. 1. Pisa/IIT SoftHand with IR Sensors

To better tackle the above described types of uncertainty, researchers have proposed the use of underactuated and/or soft hands [12], [13]. The design is simpler, easier to control and allows object contact with hand parts other than the fingertips, as well as to explore the surrounding environment in order to achieve precise and stable grasp. The robotic hand studied in this paper is the Pisa/IIT SoftHand [14], which has only one degree of actuation, and is continuously deformable in an infinity of possible shapes through interaction with objects and environment. Incipient grasp with this type of SoftHand has been successfully achieved with a wide variety of everyday objects [15]. However, problems still remain when one or several above mentioned uncertainties occur during the execution of grasping tasks with novel objects.

The lack of exact knowledge of target object shape and location in the environment can be compensated by the use of sensor feedback. To further improve the quality and reliability of robotic grasping, different strategies have been proposed to enhance the sensing capabilities of robotic manipulators. Enhancement of long-range vision sensor is one of the solutions, such as in-hand object tracking, hand extraction for object reconstruction, etc. However in general, image acquisition and processing are quite slow for online reactive response. Another solution relies on tactile sensors, which have been employed in numerous tasks [16], [17], whereas they require premature contacts with the object and may cause significant object motion.

On the other hand, short-range infrared (IR) sensors are widely used in robotic applications thanks to their low-cost, fast response time and reduced sensitivity to the environment. In robotic grasping, IR sensors have been introduced during

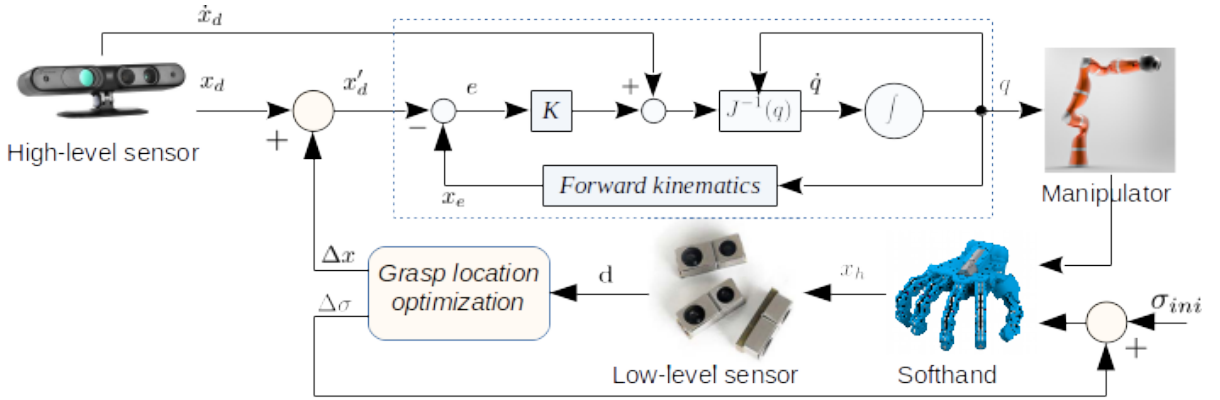


Fig. 2. Control Scheme of Sensor-based Grasping

final grasp adjustments. In [18], the authors detect the orientation of an object surface using the IR sensors that fit inside the fingers. In [19], a shared-control algorithm has been proposed based on long-range vision sensor and infrared sensors for teleoperation-based grasping. In [20], robust grasping has been achieved using an IR Net-structure proximity sensor for objects with unknown position and attitude. However, these approaches have been developed for robotic hands with sensible rigidity and high degrees of actuation (4-8). Limited number of work address the problem of grasping refinement for compliant hands based on IR sensor measurements, which looks very promising here.

In this work, an approach to grasp refinement for the Pisa/IIT Softhand under uncertainty using IR sensors is presented. Based on sensor measurement feedback, the proposed algorithm allows to center the Softhand fingers around the object and wrap the hand around it in a uniform manner. It is effective, high-speed, does not cause premature object contact nor needs re-grasping strategies. It allows the robotic hand to perform online adjustments before final grasping.

To address the above mentioned problems, the remainder of the paper is organized as follows. Section II presents the problem of grasping with our Softhand. Section III describes the IR sensor working principle and the measurements is provided. In Section IV, an algorithm of grasp location refinement of the Softhand is presented. Section V contains the experimental results obtained for IR sensor-based grasp of novel objects using Kuka-lwr and Pisa/IIT Softhand. Finally, Section VI summarizes the main results and contributions of this paper.

II. PROBLEM STATEMENT

Despite the fact that contemporary vision systems are able to reconstruct fairly good 3D object models, which allows to considerably reduce the related uncertainties, it requires enormous time and manpower to build a point cloud library for each novel object, yet still incomplete to guarantee a stable final grasp. To reduce the time of visual acquisition and processing, we propose to use only the prior

visual cue of an object, which leads the robot to a so-called pre-grasp location. In order to ensure a stable final grasp, infrared sensors are mounted on the hand fingertips to gain some additional information about the hand location with respect to the object.



Fig. 3. Types of uncertainty during grasping

For the considered compliant hand, due to the peculiarities of its embedded soft and adaptive synergy [14], its configuration and exact fingertip locations are usually unknown after a grasp is executed. Therefore, the target object is approached by the hand via controlling wrist pose and hand closing. In order to improve the quality of grasp, we proposed to minimize the distances between hand fingertips by continuously controlling the wrist pose and the amount of hand closing based on IR sensor measurements. As the hand is closed in an informed manner, the proposed method allows to reduce the chance of significantly perturbing the object during the execution of the final grasp.

The overall control scheme of the robotic arm and hand is depicted in Fig. 2. The proposed grasp location optimization algorithm provides the correction values of wrist pose and hand closing at each time step. This control strategy allows to effectively improve the quality of grasp under uncertainty, such as visual incompleteness and/or coverage, unexpected change of object location, etc. (see Fig. 3).

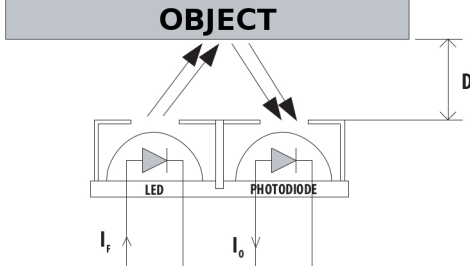


Fig. 4. IR Sensor working principle

III. SENSOR MEASUREMENTS

To measure the distances between hand fingertips and target object, we proposed to use infrared sensor. Its advantages include small size, low-cost, mechanical robustness and the simplicity to be managed with a micro-controller. The sensor consists of only one emitter and one receiver (See Fig. 4). The intensity of the transmitted infrared wave decreases according to the well known exponential law

$$E = E_0 e^{-\alpha x}, \quad (1)$$

where E_0 is the intensity of the original wave, x depends on the wave direction, and the parameter α varies with the material and increases with the wave frequency.

When the transmitted wave meets an object it splits in two, a refracted wave that spreads onto the object and a reflected one that comes back and meets the receiver. The intensity of these two waves depends on the reflection coefficient of the object material and on the angle at which the transmitted wave hits the object. The relation between the transmitted, refracted and reflected wave can be obtained using the Snell's law

$$k_1 \sin \theta_1 = k_2 \sin \theta_2, \quad (2)$$

where k_1, k_2 depend on the materials characteristics and θ_1, θ_2 are the angles between the wave travelling direction and the normal to the object surface. Usually the infrared wave is being transmitted and reflected through the same medium (the air, for instance), so $k_1 = k_2$ and, consequently, $\theta_1 = \theta_2$. Therefore, the desired distance between sensor and object can be obtained by measuring the intensities of the two waves.

However in most cases, it is hardly possible to know *a priori* the property of object material. To overcome this problem, one possible solution is to use the flight time, meaning that the sensor counts the time between the emission and reception of the infrared wave. Corresponding distance can be obtained as

$$d = \frac{vt_f}{2}, \quad (3)$$

where v is the wave propagation velocity, t_f is the flight time.

IV. GRASP REFINEMENT ALGORITHM

The IR sensors are mounted on the distal phalanges of all/a subset of the SoftHand fingers, according to the sensors' visibility w.r.t the object. Fig. 1 shows one of the possible arrangements of IR sensors, where only the thumb, index and ring finger are equipped. The sensor readings provide the distances between the phalanges and object within a range of about 60mm. It is assumed that all sensor measurements are collected in a vector $\mathbf{d} = [d_1, d_2, \dots, d_n]^T$, $d_i \geq 0$, where n indicates the number of sensors whose measurement is available (i.e. the sensor is seeing the object). Corresponding residual errors can be simply written as $r_i = d_i$. Since the goal is for the hand to approach the object in a homogeneous manner, the objective function of the optimization is defined as the root-mean-square errors of the residuals as follows

$$r_{ms} = \sqrt{\sum_{i=1}^n r_i^2} \quad (4)$$

The residual vector $\underline{\mathbf{r}} = [r_1, \dots, r_n]^T$ obtained from sensor measurements is in fact a function of control input parameters $\underline{\mathbf{x}}$, which are the decision variables of the grasp location optimization problem. The size and nature of $\underline{\mathbf{x}}$ vary with the parameters of the control input (e.g, for joint position control, $\underline{\mathbf{x}} = [j_1, \dots, j_n]^T$, for wrist pose control, $\underline{\mathbf{x}} = [p_x, \dots, p_z; r_x, \dots, r_z]^T$). In this case, $\underline{\mathbf{x}}$ is defined by the arm wrist pose ($p_x, p_y, p_z; r_x, r_y, r_z$) (6 DoF) together with the amount of hand closing, which is directly the synergy actuation (1 DoF), i.e. $\underline{\mathbf{x}} = [p_x, p_y, p_z; r_x, r_y, r_z; \sigma]^T$. The corresponding optimization problem can be formulated as

$$\min_{\underline{\mathbf{x}}} f(\underline{\mathbf{x}}), \quad \text{where } f(\underline{\mathbf{x}}) = \frac{1}{2} \underline{\mathbf{r}}(\underline{\mathbf{x}})^T \underline{\mathbf{r}}(\underline{\mathbf{x}}) \quad (5)$$

which is a *nonlinear* quadratic function w.r.t the decision variables $\underline{\mathbf{x}}$.

It is worth noting that, in the experimental setting, $f(\underline{\mathbf{x}})$ is only computable through execution of moves and measurement of sensor outputs. To reconcile the use of a gradient-based optimization algorithm with the intrinsic numerical nature of our $f(\underline{\mathbf{x}})$, we employ a Gauss-Newton strategy and form a linear approximation of the residual as follows

$$\underline{\mathbf{r}}(\underline{\mathbf{x}}) \simeq \underline{\mathbf{r}}_L(\Delta \underline{\mathbf{x}}) = \underline{\mathbf{r}}(\underline{\mathbf{x}}_k) + \mathbf{J}_r(\underline{\mathbf{x}}_k) \cdot \Delta \underline{\mathbf{x}}, \quad \text{where } \mathbf{J}_r = \frac{\partial \underline{\mathbf{r}}}{\partial \underline{\mathbf{x}}} \quad (6)$$

such that the optimal solution can be found step by step via corrections of the control inputs such that $\underline{\mathbf{r}} \rightarrow 0$. In (6), $\underline{\mathbf{r}}(\underline{\mathbf{x}}_k)$ are the residuals measured at current step k , \mathbf{J}_r is the Jacobian matrix of the residuals, and $\Delta \underline{\mathbf{x}}$ is the correction displacements, which represent the next move. Here, \mathbf{J}_r is computed numerically based on the measurement data. In particular, each column can be expressed as

$$\mathbf{J}_r(:, j) = \frac{\delta \underline{\mathbf{r}}}{\delta \underline{\mathbf{x}}_j} \quad (7)$$

where $\delta \underline{\mathbf{r}}$ collects the changes in the measurements of residuals vector with respect to the change in each control

input $\underline{\Delta x}_j$. Using Eq. (5) and (6), one can obtain the solution of the quadratic approximation at step k

$$f_Q(\underline{\Delta x}) = \frac{1}{2} \underline{\mathbf{r}}_L(\underline{\Delta x})^T \underline{\mathbf{r}}_L(\underline{\Delta x}) \quad (8)$$

of the original optimization problem (5) by seeking where $\left[\frac{\partial f_Q(\underline{\Delta x}_k)}{\partial \underline{\Delta x}_k} \right]^T = \underline{\mathbf{0}}$ which yields

$$\underline{\Delta x}_k = -\underline{\mathbf{J}}_r^+ (\underline{\mathbf{x}}_k) \underline{\mathbf{r}}_k \quad (9)$$

Note that $\underline{\mathbf{J}}_r^+ = (\underline{\mathbf{J}}_r^T \underline{\mathbf{J}}_r)^{-1} \underline{\mathbf{J}}_r^T$ is the pseudo-inverse of the residual Jacobian. This allows us to update the succeeding hand location/configuration by adding the step

$$\underline{\mathbf{x}}_{k+1} = \underline{\mathbf{x}}_k + \alpha \underline{\Delta x}_k \quad (10)$$

where $\alpha \in [0, 1]$ is a scaling factor for tuning these steps.

Based on the above presented method for grasp location optimization, the corresponding algorithm considering a robotic arm with a grasping end-effector in general are summarized in Algorithm (1). It should be mentioned that the strategies for approaching and moving the end-effector in steps no. 4 and no. 5 seem ambiguous due to the fact that these strategies highly depends on the particular circumstance of the sensors arrangement and measurements. More details will be given in the section of experimental validation.

V. EXPERIMENTAL VALIDATION

To confirm the applicability of the proposed grasp refinement algorithm and demonstrate its benefits from a practical point of view, this section presents the experimental setup and procedure, the sensor particularity as well as the experiment results of grasping performances on a set of everyday objects.

A. Experiment setup and procedure

To perform the grasping task, the experiment setup includes the following units:

- A RGB-D sensor, Asus Xtion ProLive [21], for acquisition of the object image (in our case the frontal view only);
- A 7-dof robotic manipulator, Kuka Lightweight IV [22], for object manipulation (maxim payload 7kg);
- A 19-dof robotic hand, Pisa/IIT SoftHand, for object grasping (one-dof actuation);
- Three short-range IR sensors, Avago HDSL9100, mounted on hand fingers for distance measurements;
- A experiment table and a set of selected everyday objects.

The grasp experiments are designed for two different case scenarios assuming the vision sensor captures the object frontal view only: (i) normal grasp; (ii) unexpected object locations. In case (i), all objects are assumed to be grasped at their predefined positions on the table. For objects have non-symmetrical form, grasping experiments are performed in two different object orientations. For each object and

Algorithm 1: Grasp Location Optimization

- 1: Acquiring object information from a vision system and obtain the pre-grasp location for the robotic arm;
 - 2: Moving the arm to the obtained location and bringing the grasping end-effector to a pre-grasp configuration;
 - 3: Checking the sensor measurements:
 if All sensors have no measurements on the object then
 Goto Step no. 4;
 if At least one sensor has measurement on the object then
 Goto Step no. 5;
 if All sensors have measurements on the object then
 Goto Step no. 6;
 4: Approaching the grasping end-effector to the object and returning to step no. 3;
 - 5: Moving the grasping end-effector around the object according to particular strategy (depending on the sensors measurements), returning to step no. 3;
 - 6: Moving the grasping end-effector by sequentially changing each parameter of the control input $\underline{\Delta x}$, while obtaining the differences in residual vector $\underline{\Delta r}$ based on sensor measurements and return the end-effector to its previous state;
 - 7: Computing the residual Jacobian matrix using Eq. (7);
 - 8: Computing the corrections $\underline{\Delta x}$ for the succeeding step using Eq.(9);
 - 9: Moving and Closing the grasping end-effector following Eq. (10), and reading the IR sensor measurements;
 - 10: Computing the objective function r_{ms} using the new measurements:
 if $r_{ms} > \text{threshold}$ then
 Goto Step no. 6;
 else
 Grasp the Object!
-

each object orientation, experiments are repeated for three times. In case (ii), the grasping experiments are performed where objects are slightly moved away from their predefined positions (in translations and/or in orientation, depending on the symmetry of corresponding object form).

For comparison, grasping experiments are carried out both with and without applying the IR sensor-based optimization algorithm proposed in this paper. To demonstrate the advantages of this method, the grasping performance analysis are given in the following subsections, in terms of successful rate of the grasp, evolution of measured distances and of the wrist poses.

B. Sensor particularity

In this work, the Avago HDSL9100 Infrared Sensor [23] (see Fig. 5) is selected thanks to its small size (7x3x2.5 mm), which allows it to be fit into the fingertips of Pisa/IIT SoftHand, yet provides a suitable operative range (4-65 mm)

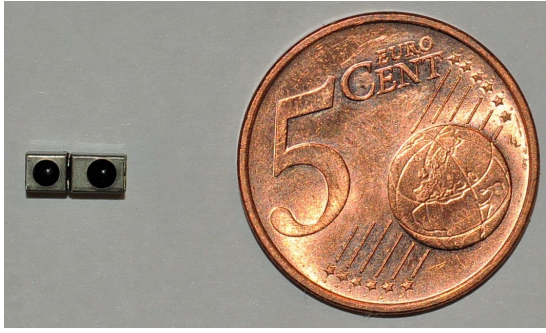


Fig. 5. Avago HDSL9100 Infrared Sensors

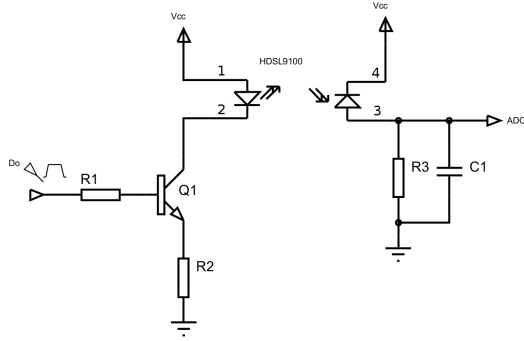


Fig. 6. Conditioning Circuit Schematic of IR Sensors

for the distance measurements. However due to the small size of the IR sensor, a conditioning circuit is required to manage the sensor input/output. It should be noted that the sensor operative range depends on the circuit components, here, they are tuned to obtain the maximum distance.

Another issue relates to closeness of the sensors due to their placements on the soft hand. In our experiment, three IR sensors are used and are mounted on the thumb, index and ring fingers (see Fig. 1). This arrangement may cause some disturbances during the measurements, for instance, the light emitted by one sensor could be misread by another. To overcome this problem, the conditioning circuit is designed to activate only one sensor at a time.

The schematic of conditioning circuit is illustrated in Fig. 6, where each sensor is activated by a square wave (D_o), and its output is read by an analog-digital converter (ADC). The physical output of the sensor is an electric voltage, which is proportional to the intensity of the reflected wave in the receiver. In other words, the higher is the output voltage, the closer is the sensor to an object. The ADC returns the output voltage in a digital value in bits (or ticks), according to its resolution (12 bits on 5 Volt for the embedded micro-controller PSoC).

To simplify the design of conditioning circuit, instead of counting the sensor flight time (see Section III), we use directly the output value of the ADC. In fact, the proposed algorithm, step by step in a differential way, works to reduce the distances between the object and the robot end-effector. In each step it moves the end-effector of the robot and

measures the distances, to understand which movements reduce these ones, so it does not need to know the exact value of distances in millimeters but considering the proportionality between distances and the intensities of the reflected waves, so the output value of the analog-digital converter is enough. Summing up this design choice allows to reduce the complexity of the conditioning circuit.

C. Checking the sensor measurements

In the Algorithm (1), before to compute the residual Jacobian matrix, one has to assure that all sensors are in the operative range. The check on the IR sensors, Step no. 3, depends on the specific configuration of the sensors installed. If at least one sensors measures a distance higher than 60 mm the current SoftHand position is changed. This displacement allows to explore the scenario exploiting the following criteria

- **case 1:** $(IR_{thumb}) > th$
 $SH_x := \rho$
 $SH_y += \rho$
- **case 2:** $(IR_{index}) > th$
 $SH_x := \rho$
 $SH_y -= \rho$
 hand-closure $\pm= v$
- **case 3:** $(IR_{ring}) > th$
 $SH_x += \rho$
 $SH_y -= \rho$
- **case 4:** $(IR_{thumb} \& IR_{index}) > th$
 $SH_x -= \rho$
 $SH_y -= \rho$
- **case 5:** $(IR_{thumb} \& IR_{ring}) > th$
 hand-closure $\pm= v$
- **case 6:** $(IR_{index} \& IR_{ring}) > th$
 $SH_y -= \rho$
- **case 7:** $(IR_{thumb} \& IR_{ring} \& IR_{ring}) > th$
 $SH_x -= \rho$
 $SH_y -= \rho$

where SH_x and SH_y are the position of the SoftHand frame in the world frame (see Fig. 7). ρ and v represent the correction about position [mm] and hand-closure [tic], while th is setted on 60mm.

D. Grasp results

The overall grasping performance of all conducted experiments are given in Table I, where the number of successful grasps are provided for each object in each case. Comparison are made for grasping with and without the proposed algorithm.

Clearly, using only the object frontal view and performing the grasp task at corresponding pre-grasp location, the number of successful grasps is very low. In the second case scenario, when the objects are deliberately moved, the successful grasp reduced to none. Applying the proposed

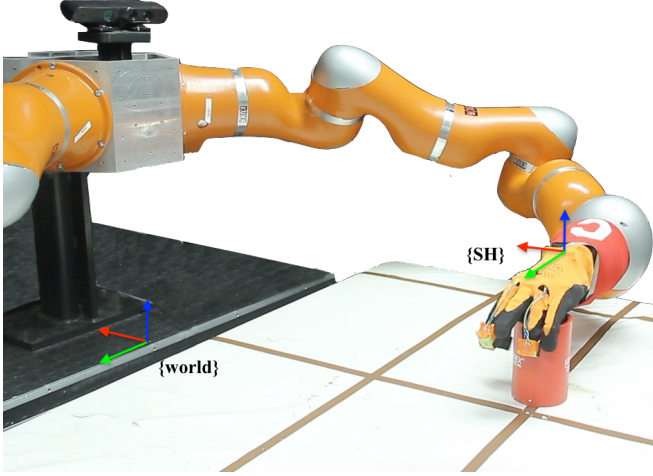


Fig. 7. Scenario

Object	Case (i)		Case (ii)	
	Algo.+	Algo.-	Algo.+	Algo.-
Cylinder	2/3	0	3	0
Baby cup	4	1	3	0
Paper box	4	1	2	0
Total	10	2	8	0

TABLE I

OVERALL GRASPING PERFORMANCE: SUCCESSFUL GRASP

grasp location optimization, the successful rate have been considerably increased by 54% and 53% in case (i) and (ii), respectively.

To evaluate the grasp results with applying the proposed sensor-based technique, the sensor measurements during the grasp have been analyzed. Fig. 8 and 9 illustrate the evolution of the measured distances between hand fingertips and objects for case scenario (i) and (ii), respectively. In particular, the blue dot line relates to the norm of all distances; the red star line shows the norm of corresponding residuals; and the markers are the distances from each fingertips to the object at each step.

In most of the performed grasp tasks, measurements of the index show that it is always further from the object than the others, whereas the thumb and ring are well centralized with respect to the object. This is due to the particular soft hand synergy, each finger closes differently driven by the hand closure. In this case, the index has relatively small amount of closure comparing to the other two fingers. However in practical grasp, such hand configuration can guarantee a stable grasp for most objects.

Table II and III present the sensor measurements before and after applying the grasp location optimization, for case scenarios (i) and (ii), respectively. The 3rd column reports the hand distance to the object, the 4th shows the residual values of all fingertips, and the last column considers only the thumb and ring. From these tables, it is clearly that

Object	Algo.	$\ \mathbf{d}\ $ (m)	$\ \mathbf{r}\ $ (m)	$\ \mathbf{r}^*\ $ (m)
Cylinder	Before	0.124	0.045	0.012
	After	0.037	0.020	0.002
Baby cup	Before	0.142	0.039	0.011
	After	0.034	0.017	0.001
Paper box	Before	0.094	0.040	0.013
	After	0.037	0.020	0.001

TABLE II
EVOLUTION OF DISTANCES AND RESIDUALS IN CASE (I)

Object	Algo.	$\ \mathbf{d}\ $	$\ \mathbf{r}\ $	$\ \mathbf{r}^*\ $
Cylinder	Before	0.119	0.021	0.010
	After	0.028	0.019	0.012
Baby cup	Before	0.139	0.018	0.004
	After	0.028	0.021	0.007
Paper box	Before	0.086	0.056	0.041
	After	0.025	0.010	0.003

TABLE III
EVOLUTION OF DISTANCES AND RESIDUALS IN CASE (II)

the proposed technique essentially reduced the distances from the hand to the object comparing to a pre-grasp configuration, and precisely centralized the thumb and ring around the object.

VI. CONCLUSIONS

In this paper we described an effective, high-speed method to refine the final grasping location, using low-cost IR sensors and optimization technique. The presented algorithm allows to center a robotic end-effector around an object, whose location and shape are acquired by a prior visual cue only. The algorithm was tested on KUKA-lwr arm and Pisa/IIT SoftHand by performing grasp tasks under different uncertainties with a set of daily objects. The grasp experiments validate the effectiveness of the proposed method and showed essential improvement in the grasping performance. Future work will address the full use of the IR sensors on all fingers, taking into account the adaptive synergy of the soft hand, to exploit the capabilities of the sensorized soft hand for perception of unstructured environments.

VII. ACKNOWLEDGMENTS

This work is supported by the grant no. 600918 PAC-MAN - Probabilistic and Compositional Representations of Object for Robotic Manipulation - within the FP7-ICT- 2011-9, and under grant agreement no. 645599 "SoMa" - Soft-bodied intelligence for Manipulation, within the H2020-ICT-2014-1.

REFERENCES

- [1] A. Bicchi and V. Kumar, "Robotic grasping and contact: a review," in *Robotics and Automation, 2000. Proceedings. ICRA '00. IEEE International Conference on*, vol. 1, 2000, pp. 348–353.
- [2] A. M. Okamura, N. Smaby, and M. R. Cutkosky, "An overview of dexterous manipulation," in *Robotics and Automation, 2000. Proceedings. ICRA'00. IEEE International Conference on*, vol. 1. IEEE, 2000, pp. 255–262.

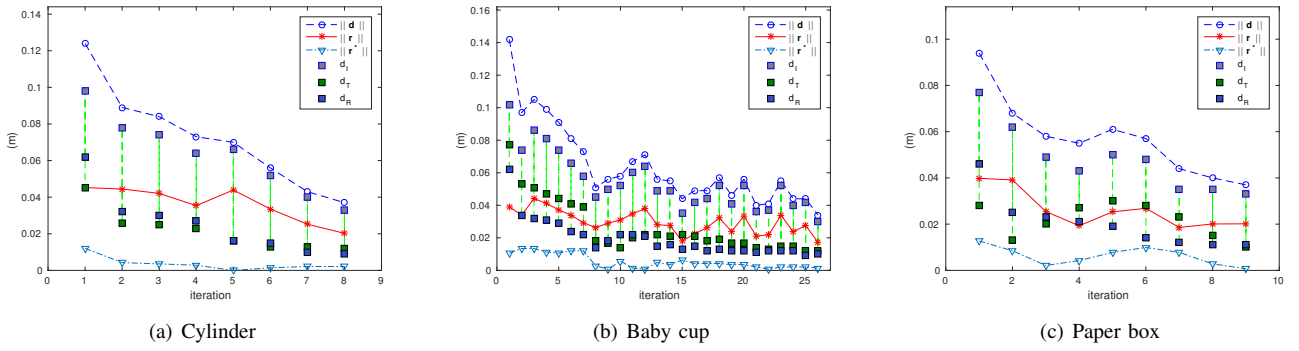


Fig. 8. Sensor measurements in case scenario (i)

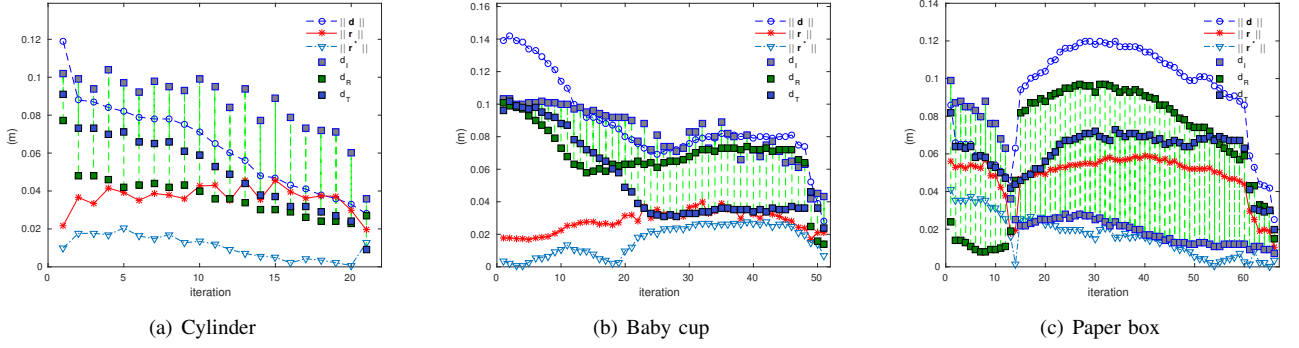


Fig. 9. Sensor measurements in case scenario (ii)

- [3] C. C. Kemp, A. Edsinger, and E. Torres-Jara, "Challenges for robot manipulation in human environments," *IEEE Robotics and Automation Magazine*, vol. 14, no. 1, p. 20, 2007.
- [4] R. Diankov and J. Kuffner, "Openrave: A planning architecture for autonomous robotics," *Robotics Institute, Pittsburgh, PA, Tech. Rep. CMU-RI-TR-08-34*, vol. 79, 2008.
- [5] A. Miller and P. Allen, "Graspit! a versatile simulator for robotic grasping," *Robotics Automation Magazine, IEEE*, vol. 11, no. 4, pp. 110–122, 2004.
- [6] C. Kemp, C. Anderson, H. Nguyen, A. Trevor, and Z. Xu, "A point-and-click interface for the real world: Laser designation of objects for mobile manipulation," in *Human-Robot Interaction (HRI), 2008 3rd ACM/IEEE International Conference on*, Mar. 2008, pp. 241–248.
- [7] A. Saxena, J. Driemeyer, and A. Y. Ng, "Robotic grasping of novel objects using vision," *The International Journal of Robotics Research*, vol. 27, no. 2, pp. 157–173, 2008.
- [8] B. Wang, L. Jiang, J. Li, and H. Cai, "Grasping unknown objects based on 3d model reconstruction," in *Advanced Intelligent Mechatronics. Proceedings, 2005 IEEE/ASME International Conference on*, Jul. 2005, pp. 461–466.
- [9] J. Tegin and J. Wikander, "Tactile sensing in intelligent robotic manipulation-a review," *Industrial Robot: An International Journal*, vol. 32, no. 1, pp. 64–70, 2005.
- [10] L. Natale and E. Torres-Jara, "A sensitive approach to grasping," in *Proceedings of the sixth international workshop on epigenetic robotics*. Citeseer, 2006, pp. 87–94.
- [11] J. Romano, K. Hsiao, G. Niemeyer, S. Chitta, and K. Kuchenbecker, "Human-inspired robotic grasp control with tactile sensing," *Robotics, IEEE Transactions on*, vol. 27, no. 6, pp. 1067–1079, Dec. 2011.
- [12] L. U. Odhner, L. P. Jentoft, M. R. Claffee, N. Corson, Y. Tenzer, R. R. Ma, M. Buehler, R. Kohout, R. D. Howe, and A. M. Dollar, "A compliant, underactuated hand for robust manipulation," *The International Journal of Robotics Research*, vol. 33, no. 5, pp. 736–752, 2014.
- [13] R. Deimel and O. Brock, "A novel type of compliant and underactuated robotic hand for dexterous grasping," *The International Journal of Robotics Research*, p. 0278364915592961, 2015.
- [14] M. G. Catalano, G. Grioli, E. Farnioli, A. Serio, C. Piazza, and A. Bicchi, "Adaptive synergies for the design and control of the pisa/it softhand," *The International Journal of Robotics Research*, vol. 33, no. 5, pp. 768–782, 2014.
- [15] M. Bonilla, E. Farnioli, C. Piazza, M. Catalano, G. Grioli, M. Garabini, M. Gabiccini, and A. Bicchi, "Grasping with soft hands," in *Humanoid Robots (Humanoids), 2014 14th IEEE-RAS International Conference on*. IEEE, 2014, pp. 581–587.
- [16] D. Gunji, Y. Mizoguchi, S. Teshigawara, A. Ming, A. Namiki, M. Ishikawa, and M. Shimojo, "Grasping force control of multi-fingered robot hand based on slip detection using tactile sensor," in *Robotics and Automation, 2008. ICRA 2008. IEEE International Conference on*, May 2008, pp. 2605–2610.
- [17] J. Felip and A. Morales, "Robust sensor-based grasp primitive for a three-finger robot hand," in *Intelligent Robots and Systems, 2009. IROS 2009. IEEE/RSJ International Conference on*. IEEE, 2009, pp. 1811–1816.
- [18] K. Hsiao, P. Nangeroni, M. Huber, A. Saxena, and A. Ng, "Reactive grasping using optical proximity sensors," in *Robotics and Automation, 2009. ICRA '09. IEEE International Conference on*, May 2009, pp. 2098–2105.
- [19] N. Chen, K. P. Tee, and C.-M. Chew, "Teleoperation grasp assistance using infra-red sensor array," *Robotica*, vol. 33, no. 04, pp. 986–1002, 2015.
- [20] S. Ye, K. Suzuki, Y. Suzuki, M. Ishikawa, and M. Shimojo, "Robust robotic grasping using IR net-structure proximity sensor to handle objects with unknown position and attitude," in *Robotics and Automation (ICRA), 2013 IEEE International Conference on*, May 2013, pp. 3271–3278.
- [21] "Asus xtion pro live home page," online; accessed 22-February-2016. [Online]. Available: https://www.asus.com/3D-Sensor/Xtion_PRO_LIVE/
- [22] R. Bischoff, J. Kurth, G. Schreiber, R. Koeppe, A. Albu-Schaffer, A. Beyer, O. Eiberger, S. Haddadin, A. Stemmer, G. Grunwald, and G. Hirzinger, "The kuka-dlr lightweight robot arm - a new reference platform for robotics research and manufacturing," in *Robotics (ISR), 2010 41st International Symposium on and 2010 6th German Conference on Robotics (ROBOTIK)*. IEEE, 2010.

[23] “Hdsl9100 datasheet page,” online; accessed 18-February-2016.
[Online]. Available: <http://www.avagotech.com/docs/AV02-2259EN>

A.3 Article: Learning and Inference of Dexterous Grasps for Novel Objects with Underactuated Hands

Authors M. Kopicki, C. J. Rosales, H. Marino, M. Gabiccini, J. L. Wyatt

Info Submitted to: [update this and the attached PDF!](#)

Abstract Recent advances have been made in learning of grasps for fully actuated hands. A typical approach learns the target locations of finger links on the object. When a new object must be grasped, new finger locations are generated, and a collision free reach-to-grasp trajectory is planned. Such a division of labour fails to transfer directly to underactuated hands, which improve grasp reliability via contacts with the object during grasping. In this paper we present a method for learning transferrable grasps for underactuated hands. Our approach learns not only the desired final grasp, and also good grasping trajectories, from a rigid body simulation. This enables us to learn how to approach the object and close the underactuated hand from a variety of poses. Our method does not rely on explicit representation of the contact sequence. The core learning method uses product of experts. This allows grasp transfer to novel objects and works despite partial shape reconstruction of less than 25% of the surface. From nine training grasps on three objects the method transferred grasps to previously unseen, novel objects, that differ significantly from the training objects, with an 80% success rate. We move beyond previous work by: i) showing the ability to learn transferrable grasps for underactuated hands; ii) extending our learning method to work with multiple training examples for each grasp type; iii) extending our method to work with multiple reach to grasp trajectories.

Relation with the deliverable this work is concerned with the problem of transferring a grasp robustly to different initial hand-object poses for underactuated hands. The present work contributes to the goals of Task 4.4.

Attachment (following pages until next annex)

Learning and Inference of Dexterous Grasps for Novel Objects with Underactuated Hands

Marek Kopicki¹ and Carlos J. Rosales² and Hamal Marino² and Marco Gabiccini² and Jeremy L. Wyatt¹

Abstract—Recent advances have been made in learning of grasps for fully actuated hands. A typical approach learns the target locations of finger links on the object. When a new object must be grasped, new finger locations are generated, and a collision free reach-to-grasp trajectory is planned. Such a division of labour fails to transfer directly to underactuated hands, which improve grasp reliability via contacts with the object during grasping. In this paper we present a method for learning transferrable grasps for underactuated hands. Our approach learns not only the desired final grasp, and also good grasping trajectories, from a rigid body simulation. This enables us to learn how to approach the object and close the underactuated hand from a variety of poses. Our method does not rely on explicit representation of the contact sequence. The core learning method uses product of experts. This allows grasp transfer to novel objects and works despite partial shape reconstruction of less than 25% of the surface. From nine training grasps on three objects the method transferred grasps to previously unseen, novel objects, that differ significantly from the training objects, with an 80% success rate. We move beyond previous work by: i) showing the ability to learn transferrable grasps for underactuated hands; ii) extending our learning method to work with multiple training examples for each grasp type; iii) extending our method to work with multiple reach to grasp trajectories.

I. INTRODUCTION

Transferring dexterous grasps to novel objects is a challenging problem. One approach is to machine learn solutions with techniques able to perform powerful generalisation. Another is to use an underactuated hand to cope with shape variation. In this paper we combine the benefits of both approaches by learning grasps for underactuated hands. Underactuated hands exploit the contacts that occur during grasping to achieve a wide variety of final grasp configurations. The final grasp configuration depends not only on the final hand pose, but also on the object shape, and on the reach to grasp trajectory. An interesting challenge is to use machine learning to exploit these interactions. The key technical challenge in applying machine learning to grasping with underactuated hands is to learn the right trajectory for a particular object shape so as to achieve a good grasp of a particular type.

One approach would be to learn the typical contact interactions that occur during a grasp, and to generate new grasps that reproduce these. The contact interactions are,

*This work was supported by EC-FP7-ICT-600918, PacMan.

¹Marek Kopicki and Jeremy L. Wyatt are with the Intelligent Robotics Laboratory, School of Computer Science, University of Birmingham, Birmingham, B15 2TT, UK.

²Carlos J. Rosales, Hamal Marino and Marco Gabiccini are with Centro Piaggio, Universita di Pisa, Pisa, Italy.

Correspond to: M.S.Kopicki at cs.bham.ac.uk



Fig. 1: We want transferrable grasps that are robust to different initial hand-object poses, and thus different interactions during reach to grasp, thus reaching similar final grasp states. We achieve this by learning a set of trajectories that, associated with a model of the final grasp state, form an attractor basin around that state.

however, rather complex and variable, even given small variations in object shape and friction. Therefore we tackle the problem by implicitly encoding the contact interactions in terms of the approach trajectory. Our method learns both the desired final contacts, the final hand shape, and possible sequences of hand pose during the reach to grasp trajectory. We build on our previous work on one-shot learning of grasps that transfer to novel objects, employing a product of experts. The novel technical contribution is that in this paper we show how to learn not only final grasp, but also the approach trajectory and control strategy for closing the dexterous hand. In particular, we learn a bundle of multiple trajectories that will all likely lead to a similar final stable grasp. We enable this by learning from examples generated in a rigid body physics simulation. Finally, at the grasp selection stage we now optimise across a space defined by this bundle of approach trajectories so as to maximise the chance of reaching a stable grasp. The method copes with partial and noisy shape information for the test objects.

A. Related Work

Previous work in learning generalisable grasps falls broadly into two classes. One class of approaches utilises the shape of common object parts or their appearance to generalise grasps across object categories [1], [2], [3], [4]. This works well for low DoF hands. Another class of approaches captures the global properties of the hand shape either at the point of grasping, or during the approach [5]. This global hand shape can additionally be associated with global object shape, allowing generalisation by warping grasps to match warps of global object shape [6]. This second

class works well for high DoF hands, but generalisation is more limited. We have previously achieved the advantages of both classes, generalising grasps across object categories with high DoF hands. In this paper we go beyond this, learning and generalising grasps for under-actuated hands.

Several hands with such behavior have been proposed in the literature with different implementations [7], [8], with a common goal: simplicity plus robustness. Their initial tests under human operation are promising, but autonomous grasping with underactuated hands faces challenges due to the almost non-observability of the finger deformation when the hand is constrained by the environment and/or a target object. Most of the existing planning algorithms for this type of hands boil down to generating good wrist poses and let the adaptive mechanism handle all variation and uncertainty while closing, such as [9], where a sequence of wrist and object poses and the corresponding interaction wrenches are generated, which are expected to exploit environmental constraints. Another approach is that by [11], where static wrist poses are sampled using different strategies around the object from where the fingers are closed using a rigid-body simulator, to finally select the areas of major success rate to generate new wrist poses.

While these approaches exploit, to some extent, the adaptive properties of the underactuated mechanism, they can be improved on. In this paper we show how we can, for the first time, learn grasps for underactuated hands that are then transferred to novel objects. This requires learning representations of the final grasp state that are amenable to transfer to new objects, grouping example grasps by the end grasp state, and learning and optimisation of reach-to-grasp trajectories.

II. OVERVIEW OF APPROACH

In our approach the main steps are as follows. A model of a training object is presented in a rigid body physics simulator. Then a number of example grasps are executed by a human, with the precise motions of hand and object during contact being determined by the simulation. Each example grasp continues until a final stable grasp state is reached. We call this the *equilibrium state*, consisting of the final hand shape, and the final set of contact relations between hand and object. For training and inference purposes each example grasp has two parts: an equilibrium state, and the reach to grasp trajectory leading to it.

We generate the example grasps in sets. Each set corresponds to a type of grasp, e.g. power or pinch. This means that the equilibrium states are similar within a set, but differ substantially between sets.

Models are then learned for each grasp and for each set. Models are learned of the reach to grasp, the hand configuration in the equilibrium state, and the contact relations between hand and object in the equilibrium state. Given these models, when a new object is presented, a (partial) model of that object is obtained by sensing. This model is combined with the models learned from the training grasps.

Then many candidate equilibrium states, and associated candidate reach to grasp trajectories are generated by sampling. Finally they are optimised so as to maximise the likelihood of the grasp according to a product of experts.

III. BASIC REPRESENTATIONS

We now sketch the representations underpinning our approach. We define several models: an object model (partial and acquired from sensing); a model of the contact between a finger link and the object; a model of the whole hand configuration; and a model of the reach to grasp trajectory. First we describe the kernel density representation for all these models. Then we describe the surface features we use to encode some of these models. Then we follow with a description of each model type. Throughout we assume that the robot's hand comprises N_L rigid *links*: a palm, and several phalanges or links. We denote the set of links $L = \{L_i\}$.

A. Kernel Density Estimation

$SO(3)$ denotes the group of rotations in three dimensions. A feature belongs to the space $SE(3) \times \mathbb{R}^2$, where $SE(3) = \mathbb{R}^3 \times SO(3)$ is the group of 3D *poses*, and surface descriptors are composed of two real numbers. We extensively use probability density functions (PDFs) defined on $SE(3) \times \mathbb{R}^2$. We represent these PDFs non-parametrically with a set of K features (or particles) x_j

$$S = \{x_j : x_j \in \mathbb{R}^3 \times SO(3) \times \mathbb{R}^2\}_{j \in [1, K]}. \quad (1)$$

The probability density in a region is determined by the local density of the particles in that region. The underlying PDF is created through *kernel density estimation* [12], by assigning a kernel function \mathcal{K} to each particle supporting the density, as

$$\text{pdf}(x) \simeq \sum_{j=1}^K w_j \mathcal{K}(x|x_j, \sigma), \quad (2)$$

where $\sigma \in \mathbb{R}^3$ is the kernel bandwidth and $w_j \in \mathbb{R}^+$ is a weight associated to x_j such that $\sum_j w_j = 1$. We use a kernel that factorises into three functions defined by the separation of x into $p \in \mathbb{R}^3$ for position, a quaternion $q \in SO(3)$ for orientation, and $r \in \mathbb{R}^2$ for the surface descriptor. Furthermore, let us denote by μ another feature, and its separation into position, orientation and a surface descriptor. Finally, we denote by σ a triplet of real numbers:

$$x = (p, q, r), \quad (3a)$$

$$\mu = (\mu_p, \mu_q, \mu_r), \quad (3b)$$

$$\sigma = (\sigma_p, \sigma_q, \sigma_r). \quad (3c)$$

We define our kernel as

$$\mathcal{K}(x|\mu, \sigma) = \mathcal{N}_3(p|\mu_p, \sigma_p) \Theta(q|\mu_q, \sigma_q) \mathcal{N}_2(r|\mu_r, \sigma_r) \quad (4)$$

where μ is the kernel mean point, σ is the kernel bandwidth, \mathcal{N}_n is an n -variate isotropic Gaussian kernel, and Θ corresponds to a pair of antipodal von Mises-Fisher distributions

which form a Gaussian-like distribution on $SO(3)$ [13], [14]. The value of Θ is given by

$$\Theta(q|\mu_q, \sigma_q) = C_4(\sigma_q) \frac{e^{\sigma_q \mu_q^T q} + e^{-\sigma_q \mu_q^T q}}{2} \quad (5)$$

where $C_4(\sigma_q)$ is a normalising constant, and $\mu_q^T q$ denotes the quaternion dot product.

Using this representation, conditional and marginal probabilities can easily be computed from Eq. (2). The marginal density $\text{pdf}(r)$ is computed as

$$\text{pdf}(r) \quad (6)$$

$$= \iint \sum_{j=1}^K w_j \mathcal{N}_3(p|p_i, \sigma_p) \Theta(q|q_i, \sigma_q) \mathcal{N}_2(r|r_i, \sigma_r) dp dq \quad (7)$$

$$= \sum_{j=1}^K w_j \mathcal{N}_2(r|r_j, \sigma_r), \quad (8)$$

where $x_j = (p_j, q_j, r_j)$. The conditional density $\text{pdf}(p, q|r)$ is given by

$$\begin{aligned} \text{pdf}(p, q|r) &= \frac{\text{pdf}(p, q, r)}{\text{pdf}(r)} \quad (9) \\ &= \frac{\sum_{j=1}^K w_j \mathcal{N}_2(r|r_j, \sigma_r) \mathcal{N}_3(p|p_j, \sigma_p) \Theta(q|q_j, \sigma_q)}{\sum_{j=1}^K w_j \mathcal{N}_2(r|r_j, \sigma_r)} \quad (10) \end{aligned}$$

B. Surface Features

All objects considered in the paper are represented by point clouds for the purpose of learning and testing. Test object models were constructed from a single view with a depth camera, and were thus incomplete⁵. We directly augment these points with a frame of reference and a surface feature that is a local curvature descriptor. For compactness, we also denote the pose of a feature as v . As a result,

$$x = (v, r), \quad v = (p, q). \quad (11)$$

The surface normal at p is computed from the nearest neighbours of p using a PCA-based method (e.g. [15]). The surface descriptors are the local *principal curvatures* [16]. Their directions are denoted $k_1, k_2 \in \mathbb{R}^3$, and the curvatures along k_1 and k_2 form a 2-dimensional feature vector $r = (r_1, r_2) \in \mathbb{R}^2$. The surface normal and the principal directions define the orientation q of a frame that is associated with the point p .

C. Object Model

Thus, given a point cloud, a set of K_O features $\{(v_j, r_j)\}$ can be computed. This set of features defines, in turn, a joint probability distribution, which we call the *object model*:

$$O(v, r) \equiv \text{pdf}^O(v, r) \simeq \sum_{j=1}^{K_O} w_j \mathcal{K}(v, r|x_j, \sigma_x) \quad (12)$$

where O is short for pdf^O , $x_j = (v_j, r_j)$, \mathcal{K} is defined in Eq. (4) with bandwidth $\sigma_x = (\sigma_v, \sigma_r)$, and where all

weights are equal, $w_j = 1/K_O$. In summary this object model O represents the object as a pdf over surface normals and curvatures.

IV. LEARNED MODELS

We now describe the representations for each of the three models that are learned from a set of grasp examples. We start with the contact model, proceed with the equilibrium state hand configuration model, and finish with the reach to grasp model.

A. Contact Model

A contact model M_i encodes the joint probability distribution of surface curvatures and of the 3D pose of the i^{th} hand link in the equilibrium state. Let us consider the hand as having grasped some given training object. The contact model for link L_i is denoted by

$$M_i(U, R) \equiv \text{pdf}_i^M(U, R) \quad (13)$$

where M_i is short for pdf_i^M , R is the random variable modelling surface curvature, and U models the pose of L_i relative to the frame of reference defined by the directions of principal curvature and the surface normal. In other words, denoting realisations of R and U by r and u , $M_i(u, r)$ is proportional to the probability of finding L_i at pose u relative to the frame of a nearby object surface patch that exhibits principal curvatures equal to r .

Given a set of features $\{x_j\}_{j=1}^{K_O}$, with $x_j = (v_j, r_j)$ and $v_j = (p_j, q_j)$, a contact model M_i is constructed from them. Features close to the link surface are more important than those lying far from the surface. Features are thus weighted, to make their influence on M_i decrease with their distance to the i^{th} link. We use a weighting function whose value decreases exponentially with the square distance to the link:

$$w_{ij} = \begin{cases} \exp(-\lambda \|p_j - a_{ij}\|^2) & \text{if } \|p_j - a_{ij}\| < \delta_i \\ 0 & \text{otherwise,} \end{cases} \quad (14)$$

where $\lambda \in \mathbb{R}^+$, there is a cut-off distance δ_i , and a_{ij} is the point on the surface of L_i that is closest to p_j . The intuitive motivation for this choice is that we require a weight function that falls off quickly so that the contact model will only take account of the local shape, while falling off smoothly.

Let us denote by $u_{ij} = (p_{ij}, q_{ij})$ the pose of L_i relative to the pose v_j of the j^{th} surface feature. In other words, u_{ij} is defined as

$$u_{ij} = v_j^{-1} \circ s_i, \quad (15)$$

where s_i denotes the pose of L_i , \circ denotes the pose composition operator, and v_j^{-1} is the inverse of v_j , with $v_j^{-1} = (-q_j^{-1} p_j, q_j^{-1})$ (see Fig. 2). The contact model is estimated as

$$M_i(u, r) \simeq \frac{1}{Z} \sum_{j=1}^{K_M} w_{ij} \mathcal{N}_3(p|p_{ij}, \sigma_p) \Theta(q|q_{ij}, \sigma_q) \mathcal{N}_2(r|r_j, \sigma_r) \quad (16)$$

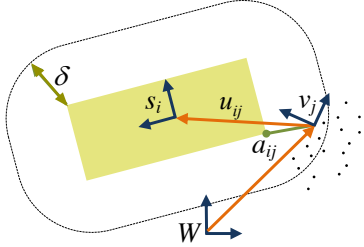


Fig. 2: Contact model. The figure shows the i -th link L_i (solid block) and its pose s_i . The black dots are samples of the surface of an object. The distance a_{ij} between a feature v_j and the closest point on the link's surface is shown. The rounded rectangle illustrates the cut-off distance δ_i . The poses v_j and s_i are expressed in the world frame W . The arrow u_{ij} is the pose of L_i relative to the frame for the surface feature v_j .

where Z is a normalising constant, $u = (p, q)$, and where $K_{M_i} \leq K_O$ is a number of features which are within cut-off distance δ_i to the surface of link L_i . If the number of features K_{M_i} of contact model M_i is not sufficiently large, contact model M_i is not instantiated and is excluded from any further computation. Consequently, the overall number of contact models N_M is usually smaller than the number of links N_L of the robotic hand. We denote the set of contact models learned from a grasp example g as $\mathcal{M}^g = \{\mathcal{M}_i^g\}$.

The parameters λ and $\sigma_p, \sigma_q, \sigma_r$ were chosen empirically. The time complexity for learning each contact model from an example grasp is $\Omega(TK_O)$ where T is the number of triangles in the tri-mesh describing the hand links, and K_O is the number of points in the object model.

B. Equilibrium State Hand Configuration Model

The equilibrium state hand configuration model, denoted $h_c^e(j) \in \mathbb{R}^D$, for the grasp examples $j = 1 \dots k$ within the set of k training examples of a particular grasp type g . The purpose of this model is to restrict the grasp search space (during grasp transfer) to hand configurations that resemble those observed during training. We combine the configurations for the examples $j = 1 \dots k$ to create a single mixture model density:

$$C^g(h_c^e) \equiv \sum_{j=1}^k \mathcal{N}_D(h_c^e | h_c^e(j), \sigma_{h_c^e}) \quad (17)$$

This expresses a density over hand configurations in the equilibrium state for a grasp type g .

C. Reach to Grasp Model

For a particular grasp type, in addition to modelling the equilibrium states of the hand, we must also model the trajectories taken to reach those equilibrium states. A single reach to grasp trajectory for an underactuated hand has three elements: the tool centre point (wrist) trajectory, the hand configuration trajectory, and the motor signal trajectory. We assume that a trajectory starts at time t_0 and ends in the

equilibrium state at time t_e . We denote the wrist trajectory $h_w^{0:e}$, the hand configuration trajectory $h_c^{0:e}$, and the motor signal trajectory $h_m^{0:e}$ respectively. The motor signal can be a wide variety of signals in practice. Here we choose it to be the position of the single actuator. When the hand is not in contact with an object the motor signal and the wrist pose together determine the hand configuration. When in contact, the actual hand configuration will differ. The reach to grasp model is simply the concatenation of each component $(h_w^{0:e}, h_c^{0:e}, h_m^{0:e})$. The set of reach to grasp trajectory models define an attractor basin, leading towards the final hand configuration.

In the next section we explain how we gather the grasp examples that are used to learn these models. Then in Section VI the inference method—by which the models are used to generate grasps for new objects—is described.

V. DATA GENERATION

There are several ways to implement underactuation in a dexterous hand. In this paper we employ an approach based on adaptive synergy transmission, due to its simplicity and robust design, and its ability for complex interaction with the environment. The Pisa/IIT SoftHand [7] implements such a transmission mechanism. This hand has 19 degrees of freedom (DoF) distributed over four fingers and an opposable thumb, but only 1 degree of actuation (DoA). The synergy motion of the hand in free space has been derived from databases of human hand postures. The overall behaviour parameters are the matrices that correspond to the transmission ratio, R , to the joint stiffness, K_q . The actuation is done through a single tendon routed through all joints, making the fingers flex and abduct.

Moving such a hand to grasp an object results in a hard-to-predict contact and hand shapes due to the adaptivity. We thus generate a variety of grasp examples to cover a portion of the interaction space. However, recording many trajectories of all the finger elements that affect the grasp in the real world is non-trivial. For this reason, we generate the example interactions for training using a rigid-body physics simulator, where these problems are avoided. The main two simulation elements we have developed are the contact stability model and the hand behavior model. In the case of the Pisa/IIT softhand, the latter depends heavily on the former. We used the standard distribution of Gazebo and Open Dynamic Engine, both in widespread use. The adaptive synergy equations have been implemented as a plugin to these, and accompany the proper kinematic description of the Pisa/IIT SoftHand¹.

At the current state, there are no generally accepted measures concerning whether a grasp by an underactuated hand is good or not, hence the lack of robust grasp planners for them is not a surprise. Thus, generating a large dataset at this point is useless, and there are plans in the future to cover this area. As a result, we generated the examples by

¹The Pisa/IIT SoftHand ROS/Gazebo packages are available at <https://github.com/CentroEPiaggio/pisa-iit-soft-hand>

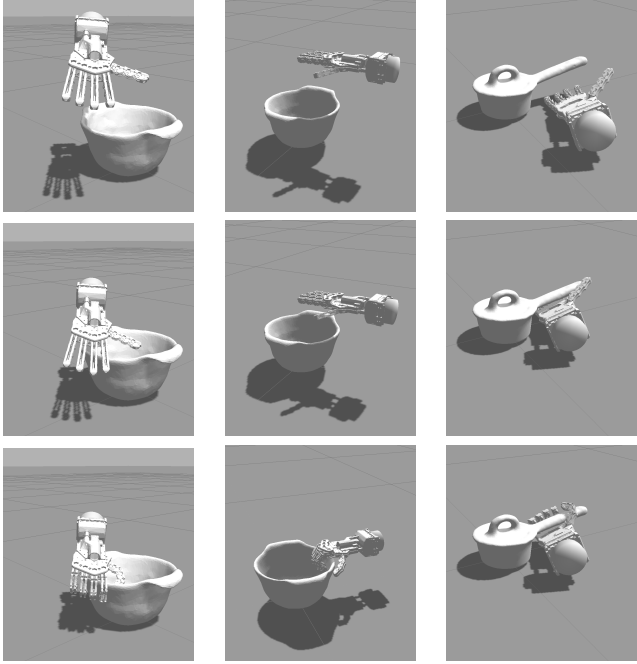


Fig. 3: Snapshots of the simulation of a pinch and rim grasp types for the colander (first and second columns), and handle grasp for the pot (last column).

guiding manually the hand to a “nice” grasp as shown in Fig. 3. In this simpler scenario, we assume without loss of generality that the grasps are labelled by type. In our example dataset, we have three grasp types namely pinch, rim and by-the-handle. The main difference between pinch and rim is the fingers configuration w.r.t. the top border of objects. In the pinch grasp, the thumb goes inside whereas in the rim grasp, the fingers go inside. In the latter, the container can be filled with liquid while holding, for instance. For each grasp example, the corresponding dataset comprises the set of trajectories as described in the previous section.

VI. INFERENCE

After acquiring the models from a set of training grasps, we present the robot with a test (query) object. The goal is to find a generalisation of the training grasp that is likely according to all of the model types simultaneously. First of all, we obtain a point cloud for the test object, and thus an object model. We then combine every contact model with that object model, so as to obtain a set of *query densities*, one for each link with a contact model defined for the example grasp. The i -th query density Q_i is a density modelling where the i -th link can be placed, in the equilibrium state, with respect to the surface of a new object.

From the query densities, a candidate equilibrium grasp state is generated. This is then augmented with a reach to grasp trajectory that finishes close to the candidate equilibrium grasp state. Finally we refine the equilibrium grasp and reach to grasp by performing a simulated annealing search in the space of equilibrium state wrist poses and

Algorithm 1: Pose sampling (M_i, O)

```

For samples  $j = 1$  to  $K_{Q_i}$ 
    Sample  $(\hat{v}_j, \hat{r}_j) \sim O(v, r)$ 
    Sample from conditional density  $(\hat{u}_{ij}) \sim M_i(u|\hat{r}_j)$ 
    Compute sample weight  $w_{ij} = M_i(\hat{r}_j)$ 
     $\hat{s}_{ij} = \hat{v}_j \circ \hat{u}_{ij}$ 
    separate  $\hat{s}_{ij}$  into position  $\hat{p}_{ij}$  and quaternion  $\hat{q}_{ij}$ 
return  $\{(\hat{p}_{ij}, \hat{q}_{ij}, w_{ij})\}, \forall j$ 
```

hand configurations, so as to maximise the grasp likelihood. We repeat the entire process many times. This procedure generates many possible grasps, ranked by likelihood. We give details below.

A. Query Density

A query density is, for a hand link and an object model, a density over the pose of that hand link relative to the object. Intuitively the query density encourages a finger link to make contact with the object at locations that have similar local surface curvature to that in the training example. Specifically, we use K_{Q_i} kernels centred on the set of weighted finger link poses:

$$Q_i(s) \simeq \sum_{j=1}^{K_{Q_i}} w_{ij} \mathcal{N}_3(p|\hat{p}_{ij}, \sigma_p) \Theta(q|\hat{q}_{ij}, \sigma_q) \quad (18)$$

with j -th kernel centre $(\hat{p}_{ij}, \hat{q}_{ij}) = \hat{s}_{ij}$, and weights are normalised $\sum_j w_{ij} = 1$. When a test object is presented, a set of query densities Q^g is calculated for the equilibrium state for each training grasp b for the grasp type g . The set $Q_b^g = \{Q_{b,i}^g\}$ has $N_Q^g = N_M^g$ members, one for each contact model M_i^g in \mathcal{M}^g . We estimate the query density using a Monte Carlo procedure detailed in Alg.1.

B. Equilibrium Grasp Generation

Once query densities have been created for the new object for each training example, an initial set of equilibrium state grasps is generated for each grasp type g . For each candidate equilibrium grasp of a particular grasp type we proceed as follows. First an example grasp is selected at random. Then a finger link is selected at random. This ‘seed’ link indexes its query density Q_i^g . A link pose s_i is then sampled from that query density. Then an equilibrium state hand configuration h_c^e is sampled from C^g . Together the seed link and the hand configuration define a complete equilibrium state hand pose h in the workspace via forward kinematics. This is an initial ‘seed’ grasp, which will subsequently be refined. A large set of such initial solutions is generated, where $h_e^g(j) = (h_w^e(j), h_c^e(j))$ means the j^{th} initial solution for grasp type g .

C. Reach to Grasp Generation

Given an equilibrium grasp, a reach to grasp trajectory is selected and adapted to maximise the chance of reaching that equilibrium grasp state. Specifically, we sample a reach to grasp model $(h_w^{0:e}, h_c^{0:e}, h_m^{0:e})$ according to a multinomial

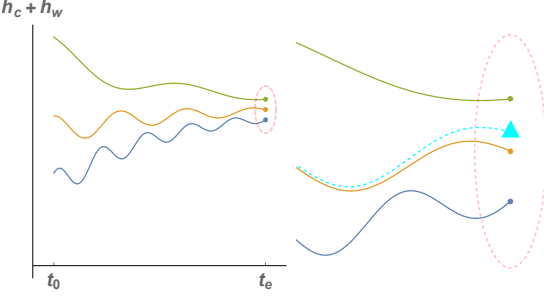


Fig. 4: (Left) We acquire set of reach to grasp trajectories that, associated with a model of the final equilibrium grasp state, form an attractor basin around that state. (Right) When an equilibrium state hand configuration is generated (triangle) a reach to grasp trajectory is sampled, and then the configuration component of the trajectory is smoothly interpolated between the selected reach to grasp and the generated equilibrium state grasp.

probability distribution created by the normalised values of a Gaussian centred on the candidate equilibrium grasp $h_e^g(j)$. To align the selected reach to grasp to the candidate equilibrium grasp, the wrist trajectory $h_w^{0:e}$ is trivially redefined to be relative to the frame $h_e^g(j)$. Then the configuration trajectory only $h_c^{0:e}$ is warped (see Fig. 4) so that it smoothly shifts from h_c^0 to $h_e^g(j)$ from the beginning to the end of the trajectory. Having generated an initial solution set \mathcal{H}^1 stages of optimisation and selection are then interleaved.

D. Grasp Optimisation

The objective of the grasp optimisation steps is, given a candidate equilibrium grasp and a reach to grasp model, to find a grasp that maximises the product of the likelihoods of the query densities and the hand configuration density

$$\operatorname{argmax}_{(h)} \mathcal{L}^g(h) \quad (19)$$

$$= \operatorname{argmax}_{(h)} \mathcal{L}_C^g(h) \mathcal{L}_Q^g(h) \quad (20)$$

$$= \operatorname{argmax}_{(h_w, h_c)} C^g(h_c) \prod_{Q_i^g \in \mathcal{Q}^g} Q_i^g(k_i^{\text{for}}(h_w, h_c)) \quad (21)$$

where $\mathcal{L}^g(h)$ is the overall likelihood, where $C^g(h_c)$ is the hand configuration model (17), Q_i^g are query densities (18). Thus whereas each initial grasp is generated using only a single query density, grasp optimisation requires evaluation of the grasp against all query densities. It is only in this improvement phase that all query densities must be used. Improvement is by simulated annealing (SA) [17]. The SA temperature T is declined linearly from T_1 to T_K over the K steps. In each time step, one step of simulated annealing is applied to every grasp m in \mathcal{H}^k .

E. Grasp Selection

At predetermined selection steps (here steps 1 and 50 of annealing), grasps are ranked and only the most likely 10% retained for further optimisation. During these selection steps

the criterion in (21) is augmented with an additional expert $W(h_w, h_c)$ penalising collisions for the entire reach to grasp trajectory in a soft manner. This soft collision expert has a cost that rises exponentially with the greatest degree of penetration through the object point cloud by any of the hand links. We thus refine Eq. 21:

$$\mathcal{L}^g(h) = \mathcal{L}_W^g(h) \mathcal{L}_C^g(h) \mathcal{L}_Q^g(h) \quad (22)$$

$$= W(h_w, h_c) C^g(h_c) \prod_{Q_i \in \mathcal{Q}^g} Q_i^g(k_i^{\text{for}}(h_w, h_c)) \quad (23)$$

where $\mathcal{L}^g(h)$ is now factorised into three parts, which evaluate the collision, hand configuration and query density experts, all at a given hand pose h . A final refinement of the selection criterion is due to the fact the number of links involved in a grasp varies across grasp types. Thus the number of query densities $N_Q^{g_1}, N_Q^{g_2}$ for different grasp models $g_1 \neq g_2$ also varies, and so the values of \mathcal{L}^{g_1} and \mathcal{L}^{g_2} cannot be compared directly. Given the grasp with the maximum number of involved links N_Q^{\max} , we therefore normalise the likelihood value (22) with

$$\|\mathcal{L}^g(h)\| = \mathcal{L}_W^g(h) \mathcal{L}_C^g(h) \left(\mathcal{L}_Q^g(h) \right)^{\frac{N_Q^{\max}}{N_Q^g}}. \quad (24)$$

It is this normalised likelihood $\|\mathcal{L}^g\|$ that is used to rank all the generated grasps across all the grasp types during selection steps. After simulated annealing has yielded a ranked list of optimised grasp poses, they are checked for reachability given other objects in the workspace, and unreachable poses are pruned.

F. Grasp Execution

The remaining best scoring hand pose h^* is then used to generate a reach to grasp trajectory. Since the hand is underactuated this consists of the wrist pose trajectory, and the motor signal trajectory. This is the command sequence that is executed on the robot.

VII. RESULTS

The experiments were conducted as follows. Training consisted of nine example grasps, executed in simulation, with a human in control. These nine grasps were grouped into three grasp types (rim, pinch, and handle). The rim and pinch grasp types were trained on the colander object, and the handle grasp type was demonstrated on the saucepan. During testing an object was placed on the table. Every grasp type was compared automatically, and one selected for execution according to the methods described above. The models of the test objects consisted of a point cloud taken from just one view. Thus reconstructions were partial, typically less than 25% of the object's surface area. No test objects had been seen previously by the robot, and it can be seen from Fig. 5. Fifteen test objects were presented, and 12 of the 15 test grasps succeeded, giving a generalisation success rate of 80%. While the difference is not statistically significant, this is slightly higher than the 77.7% success rate we recorded

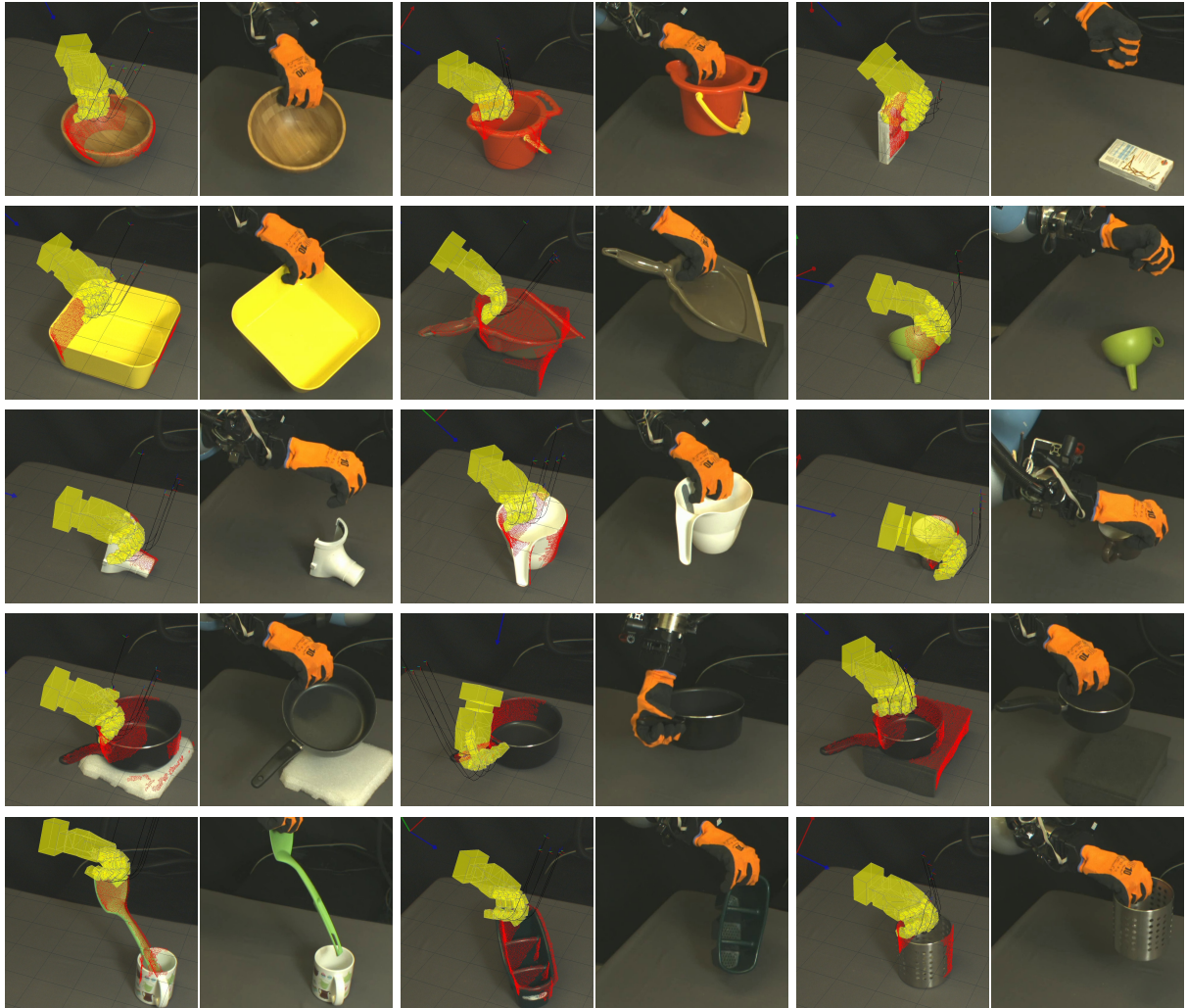


Fig. 6: The fifteen test grasps. Each one has a pair of images. The predicted equilibrium grasp state is shown on the left of each pair, and the actual grasp on the right. Counting from top left it can be seen that grasps 3,6, and 7 failed. All other grasps succeeded.



Fig. 5: The two training objects are on the far left. The testing objects on the right. 12 from 15 test grasps on novel objects were successful.

on a larger test set for a fully actuated hand also working from a single view of an object [18].

Finally, it is worth noting the similarity between the location of the actual and target final grasp states. In a majority of cases the grasp involved interactions with the object, moving it to the stable grasp pose. This is a natural property of the hand, but it might have been supposed that the learning method would not be robust to such interactions in terms of the accuracy of the grasp.

REFERENCES

- [1] A. Saxena, L. Wong, and A. Ng, “Learning grasp strategies with partial shape information,” in *Proceedings of AAAI*. AAAI, 2008, pp. 1491–1494.
- [2] R. Detry, C. H. Ek, M. Madry, and D. Kragic, “Learning a dictionary of prototypical grasp-predicting parts from grasping experience,” in *International Conference on Robotics and Automation*. IEEE, 2013, pp. 601–608.

- [3] A. Herzog, P. Pastor, M. Kalakrishnan, L. Righetti, J. Bohg, T. Asfour, and S. Schaal, "Learning of grasp selection based on shape-templates," *Autonomous Robots*, vol. 36, no. 1-2, pp. 51–65, 2014.
- [4] O. Kroemer, E. Ugur, E. Oztop, and J. Peters, "A kernel-based approach to direct action perception," in *IEEE International Conference on Robotics and Automation*. IEEE, 2012, pp. 2605–2610.
- [5] H. Ben Amor, O. Kroemer, U. Hillenbrand, G. Neumann, and J. Peters, "Generalization of human grasping for multi-fingered robot hands," in *International Conference on Intelligent Robots and Systems*. IEEE, 2012, pp. 2043–2050.
- [6] U. Hillenbrand and M. Roa, "Transferring functional grasps through contact warping and local replanning," in *IEEE/RSJ International Conference on Robotics and Systems*. IEEE, 2012, pp. 2963–2970.
- [7] M. G. Catalano, G. Grioli, E. Farnioli, A. Serio, C. Piazza, and A. Bicchi, "Adaptive synergies for the design and control of the Pisa/IIT SoftHand," *The International Journal of Robotics Research*, vol. 33, no. 5, pp. 768–782, 2014.
- [8] A. M. Dollar and R. D. Howe, "The highly adaptive SDM hand: Design and performance evaluation," *The International Journal of Robotics Research*, vol. 29, no. 5, pp. 585–597, 2010.
- [9] C. Eppner and O. Brock, "Planning grasp strategies that exploit environmental constraints," in *Proceedings of the IEEE International Conference on Robotics and Automation*, 2015.
- [10] M. Bonilla, E. Farnioli, C. Piazza, M. G. Catalano, G. Grioli, M. Garabini, M. Gabiccini, and A. Bicchi, "Grasping with soft hands," in *In Proceedings of the IEEE/RAS International Conference on Humanoid Robots*, 2014.
- [11] M. Bonilla, D. Resaco, M. Gabiccini, and A. Bicchi, "Grasp planning with soft hands using bounding box object decomposition," in *In Proceedings of the IEEE International Conference of Intelligent Robots and Systems*, 2015.
- [12] B. W. Silverman, *Density Estimation for Statistics and Data Analysis*. Chapman & Hall/CRC, 1986.
- [13] R. A. Fisher, "Dispersion on a sphere," in *Proc. Roy. Soc. London Ser. A.*, vol. 217, no. 1130. Royal Society, 1953, pp. 295–305.
- [14] E. B. Sudderth, "Graphical models for visual object recognition and tracking," Ph.D. dissertation, MIT, Cambridge, MA, 2006.
- [15] K. Kanatani, *Statistical optimization for geometric computation: theory and practice*. Courier Dover Publications, 2005.
- [16] M. Spivak, *A comprehensive introduction to differential geometry*. Publish or Perish Berkeley, 1999, vol. 1.
- [17] S. Kirkpatrick, C. D. Gelatt, and M. P. Vecchi, "Optimization by simulated annealing," *Science*, vol. 220, no. 4598, pp. 671–680, 1983.
- [18] M. Kopicki, R. Detry, M. Adjigble, A. Leonardis, and J. L. Wyatt, "One shot learning and generation of dexterous grasps for novel objects," *International Journal of Robotics Research*, 2015.

A.4 Article: Data-Driven Human Grasp Movement Analysis

Authors H. Marino, M. Gabiccini, A. Leonardis, and A. Bicchi

Info Submitted to: [update this and the attached PDF!](#)

Abstract The description of human hand motions is very complex, and methods to reduce this complexity have attracted much attention in the motor control literature. Important implications in robot hand design and programming have also generated a wide interest in the robotics research community. Early studies prevalently used direct analysis methods such as visual inspection to define grasp taxonomies. More recently, analytical methods have been employed to perform grasping data dimensionality reduction. In this paper, we present a methodology to reconcile these two distinct and apparently incompatible approaches under a unified framework: this allows us to obtain a data-generated grasp taxonomy along with low-dimensional representations which could be used for human grasping data classification and posture reconstruction, as well as for simplifying grasp planning algorithms and robotic hands programming.

Relation with the deliverable this work is concerned with the problem of finding a principled way of analyzing human grasping motion in order to obtain guidelines for the design of hand underactuation mechanisms based on specific tasks to be accomplished.

Attachment (following pages until next annex)

Data-Driven Human Grasp Movement Analysis

Hamal Marino, Marco Gabiccini, Aleš Leonardis, and Antonio Bicchi

Abstract—The description of human hand motions is very complex, and methods to reduce this complexity have attracted much attention in the motor control literature. Important implications in robot hand design and programming have also generated a wide interest in the robotics research community. Early studies prevalently used direct analysis methods such as visual inspection to define grasp taxonomies. More recently, analytical methods have been employed to perform grasping data dimensionality reduction. In this paper, we present a methodology to reconcile these two distinct and apparently incompatible approaches under a unified framework: this allows us to obtain a data-generated grasp taxonomy along with low-dimensional representations which could be used for human grasping data classification and posture reconstruction, as well as for simplifying grasp planning algorithms and robotic hands programming.

Keywords: Human Grasp Movement; Grasp Taxonomy; Posture Reconstruction; Multiple Eigenspaces

I. INTRODUCTION

In the past 60 years, attempts made towards the generation of a grasp taxonomy (such as [1] in the 50s and [2] in the 80s) have mostly relied on direct visual inspection. Still recently (see e.g. [3] and [4]), the most successful approaches to classify human grasping postures and movements apply the same method.

On an apparently separate side, a large number of models and techniques for dimensionality reduction have lately been applied to postural and grasping data. Santello et al. [5] asked subjects to grasp a large number of imagined objects and used Principal Component Analysis (PCA, [6]) to extract the so called *postural synergies*; the more recent work from Vinjamuri and co-workers [7], [8] extended the concept to *temporal* and *kinematic* postural synergies; Thakur et al. [9] analyzed hand posture data obtained from a motion capture system during an unconstrained haptic exploration task still applying the same technique, which to date remains the most

This work is supported by the European commission project PaCMan EU FP7-ICT, 600918.

H. Marino is with the Dep. of Advanced Robotics, Istituto Italiano di Tecnologia, via Morego, 30, 16163 Genova, and with the Res. Center “E. Piaggio”, University of Pisa, 56122 Pisa, Italy (hamal.marino@centripiaggio.unipi.it)

M. Gabiccini is with the DICI and Res. Center “E. Piaggio” University of Pisa, 56122 Pisa, Italy, and with the Dep. of Advanced Robotics, Istituto Italiano di Tecnologia, via Morego, 30, 16163 Genova (phone: +39-050-221.80.77, fax: +39-050-221.80.65, email: m.gabiccini@ing.unipi.it)

A. Leonardis is with The University of Birmingham, School of Computer Science and Centre for Computational Neuroscience and Cognitive Robotics, Edgbaston, Birmingham B15 2TT, United Kingdom (email: a.leonardis@cs.bham.ac.uk)

A. Bicchi is with the Dep. of Advanced Robotics, Istituto Italiano di Tecnologia, via Morego, 30, 16163 Genova, and with the Res. Center “E. Piaggio”, University of Pisa, 56122 Pisa, Italy (email: antonio.bicchi@iit.it)

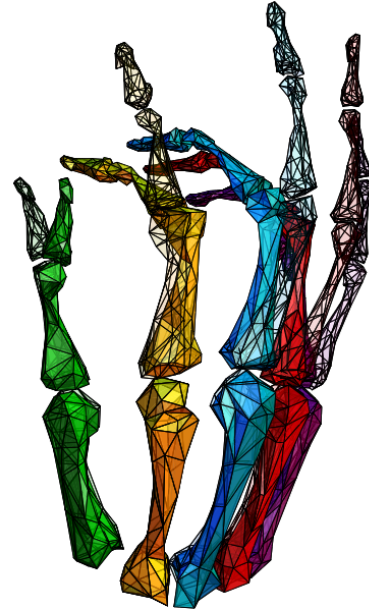


Fig. 1: An example of a 1-dimensional linear space in hand posture space obtained using the kinematic model from [20] and the technique from [21] adapted for postural data analysis. Subject ED, spherical grasp movement.

largely used; this type of reduction was then exploited in many areas, from robotic hands programming (see e.g. [10]), sensing (see e.g. [11] and [12]), and building of simpler, underactuated hands (e.g. [13] and [14]).

Other types of dimensionality reductions have been used too: e.g., Bernardin et al. [15] approached the problem of fusing data glove and tactile sensor information applying an Hidden Markov Model (HMM, [16]) recognizer to distinguish among different grasp types; the same technique was used by Ekvall et al. [17] to recognize grasp types based on entire grasping timeseries; on different data types, Jenkins et al. [18] extended the concept of ISOMaps to spatio-temporal ISOMaps in order to approach more general human data analysis; Peternel and Leonardis [19] showed that even movements as complex as human locomotion can be modeled by a small number of Degrees of Freedom (DoFs), i.e. 15 Gaussian Mixture Model (GMM) in 4-D space.

All these automatic techniques have been applied to show that there is an underlying structure in the way humans perform any action, in particular grasping, which seems to be an apparently irreconcilable topic with respect to the generation of a grasp taxonomy.

Some attempts at automating the procedure of data segmentation have been made in the last decade (e.g., [22], [23]), and even very recently (see [24]): still they start by performing dimensionality reduction on the full dataset, and then look for a valid segmentation in the reduced dimensional space which is, indeed, affected by the population employed. Specifically, [24] uses functional PCA (fPCA, [25]) to analyze grasping motions which are first projected over 3 PCs, and then each PC is decomposed along 2 fPCs to obtain movement 6-D representations: the grasping movements, generated on instruction from a subset of Cutkosky's grasp taxonomy, are then clustered using K-means (see [26]) into a new grasp taxonomy.

This work aims to find a systematic, data-driven way to explain grasp taxonomy from generic grasping data, which could then be used for automatic movement classification, hand-posture database indexing (see e.g. the DB at [27]), and as a way of reducing grasp planning algorithms and robotic hands programming complexity, moving towards the unification of human grasp movement analysis and robotic grasp synthesis procedures.

Although global dimensionality reduction techniques are well-suited for building simpler, underactuated robotic hands and to more easily program fully actuated hands, different approaches can be exploited which can benefit from the locally low-dimensional structure of the data to be used (see e.g. the work by Ciocarlie et al [10] on dexterous robotic grasping with a variety of hands, or [28] for a recent application of Programming by Demonstration, PbD [29]). A low number of DoFs is desirable for these methods, and a technique which automatically groups together similar movements could relieve the programmer from most of the pre-processing of a suitable dataset for the task at hand.

As a means to our goal, we borrow form computer vision the technique of Multiple Eigenspaces (originally from [21], see Section III), and adapt it to our data. The reason behind this choice is that Multiple Eigenspaces are a generalization of PCA, which can be viewed as a single eigenspace which tries to explain the whole dataset. Using more than one eigenspace the dataset is automatically clustered and, differently from other clustering techniques like K-means, each cluster can have a different dimension. Moreover, the used approach gives lower dimensional subspaces w.r.t. PCA, which means that they can be used for interpolation (the whole space is meaningful, which is not true when a single high order space is considered): we thus try not to neglect the low dimensional local structure of the data, which is instead usually ignored.

The paper is organized as follows: in Section II we report the data collection procedure for obtaining a test bed dataset, along with a brief explanation of the fully parameterized hand model we use to reconstruct the postures from those data; in Section III the technique of Multiple Eigenspaces is briefly recalled, with some advantages highlighted over global dimensionality reduction techniques, and a specializa-

tion of the algorithms for our type of data is illustrated; in Section IV we show qualitatively and quantitatively how our approach fits in between a taxonomy-generation problem and a human grasp movement dimensionality reduction problem for analysis and synthesis of grasping behaviors. Finally, conclusions and ongoing research are presented in Section V.

II. HAND MODEL DESCRIPTION AND POSTURAL DATA GATHERING

To test the algorithm which we will fully describe in the following Section, the grasping movement data are obtained from timed sequences of postural data constructed with the procedure described in [20]. In particular:

- a volunteer (*subject*) has his/her hand prepared with active markers (LEDs) placed on the skin;
- a motion capture system (Phase Space, San Leandro, CA - USA) is used to record the 3-D movement of the markers; the recording frequency is 480 Hz;
- upon timed intervals (every 12 sec), a random image from a set of possible objects is shown to the subject for 3 seconds (see Table I for a partial list of the objects used, or [5] for a full list of the 57 objects);
- as a correspondence to the experiment performed in [5], after each image disappears the subject is asked to perform the grasp as if the object just shown was in front of them.

1. Bucket	11. Hammer
2. Calculator	12. Ice cube
3. Chalk	13. Jar lid
4. Cherry	14. Light bulb
5. Computer mouse	15. Pen
6. Dinner plate	16. Rope
7. Espresso cup	17. Telephone handset
8. Fishing rod	18. Tennis racket
9. Frisbee	19. Toothpick
10. Hair dryer	20. Wrench

21 ÷ 57 ...

TABLE I: A partial list of objects used for data gathering.

The marker position data are then used to reconstruct joint movements of the subject via a fully parameterized 26 DoFs kinematic hand model which includes a mechanism to compensate for movements of the markers positioned close to joints due to movements of the skin relative to the bones (the so called “soft-tissue artifact”). The procedure, applied for computational time reasons to a version of the data downsampled to 15 Hz, goes as follows:

- a calibration phase estimates the geometric parameters of the specific subject hand to adapt the general model; these parameters are mainly bone lengths and position of the markers with respect to bones;
- keeping constant the calibration data, an identification with an Extended Kalman Filter is performed on the whole movement data.

From the 26 DoFs data, which includes also 2 wrist DoFs, only the remaining 24 “inner-hand” DoFs are considered. A visual example of how the model looks like when a posture is reconstructed is shown in Fig. 1, which represents the extrema of a 1-DoF movement in joint space reconstructed using the procedure highlighted in Sec. III.

To reduce the computational burden of the following analyses, only 20 frames of each interval, which contain in full the grasping movement, are considered. No other pre-processing is performed.

Data from two subjects (ED and VB, both right handed and unimpaired, between 20 and 30 years old), each performing the full experiment twice, have been used: the full dataset for each subject contains twice the full experiment consisting of 57 grasping movements, lasting 20 frames, i.e. $2 \times 57 \times 20 = 2280$ datapoints.

III. MULTIPLE EIGENSPACES TECHNIQUE

In order to proceed towards our goal of finding a data-driven way to explain grasp taxonomy, we decide to use the technique of Multiple Eigenspaces [21].

The word *Eigenspace* stands for a representation of a subset of the data which consists of a mean datapoint and a certain number of linear directions, taken as the direction of maximum variance in the data: this number is called *dimension* of the eigenspace.

The problem of generating the eigenspaces is twofold, i.e. has to consider these two aspects:

- which datapoints belong together in the same eigenspace
- what should the dimension of each eigenspace be.

We will now illustrate the original technique as proposed in [21], along with its advantages over more classical approaches, and necessary modifications which have been applied to the algorithm to work with our different type of data.

A. Original Algorithm

In [21] the procedure of generating multiple eigenspaces is structured as follows:

- generate a large number of *seeds* with a certain amount of datapoints (DP’s) in the dataset (Sec. III-A.1)
- apply a cyclical growing procedure
 - grow them independently of each other (Sec. III-A.2.a)
 - prune the eigenspaces using a selection procedure (Sec. III-A.2.b)

which terminates when no eigenspace can further be grown.

1) *Seeds generation*: Seeds, which are the initial stage of the eigenspaces, are generated from the dataset with a proximity criterion, to have a good set of seeds, based on spatial or temporal proximity in the acquisition: once the initial scope of the seeds has been chosen (being the scope the number of DP’s in the eigenspace), corresponding DP’s are incorporated in an eigenspace which, at the beginning, simply represents their mean value (i.e., has dimension zero).

Notice that the scope has to be chosen small enough to let the seeds be free to evolve in the best possible direction as dictated by the data. Notation: in the following, the j -th eigenspace at stage t will be denoted by E_j^t , thus the seeds are denoted by E_j^0 .

2) *Eigenspace cyclical formation*: The eigenspaces are then obtained with a cyclical procedure, which terminates when they cannot be further grown.

a) *Eigenspace independent growing*: Each eigenspace is independently grown inserting the DP’s which are more closely related to it, sorted considering their reconstruction error δ . The δ_{ij}^t error of the i -th DP w.r.t. eigenspace j at stage t is simply the norm of the distance between the DP \mathbf{x}_i and its reconstruction $\hat{\mathbf{x}}_{ij}^t$ obtained in E_j^t

$$\delta_{ij}^t = \|\mathbf{x}_i - \hat{\mathbf{x}}_{ij}^t\| \quad (1)$$

where the reconstruction $\hat{\mathbf{x}}_{ij}^t$ is the projection of \mathbf{x}_i onto the eigenspace.

An allowable error level σ (see Table II), has to be chosen depending on the data at hand (i.e., what we consider to be an average level of error in a group of DP’s). The δ error has thus to be below a pre-specified threshold δ_{th} to avoid inserting in the eigenspace DP’s which are too far from it, still trying to expand the scope; a value of $\delta_{\text{th}} = 2.0\sigma$ is used.

At every iteration, the maximum number of DP’s allowed to enter an eigenspace is equal to its scope. If for an eigenspace there are no DP’s which respect the threshold on δ error, the growing of that eigenspace is terminated.

When a certain set of DP’s is considered compatible with an eigenspace (based on δ error), it is temporarily included in E_j^{t+1} , and the overall reconstruction error ρ is computed

$$(\rho_j^t)^2 = \frac{1}{\#E_j^t} \sum_{\mathbf{x}_i \in E_j^t} (\delta_{ij}^t)^2, \quad (2)$$

where the symbol $\#$ means the number of postures in E_j^t , i.e. its scope.

This error is used to decide whether an eigenspace is expanding correctly, and when it would be useful to increase its dimension; this is achieved using two thresholds $\rho_{\text{th1}} \leq \rho_{\text{th2}}$ (chosen as in Table II) and the following procedure:

- if the eigenspace E_j^{t+1} is already a good representation for the postures in it, i.e. $\rho_j^{t+1} < \rho_{\text{th2}}$, accept the eigenspace and make the inclusion permanent

- otherwise try increasing the dimension of E_j^{t+1} by one (generating \hat{E}_j^{t+1}) and compute again its error $\hat{\rho}_j^{t+1}$
 - if the error of this new eigenspace is significantly reduced, i.e. $\hat{\rho}_j^{t+1} < \rho_{\text{th1}}$, accept this new eigenspace
 - otherwise discard the last set of inserted DP's, revert the eigenspace to its previous stage (assigning $\hat{E}_j^{t+1} = \hat{E}_j^t$) and stop growing it.

b) *Eigenspace selection:* The selection procedure is the step used to take some eigenspaces out during the cyclical growing, to make it computationally feasible. Which eigenspaces have to remain is decided based on a Minimum Description Length (MDL) principle considering the following cost function

$$F(\mathbf{h}) = \mathbf{h}^T C \mathbf{h} = \mathbf{h}^T \begin{bmatrix} c_{11} & \cdots & c_{1r} \\ \vdots & & \vdots \\ c_{r1} & \cdots & c_{rr} \end{bmatrix} \mathbf{h} \quad (3)$$

where each c_{jj} is the *saving* associated with leaving the eigenspace j in, and each c_{jk} is the *saving* associated to leaving in both eigenspaces j and k ; finally, \mathbf{h} is a vector whose i -th entry is 1 if E_i is included, 0 otherwise. Notice that, for the sake of readability, all superscript t are omitted in the following equations. c_{jj} have the structure

$$c_{jj} = K_0(\#E_j) - (K_1 d_j + K_2(\#E_j)d_j + K_3(\#E_j)\rho_j), \quad (4)$$

where d_j is the dimension of E_j , while K_0 , K_1 , K_2 , and K_3 are constant (see Table II). K_0 is related to the cost of encoding one DP in the absence of the eigenspace, and K_1 to the cost of encoding each eigendirection: these costs are considered to be equal, being all images in the original work of the same size, and will be kept equal as all postures have 24 DoFs. K_2 is the cost related to encoding the coefficients of each DP in the eigenspace, and is neglected as much smaller than the others. Finally, K_3 is related to the average cost due to the error, and is a parameter which have to be chosen appropriately. c_{jj} is thus simplified to

$$c_{jj} = K_0(\#E_j - d_j) - K_3(\#E_j)\rho_j. \quad (5)$$

Elements c_{jk} out of the diagonal are elements which are used to consider that savings only occur only once even when the DP's are inserted in more than one eigenspace.

$$c_{jk} = (\#E_{j \cap k})(-K_0 + K_3\rho_{jk}), \quad (6)$$

where $E_{j \cap k}$ represent the datapoint intersection of E_j and E_k , and ρ_{jk} is the maximal error of the DP's in $E_{j \cap k}$ w.r.t. E_j and E_k .

For the choice of these out-of-diagonal coefficients, the procedure work well when the overlaps of each DP are mainly pairwise (each DP is at most present in 2 eigenspaces), but does not generalize well for higher order overlaps.

The sub-optimal choice of \mathbf{h} is performed via greedy search, as the optimal cost (3) would require the solution of a binary search problem which is computationally unfeasible as soon as the number of eigenspaces exceeds few entries.

Parameters	Description	Value
σ	level of allowed error	N.A.
δ_{th}	threshold: allow a datapoint in	2.0σ
ρ_{th2}	threshold: request a dimension upgrade	$> 1.2\sigma$
ρ_{th1}	threshold: accept a dimension upgrade	$< 1.0\sigma$
K_3/K_0	relative cost of the reconstruction error	1.1

TABLE II: Parameters and their values in the original algorithm. Notice that the value of σ was chosen based on normalized image errors and is thus not meaningful for our analyses.

B. Advantages Over Global Techniques

Global dimensionality reduction techniques can generally be very effective in representing the data, but usually do not consider the locally low-dimensional structure of the data. Clustering methods such as K-means [26], on the other hand, force all clusters to have an a priori fixed dimension.

In terms of ability to explain the data, a global technique may give poor results, even if the error in reconstructing each DP is very low. As an example to illustrate this concept, we use in Fig. 2 a Figure from [5] for an example of a space (the first 2 PCs of hand postures) which is mainly meaningful only along two lower dimensional (1-D) subspaces.

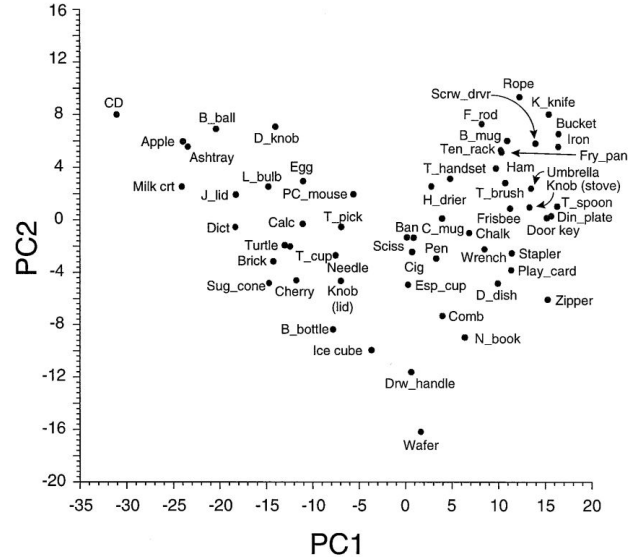


Fig. 2: Distribution of hand postures in the plane of the first two principal components. Note the distributions of the coefficients along two main axes. Reproduction from [5].

C. Modifications for Postural Data Analysis

The technique illustrated so far, although working well on images, does not give meaningful results when applied to postural data: the main reason for this is the fact that the selection procedure shown in Sec. III-A.2.b cannot handle high order overlaps, which happen rather frequently in human grasping data.

In order to overcome this issue, we include the following modifications:

- before the selection, include a *datapoint reduction* phase to avoid high order overlaps (Sec. III-C.1)
- change the coefficients c_{jk} because, from an MDL point of view, the cost of encoding the coefficients is in these data not negligible (Sec. III-C.2)
- at the end of the growing phase, increase the specificity of the eigenspaces performing an additional reduction step in order to keep each posture in no more than one eigenspace (Sec. III-C.3).

1) Datapoint reduction: After all eigenspaces have passed a stage of growing, a datapoint reduction procedure is performed to keep each posture in at most two eigenspaces. This is done keeping each posture in the two eigenspaces which best reconstruct it, i.e. selecting the two lowest δ errors amongst all possible ones across the various eigenspaces which include that posture. After reducing the datapoints in each eigenspace, if the dimension of the changed eigenspaces can be lowered still respecting error threshold, we do so. Again, this step serves as a preparation to the selection procedure (Sec. III-A.2.b), which can handle well pairwise overlaps, but suffers when much higher order overlaps exist.

2) New savings coefficients: Because the dimensionality of the data we use, the cost K_2 of encoding coefficients is not negligible. We thus use c_{jj} as in (4) and

$$c_{jk} = (\#E_j \cap k)(-K_0 + K_2 d_{jk} + K_3 \rho_{jk}), \quad (7)$$

with $K_2/K_0 = 1/24$ as one posture has 24 elements (see Table III).

Moreover, the choice of σ is related to the covariance of the dataset X used for generating the eigenspaces.

Parameters	Description	Value
σ	level of allowed error	$0.75 \sqrt{\ \text{Cov}(X)\ }$
K_2/K_0	cost of a coefficient	$1/24$

TABLE III: Parameters and their values in the modified algorithm. In this case, K_2 is not negligible, and σ is chosen based on the dataset covariance.

3) Final selection and unification: When the eigenspaces reach a steady state and, thus, the growing procedure terminates, we unify the eigenspaces, allowing each posture to belong to no more than one eigenspace: this step reduces the overlaps to zero.

Moreover, as we are interested in movements rather than just static posture classification, before performing this merging, we kill all the eigenspaces which have an order of zero (i.e., the postures in those are represented only by a mean value).

IV. RESULTS

The technique described in the previous Section has then been applied to each subject dataset obtained as explained in Section II.

A. Qualitative results: Grasp taxonomy classification of eigenspaces

Eigenspaces resulting from this procedure have been directly inspected to assess their similarity to a classical grasp taxonomy entries. Most similar grasps from the taxonomy in [2] are as follows:

ED: medium wrap (see Figure 3), tripod, light tool (see Figure 4), thumb - 4 finger, sphere (see Figure 1);
VB: tripod, lateral pinch, medium wrap, thumb - 2 finger, large diameter, thumb-index, prismatic with adducted thumb, light tool (see the attached video for a graphic representation of these movements).

Given their similarity to entries in a classical grasp taxonomy and their inherent low-dimensional nature, eigenspaces are great candidates as basic components of robotic hands programming as in [10], human grasping sequence classification from noisy data as in [11], and low-dimensional grasp planning as in [30].

About Programming by Demonstration side, and especially w.r.t. [24] in which the authors reduce the dimensionality of a 14 DoFs hand movements first to 3 Principal Components and then to 6 functional PCs, our algorithm does not need any pre-processing nor extra clustering and is able to reduce 24 DoFs hand motions in few 1-D or 2-D simple linear spaces which could then be used as training sets for the robot.

Of course, fPCA is a more powerful tool compared to PCA and, thus, its application inside a Multiple Eigenspaces framework remains of interest for future work.

B. Quantitative results: Parallel with PCA

As the multiple eigenspaces algorithm here used is somehow a generalization of PCA, a fair comparison of the results is with the application of simple PCA. A number of 5 or 7 Principal Components is used when employing PCA in order to show results which are of a comparable order w.r.t. the results of this work. An analogous comparison could be done with a different number of PCs, and would give expected results, which are thus not reported for the sake of space.

In Table IV, a comparison of explained variance across the postures included in each eigenspace are reported. The first columns indicates the subject to whom the data belong, then the second column says whether we consider a PCA or an eigenspace, and the third column shows the number of PCs (or eigenspace dimension). Fourth and fifth columns are, respectively, number of postures and explained variance, in



Fig. 3: Subject ED: medium wrap grasping; hand closing from left to right.



Fig. 4: Subject ED: light tool grasping; hand closing from left to right.

percentage over total variance, of the corresponding dataset. Finally, last column, inserted for completeness, displays how many PCs coming from a PCA on the full dataset would be needed to explain the same amount of percentage variance on all the postures: notice that this measure can be misleading, as averaging effects can take place when considering a dataset which is much broader than the ones of each eigenspace.

A fairer comparison can be made using reconstruction error (δ error) of each posture. In Figure 5, histograms of δ error using, from left to right, multiple eigenspaces, 5 PCs, and 7 PCs respectively, are shown. It is possible to see that, using multiple eigenspaces, the amount of postures reconstructed with an error up to 0.5 is similar to a PCA in which 5 PCs are considered. Using more PCs obviously leads to better results about reconstruction. Still, interpretation is a total different matter. Also notice that, in the first of these images, there are no postures with a δ error as high as in the other two, and this is because datapoints with such a high error, if any, get automatically discarded by the procedure.

V. CONCLUSIONS AND FUTURE WORK

In this work, the problem of conciliating direct, data-driven human grasp movement analysis towards classification and taxonomy generation, and analytical analysis for obtaining low-dimensional representation of grasping data has been considered.

To do this, the algorithm of Multiple Eigenspaces from [21] has been adapted and applied to a dataset of imagined grasping movements obtained following the procedure from

Subject(s)		dim.	# postures	variance	# of corr. PCs
VB + ED	PCA	5	4560	75%	-
VB + ED	PCA	7	4560	84%	-
VB	E_1	1	191	66%	4
VB	E_2	1	293	67%	4
VB	E_3	1	243	57%	3
VB	E_4	1	369	58%	3
VB	E_5	1	166	63%	3
VB	E_6	1	373	63%	3
VB	E_7	1	307	66%	4
VB	E_8	1	129	79%	6
ED	E_1	1	287	70%	5
ED	E_2	2	1302	60%	3
ED	E_3	1	236	61%	3
ED	E_4	1	210	40%	1
ED	E_5	1	182	44%	2

TABLE IV: Comparison of percentage explained variance values using PCA or Multiple Eigenspaces. PCA is performed on the whole dataset, while eigenspaces are generated on separate subjects as they become clustered from the very beginning. Number of Principal Components (PCs) used, or dimension of the eigenspace, are shown, along with number of datapoints included and percentage of total variance in the data explained. In the last column, the corresponding number of PCs required to explain the same amount of total variance across the whole dataset is reported.

[20]. Noteworthy, grasping movements analogous to classical grasp taxonomy entries (from, e.g., [2]) are automatically found from the data, as shown in Figures 1, 3, and 4, and in the video attachment.

The presented procedure builds in the direction of increasingly automating classification of movements, and using its

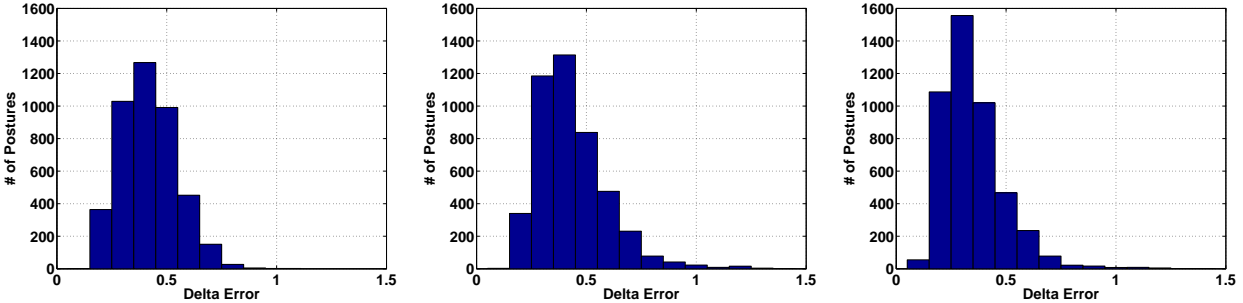


Fig. 5: Histograms of delta error across datapoints. From left to right: delta error obtained with a Multiple Eigenspace representation; delta error with 5 PCs from PCA; again PCA, taking into account 7 PCs. Notice that the total of postures in the first (left-most) figure is lower than the other two, as only postures represented by the selected eigenspaces are considered.

results for speeding-up grasp planning algorithms (given the great advantages of searching in more than one smaller spaces w.r.t. a single, higher dimensional space - see e.g. [30] for an example of grasp planning with 1-DoF motion), for Programming by Demonstration dataset generation, for human grasping movement classification, and for data-driven posture database indexing.

Ongoing research involves the implementation of the automatically generated taxonomy-like grasping movements in a grasp planner to control a fully actuated robotic hand. Moreover, future work also includes the idea of using Multiple Eigenspaces procedure, which is based on PCA, building upon more complex (maybe nonlinear) dimensionality reduction techniques, finding a principled way to change error thresholds in order to deal with different levels in the grasp taxonomy hierarchy, and using parabolic mirrors in order to make the imagined grasp experience closer to reality by having the object to be grasped shown exactly where it should be.

REFERENCES

- [1] J. R. Napier, “The prehensile movements of the human hand,” *Journal of bone and Joint surgery*, vol. 38, no. 4, pp. 902–913, 1956.
- [2] M. Cutkosky, “On grasp choice, grasp models, and the design of hands for manufacturing tasks,” *Robotics and Automation, IEEE Transactions on*, vol. 5, no. 3, pp. 269–279, 1989.
- [3] I. Bullock, R. Ma, and A. Dollar, “A hand-centric classification of human and robot dexterous manipulation,” *Haptics, IEEE Transactions on*, vol. 6, no. 2, pp. 129–144, 2013.
- [4] I. Bullock, J. Zheng, S. De La Rosa, C. Guertler, and A. Dollar, “Grasp frequency and usage in daily household and machine shop tasks,” *Haptics, IEEE Transactions on*, vol. 6, no. 3, pp. 296–308, 2013.
- [5] M. Santello, M. Flanders, and J. F. Soechting, “Postural hand synergies for tool use,” *The Journal of Neuroscience*, vol. 18, no. 23, pp. 10 105–10 115, 1998.
- [6] I. Jolliffe, “Principal component analysis and factor analysis,” *Principal Component Analysis*, pp. 150–166, 2002.
- [7] R. Vinjamuri, M. Sun, C.-C. Chang, H.-N. Lee, R. J. Scabassi, and Z.-H. Mao, “Temporal postural synergies of the hand in rapid grasping tasks,” *Information Technology in Biomedicine, IEEE Transactions on*, vol. 14, no. 4, pp. 986–994, 2010.
- [8] ———, “Dimensionality reduction in control and coordination of the human hand,” *Biomedical Engineering, IEEE Transactions on*, vol. 57, no. 2, pp. 284–295, 2010.
- [9] P. H. Thakur, A. J. Bastian, and S. S. Hsiao, “Multidigit movement synergies of the human hand in an unconstrained haptic exploration task,” *The Journal of neuroscience*, vol. 28, no. 6, pp. 1271–1281, 2008.
- [10] M. T. Ciocarlie and P. K. Allen, “Hand posture subspaces for dexterous robotic grasping,” *The International Journal of Robotics Research*, vol. 28, no. 7, pp. 851–867, 2009.
- [11] M. Bianchi, P. Salaris, and A. Bicchi, “Synergy-based hand pose sensing: Reconstruction enhancement,” *The International Journal of Robotics Research*, p. 0278364912474078, 2013.
- [12] ———, “Synergy-based hand pose sensing: Optimal glove design,” *The International Journal of Robotics Research*, vol. 32, no. 4, pp. 407–424, 2013.
- [13] C. Y. Brown and H. H. Asada, “Inter-finger coordination and postural synergies in robot hands via mechanical implementation of principal components analysis,” in *Intelligent Robots and Systems, 2007. IROS 2007. IEEE/RSJ International Conference on*. IEEE, 2007, pp. 2877–2882.
- [14] M. G. Catalano, G. Grioli, E. Farnioli, A. Serio, C. Piazza, and A. Bicchi, “Adaptive synergies for the design and control of the pisal/it softhand,” *The International Journal of Robotics Research*, vol. 33, no. 5, pp. 768–782, 2014.
- [15] K. Bernardin, K. Ogawara, K. Ikeuchi, and R. Dillmann, “A hidden markov model based sensor fusion approach for recognizing continuous human grasping sequences,” in *Proc. 3rd IEEE International Conference on Humanoid Robots*, 2003, pp. 1–13.
- [16] L. R. Rabiner, “A tutorial on hidden markov models and selected applications in speech recognition,” *Proceedings of the IEEE*, vol. 77, no. 2, pp. 257–286, 1989.
- [17] S. Ekwall and D. Kragic, “Grasp recognition for programming by demonstration,” in *Robotics and Automation, 2005. ICRA 2005. Proceedings of the 2005 IEEE International Conference on*. IEEE, 2005, pp. 748–753.
- [18] O. C. Jenkins and M. J. Mataric, “Deriving action and behavior primitives from human motion data,” in *Intelligent Robots and Systems, 2002. IEEE/RSJ International Conference on*, vol. 3. IEEE, 2002, pp. 2551–2556.
- [19] M. Peternel and A. Leonardis, “Visual learning and recognition of a probabilistic spatio-temporal model of cyclic human locomotion,” in *Pattern Recognition, 2004. ICPR 2004. Proceedings of the 17th International Conference on*, vol. 4. IEEE, 2004, pp. 146–149.

- [20] M. Gabiccini, G. Stillfried, H. Marino, and M. Bianchi, "A data-driven kinematic model of the human hand with soft-tissue artifact compensation mechanism for grasp synergy analysis," in *Intelligent Robots and Systems, 2013. Proceedings., 2013 IEEE/RSJ International Conference on*. IEEE, 2013.
- [21] A. Leonardis, H. Bischof, and J. Maver, "Multiple eigenspaces," *Pattern Recognition*, vol. 35, no. 11, pp. 2613–2627, 2002.
- [22] L. Y. Chang, N. S. Pollard, T. M. Mitchell, and E. P. Xing, "Feature selection for grasp recognition from optical markers," in *Intelligent Robots and Systems, 2007. IROS 2007. IEEE/RSJ International Conference on*. IEEE, 2007, pp. 2944–2950.
- [23] J. Barbić, A. Safanova, J.-Y. Pan, C. Faloutsos, J. K. Hodgins, and N. S. Pollard, "Segmenting motion capture data into distinct behaviors," in *Proceedings of Graphics Interface 2004*. Canadian Human-Computer Communications Society, 2004, pp. 185–194.
- [24] W. Dai, Y. Sun, and X. Qian, "Functional analysis of grasping motion," in *Intelligent Robots and Systems (IROS), 2013 IEEE/RSJ International Conference on*. IEEE, 2013, pp. 3507–3513.
- [25] J. O. Ramsay and B. W. Silverman, *Applied functional data analysis: methods and case studies*. Springer New York, 2002, vol. 77.
- [26] J. A. Hartigan, *Clustering algorithms*. John Wiley & Sons, Inc., 1975.
- [27] M. Bianchi and M. V. Liarokapis, "HandCorpus, a new open-access repository for sharing experimental data and results on human and artificial hands," in *IEEE World Haptics Conference (WHC)*, April 2013.
- [28] P. Kingston and M. Egerstedt, "Time and output warping of control systems: Comparing and imitating motions," *Automatica*, vol. 47, no. 8, pp. 1580–1588, 2011.
- [29] S. Calinon, "Robot programming by demonstration," in *Springer Handbook of Robotics*. Springer, 2008, pp. 1371–1394.
- [30] M. Bonilla, E. Farnioli, C. Piazza, M. Catalano, G. Grioli, M. Garabini, M. Gabiccini, and A. Bicchi, "Grasping with soft hands," in *Humanoids*, 2014.

A.5 Article: A computational framework for environment-aware robotic manipulation planning

Authors M. Gabiccini, A. Artoni, G. Pannocchia, J. Gillis

Info Published in: 17th International Symposium on Robotics Research (ISRR), Sestri Levante (Genova), Italy, September 12-15, 2015

Abstract In this paper, we present a computational framework for direct trajectory optimization of general manipulation systems with unspecified contact sequences, exploiting *environmental constraints* as a key tool to accomplish a task. Two approaches are presented to describe the dynamics of systems with contacts, which are based on a penalty formulation and on a velocity-based time-stepping scheme, respectively. In both cases, object and environment contact forces are included among the free optimization variables, and they are rendered consistent via suitably devised sets of complementarity conditions. To maximize computational efficiency, we exploit sparsity patterns in the linear algebra expressions generated during the solution of the optimization problem and leverage Algorithmic Differentiation to calculate derivatives. The benefits of the proposed methods are evaluated in three simulated planar manipulation tasks, where essential interactions with environmental constraints are automatically synthesized and opportunistically exploited.

Relation with the deliverable grasp and manipulation planning for systems with a-priori unspecified contact sequences.

Attachment (following pages until next annex)

A Computational Framework for Environment-Aware Robotic Manipulation Planning

Marco Gabiccini, Alessio Artoni, Gabriele Pannocchia and Joris Gillis

Abstract In this paper, we present a computational framework for direct trajectory optimization of general manipulation systems with unspecified contact sequences, exploiting *environmental constraints* as a key tool to accomplish a task. Two approaches are presented to describe the dynamics of systems with contacts, which are based on a penalty formulation and on a velocity-based time-stepping scheme, respectively. In both cases, object and environment contact forces are included among the free optimization variables, and they are rendered consistent via suitably devised sets of complementarity conditions. To maximize computational efficiency, we exploit sparsity patterns in the linear algebra expressions generated during the solution of the optimization problem and leverage Algorithmic Differentiation to calculate derivatives. The benefits of the proposed methods are evaluated in three simulated planar manipulation tasks, where essential interactions with environmental constraints are automatically synthesized and opportunistically exploited.

1 INTRODUCTION

Careful observation of how humans use their hands in grasping and manipulation tasks clearly suggests that their limbs extensively engage functional interactions with parts of the environment. The physical constraints imposed by the manipulandum and the environment are not regarded as obstacles, but rather as opportunities to guide functional hand pre-shaping, adaptive grasping, and affordance-guided manipulation of objects. The exploitation of these opportunities, which can be referred to as *environmental constraints* (EC), enables robust grasping and manipulation in dynamic and highly variable environments. When one considers the exploitation of EC, i.e. when manipulation actions are performed *with the help* of the environment, the boundary between grasping and manipulation is blurred, and traditional categories such as grasp and manipulation analysis, trajectory planning and interaction control appear somewhat artificial, as the problem we aim to solve seems to inextricably entangle all of them.

In this paper, we set out to formulate environment-aware manipulation planning as a nonlinear optimal control problem and discretize it according to a *direct transcription* scheme [3]. In Sec. 3, two approaches to describe the dynamics of systems with contacts are proposed and evaluated:

M. Gabiccini, A. Artoni, G. Pannocchia
Department of Civil and Industrial Engineering, Univ. of Pisa, Italy.
e-mail: name.lastname@unipi.it

J. Gillis
Department of Electrical Engineering, KU Leuven, Belgium.
e-mail: joris.gillis@kuleuven.be

in the first one, continuous contact reaction forces are generated by nonlinear virtual springs, and the requirement to avoid sliding contacts is handled in an apparently original way; in the second one, contact collisions are approximated as impulsive events causing discontinuous jumps in the velocities according to a modified version of the Stewart-Trinkle time-stepping scheme [47]. The introduction of two different models is motivated by the relative ease for the first (second) one to enforce EC exploitation primitives that avoid (profitably exploit) sliding motions during interaction.

Both formulations lead to a nonlinear programming (NLP) problem (Sec. 4) that we solve by using the Interior-Point (IP) method implemented in IPOPT [4] and discussed in Sec. 5. To improve computational efficiency, we also annotate sparsity in the linear algebra expressions and leverage algorithmic differentiation (AD) [22] to calculate derivatives both quickly and accurately: the adoption of the CasADI framework [2], described in Sec. 5, provides a profitable interface to all the above tools with a consistent API.

In Sec. 6, we evaluate our approaches in three simulated planar manipulation tasks: (i) moving a circular object in the environment with two independent fingers, (ii) rotating a capsule with an underactuated two-fingered gripper, and (iii) rotating a circular object in hand with three independent fingers. Tasks (i) and (ii) show that our algorithm quickly converges to locally optimal solutions that opportunistically exploit EC. Task (iii) demonstrates that even dexterous fingertip gaits can be obtained as a special solution in the very same framework. Conclusions are drawn in Sec. 7.

It is worth noting that with our method, approach planning, grasping, manipulation, and environment constraint exploitation phases occur automatically and opportunistically for a wide range of tasks and object geometries, with no *a-priori* specification of the ordering of the different stages required.

2 RELATED WORK

2.1 Exploitation of Environmental Constraints

The concept of exploiting environmental constraints is well-rooted in robotics. Pioneering work was performed already in the eighties in the context of motion planning [33] and manipulation [34]. However, these concepts did not have the proper influence on many of the recent developments on either area, perhaps due to the inadequacy of the mechanical impedance properties of contemporary industrial manipulators to achieve sliding motion primitives stably, thus precluding the adoption of strategies that exploit environmental constraints, e.g. by sliding one object over another [10]. Also the idea of programming using environmental constraints is well entrenched in robotics literature, starting with the seminal work [1], proceeding with [44], and culminating in the *iTaSC* framework [46].

The exploitation of complex interactions with the environment in a manipulation task also plays a central role in automation and manufacturing to design fixtures [7] and part feeders [6]. However, these works are highly specialized and they are limited to the case of handling a single object geometry.

2.2 Traditional Grasp Planners

State-of-the-art general grasping algorithms and dexterous mechanical hands lie at the opposite end of the spectrum: they are designed to perform grasping and manipulation of a wide range of object geometries and for many different tasks. Traditional grasp planners (such as OpenRAVE [11] and GraspIt! [35]) rely on precise finger-to-object contact points while avoiding the

surrounding environment. In real-world scenarios these models, as well as the motion of the hand, will be highly uncertain leading to poor grasping performance for grasps that were deemed highly robust based on theoretical considerations.

The recent paper [5] has proposed a pipeline for automated grasp synthesis of common objects with a compliant hand by developing a full-fledged multi-body simulation of the whole grasping process in the presence of EC: however, to date, the approach seems time consuming and the sequence of primitive actions needed to perform complex tasks must be scripted in advance. Also recently, both grasp planning algorithms and grasping mechanisms have begun to take advantage of EC [13], albeit not systematically. While sequences of EC exploitation primitives have been shown to be robust and capable [9], [27], there has been no comprehensive research on how to enumerate and describe these primitives or how to sequence them into task-directed manipulation plans. A noteworthy exception where a sequence of task-directed manipulation plan exploiting EC is created and performed on-line with minimalistic sensory information and limited previous assumptions about the scene was recently presented in [15].

2.3 General Purpose Planning Algorithms

State-of-the-art sampling-based planning algorithms like RRT*[26] seem not tailored for situations where *a-priori* unknown contact interactions may cause a combinatorial explosion of system configurations. Recent extensions, initially presented in [19] for RRT, and successively devised for RRT* in [41], were able to cope with systems described by complex and underactuated dynamics. In [29], the authors presented an approach to moving an object with several manipulators. This problem presents some similarities to ours, since a sequence of phases has to be both planned and solved. The strong assumption that the plan called by the high-level scheduler will succeed — which is not always possible — has been removed in the recent contribution [8].

However, situations where intermittent contact sequences are not easily enumerated from the outset, but are key for the success of environment-aware manipulation plans, still appear to be out of their reach.

2.4 Machine Learning Approaches

Although significant progresses have been made in this area in recent years [28], learning robot motion skills still remains a major challenge, especially for systems with multiple intermittent contacts. Policy search is often the preferred method as it scales gracefully with system dimensionality, even if its successful applications typically rely on a compact representation that reduces the numbers of parameters to learn [30], [49], [42]. Innovative policy classes [24] have led to substantial improvements on real-world systems. However, designing the right low-dimensional representation often poses significant challenges. Learning a state representation that is consistent with physics and embeds prior knowledge about interactions with the physical world has recently been proposed in [25] and seems a promising venue to find effective methods to help improve generalization in reinforcement learning: however, the simulated robotic tasks solved by this methods are still far in complexity from environment-aware manipulation scenarios.

The recent contribution [31] developed a policy search algorithm which combines a sample-efficient method for learning linear-Gaussian controllers with the framework of guided policy search, which allows the use of multiple linear-Gaussian controllers to train a single nonlinear policy with any parametrization, including complex and high-dimensional policies represented by large neural networks. In [32], this method has been recently applied, with some modifications

that make it practical for deployment on a robotic platform, to solve contact-rich manipulation tasks with promising results.

2.5 Optimization-based Trajectory Planning

Various research groups are currently pursuing direct trajectory optimization to synthesize complex dynamic behaviors for systems with intermittent contacts. Those working in locomotion [45] mainly adopt a multi-stage hybrid-mode approach (usually employing multiple-shooting), where the optimization is constrained to operate within an *a priori* specification of the mode ordering. Interestingly, a recent contribution [52] explored the synthesis of optimal gaits for legged robots without the need to specify contact sequences. Certainly, the adoption of such an approach seems the only viable solution for a multi-fingered hand manipulating an object also by exploiting EC. Along this line, it is worth mentioning the contact-invariant approach originally proposed in [37] to discover complex behaviors for humanoid figures and extended to the context of manipulation in [36]. The previously described trajectory optimization method has been recently employed to gradually train a neural network by following an Alternating Direction Method of Multipliers (ADMM) strategy with interesting results [38].

The approach presented in [43] inspired our work and is the one which is definitely closest. However, remarkable differences in the formulation of the dynamics for systems with contacts, in the choice of the solution algorithm, solver and framework, and in the focus of the paper — here, EC exploitation is sought as a key factor — render our work significantly different.

3 DYNAMICS OF SYSTEMS WITH CONTACTS

3.1 Penalty-based contact model

To our eyes, manipulation planning has to rely on a dynamic model of the system, namely of manipulandum, manipulator, and the environment, and of their mutual interactions through contact. We consider here deterministic systems with continuous state and control spaces, denoted by x and u respectively. The dynamic evolution of our controlled (non-autonomous) system can be described in continuous time t by a set of Ordinary Differential Equations (ODEs):

$$\dot{x}(t) = F(x(t), u(t)) \quad \text{or} \quad \tilde{F}(\dot{x}(t), x(t), u(t)) = 0 \quad (1)$$

(explicit dependence on t is omitted hereafter). Together with an initial value $x(0) = x_0$, equation (1) defines an initial value problem. In general, additional algebraic dependencies may exist among \dot{x} , x and u leading to a dynamic system governed by differential-algebraic equations (DAEs). In the presence of contact, for instance, and if contact forces are included among the controls u , contact interactions establish functional dependencies between u and x through a set of algebraic equations/inequalities. As an example, if f_N is the normal contact force and $g_N = g_N(x)$ the normal gap (shortest distance) between a finger and the object being manipulated, the complementarity and non-negativity conditions $0 \leq f_N \perp g_N(x) \geq 0$ must hold. The contact model described in this section is based on a special treatment of the contact forces and the relative velocities that arise during interaction between manipulandum, manipulator, and environment. Such a model has proved to be successful in solving trajectory planning problems for manipulation tasks with *no sliding*, in the presence of EC.

For normal contact forces, the underlying idea is borrowed from classical penalty-based approaches, where contact interactions are modeled by spring-dampers. In our model, no damping is introduced, while a nonlinear exponential spring relates the normal contact force and the nor-

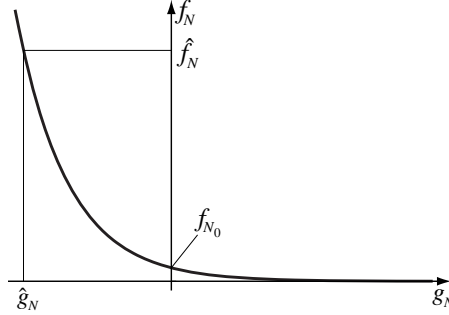


Fig. 1 Normal contact force as a function of the normal gap.

mal gap through the constitutive equation (Fig. 1)

$$f_N(g_N(x)) = f_{N_0} \left(\frac{\hat{f}_N}{f_{N_0}} \right)^{g_N(x)/\hat{g}_N} \quad (2)$$

where $g_N(x)$ is the normal gap function and \hat{g}_N the negative normal gap value (penetration) corresponding to the normal force value \hat{f}_N . The (fixed) parameters (\hat{f}_N, \hat{g}_N) provide a straightforward way to properly “calibrate” the model and adapt it to the problem at hand. Relation (2) is a relaxation of the above-stated complementarity condition: it avoids discontinuities while being sufficiently representative of physical reality. In order to describe (unilateral) contacts with friction, the classical Coulomb model is adopted. The focus is placed here on point-contact with *static* friction, whereby normal force f_N , tangential force f_T and the coefficient of static friction μ_s are related by the well known relation

$$f_T \leq \mu_s f_N \quad (3)$$

No-sliding conditions must be enforced by requiring that sliding velocities at contact points be zero. The normal gap $g_N(x)$ and the sliding velocity $\dot{g}_T(\dot{x}, x)$ (i.e., the time derivative of the tangential gap [51]) would call for an additional complementarity condition. We devised a smooth relaxation of this discontinuous condition through the *sliding velocity funnel* shown in Fig. 2 and described by:

$$\dot{g}_T^{(l)}(g_N) \leq \dot{g}_T \leq \dot{g}_T^{(u)}(g_N) \quad (4)$$

where the functions $\dot{g}_T^{(l)}(g_N)$ and $\dot{g}_T^{(u)}(g_N)$ are lower and upper bounds, respectively, for the sliding velocity. It is reasonable to have a symmetric funnel, hence $\dot{g}_T^{(l)}(g_N) = -\dot{g}_T^{(u)}(g_N)$. The bounds are modeled here as:

$$\dot{g}_T^{(u)}(g_N) = \exp(c_1(g_N + c_2)) + c_3 \quad (5)$$

where the three parameters (c_1, c_2, c_3) are used for proper, problem-dependent calibration. No-sliding manipulation planning benefits from this approach as the sliding velocity funnel smoothly and gradually guides the fingers towards the object, eventually driving relative velocities to (nearly) zero at their contact points. The trajectory planning methods employed in this work are based on numerical optimization techniques that require a discrete-time model of the dynamic system, therefore discrete-time versions of eqs. (1)–(4) are adopted in the following. In our implementation, the state vector $x_k = x(t_k)$ collects configuration and velocity of each body, while control vector $u_k = u(t_k)$ includes acceleration of each finger (or actuator) and contact forces at each candidate contact point. The dynamic equation (1) is used in a direct transcription scheme based on *collocation points*: using a single collocation point as midpoint in the interval $[t_k, t_{k+1}]$,

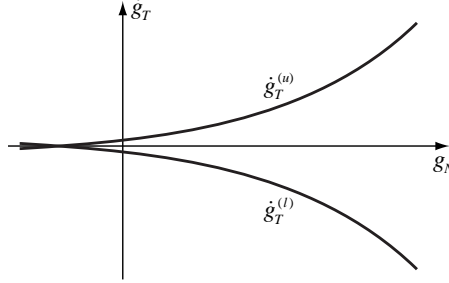


Fig. 2 Example of sliding velocity funnel.

and denoting $\bar{t}_k = (t_{k+1} + t_k)/2$, $\bar{x}_k = x(\bar{t}_k)$ and $h = t_{k+1} - t_k$ (fixed), the discretized dynamic equation becomes

$$x_{k+1} = x_k + hF(\bar{x}_k, u_k) \quad (6)$$

In the above implementation, states are linear and controls are constant over each discretization interval. The integration scheme (6) is known as implicit midpoint rule ($O(h^2)$), and it is the special one-point case of the Gauss-Legendre collocation method. As it is a symplectic integrator, it is suitable to cope with stiff, conservative mechanical systems. While eqs. (3)–(4) are straightforward to discretize, eq. (2) needs some attention: as it involves both states and controls, its discretization must adhere to the scheme dictated by eq. (6), to wit

$$f_{N_k} = f_N(g_N(\bar{x}_k)) = f_{N_0} \left(\frac{\hat{f}_N}{f_{N_0}} \right)^{g_N(\bar{x}_k)/\hat{g}_N} \quad (7)$$

Failing to do so (e.g., evaluating g_N at x_k) would result in a “causality violation”, with contact forces being inconsistent with the interpenetrations between bodies governed by (6).

3.2 Velocity-based time stepping scheme

In this section, we present the complementarity formulation of the time-stepping scheme employed for the dynamic modeling of manipulation systems exploiting *sliding over* EC. To keep the treatment general enough, we refer to a 3D system of m bodies with c contacts. We assume a polyhedral approximation of the friction cone, with d friction directions uniformly distributed to positively span the contact tangent plane¹. For ease of notation, we write $M_k = M(q_k)$ and likewise for other vector/matrix functions. Let h be again the time step, and let $\Delta v := v_{k+1} - v_k$. For $k \in \{0, \dots, N-1\}$, we adopt a Backward-Euler transcription scheme by writing the *kinematic reconstruction* and the *dynamic* equations as

$$q_{k+1} - q_k - h v_{k+1} = 0 \quad (8a)$$

$$M_{k+1} \Delta v - h [\kappa(q_{k+1}, v_k) + B_{k+1} u_{k+1}] - G_{k+1} \lambda_{k+1} = 0, \quad (8b)$$

where: $q \in \mathbb{R}^{6m}$ and $v \in \mathbb{R}^{6m}$ represent system configuration and velocity, respectively, $M \in \mathbb{R}^{6m \times 6m}$ is the generalized mass matrix, $\kappa \in \mathbb{R}^{6m}$ collects centrifugal, Coriolis and gravitational forces, $u \in \mathbb{R}^t$ is the control torque vector, $B \in \mathbb{R}^{6m \times t}$ is the actuation matrix, $G = [N \ T]$ is a

¹ For simplicity of description, we assume that the number of friction directions d is the same at each contact, although this is not necessary.

generalized grasp matrix, where $N \in \mathbb{R}^{6m \times c}$ and $T \in \mathbb{R}^{6m \times nd}$ are normal and tangential wrench bases, and $\lambda = [\lambda_N^\top \ \lambda_T^\top]^\top$ is the generalized wrench impulse vector, wherein λ_N and λ_T are the normal and tangential contact wrench impulses. Matrix N appears as $N = [N^{(1)} \dots N^{(c)}]$, and each column $N^{(i)} \in \mathbb{R}^{6m}$ corresponds to contact i and contains, for each body ℓ connected to contact i , a block of rows of the form $\pm[n_i^\top \ (p_{\ell,i} \times n_i)^\top]^\top$ ². Since there are at most two bodies connected to a contact, each $N^{(i)}$ has at most 12 non-zero elements. Similarly, $T = [T^{(1)} \dots T^{(c)}]$, and in the generic block $T^{(i)} \in \mathbb{R}^{6m \times d}$, each column $T^{(i,j)} \in \mathbb{R}^{6m}$ contains, for each body ℓ connected to contact i , a block of rows of the form $\pm[t_{i,j}^\top \ (p_{\ell,i} \times t_{i,j})^\top]^\top$, where $t_{i,j}$ denotes friction direction j at contact i . Opposite signs must be selected for each of the two bodies connected to contact i , and each column of T will contain, at most, 12 non-zero elements.

In partial accordance to [47], *unilateral* contacts with friction can be described by the following set of *inequality* and *complementarity* conditions

$$0 \leq \lambda_{N_{k+1}} \perp g_N(q_{k+1}) \geq 0 \quad (9a)$$

$$0 \leq \lambda_{T_{k+1}} \perp (\dot{g}_T(q_{k+1}, v_{k+1}) + E\gamma_{k+1}) \geq 0 \quad (9b)$$

$$0 \leq \gamma_{k+1} \perp [\mu \lambda_{N_{k+1}} - (\lambda_{T_{k+1}}^\top H \lambda_{T_{k+1}})^{\frac{1}{2}}] \geq 0, \quad (9c)$$

where $g_N(\cdot)$ is the normal gap function and $\dot{g}_T(\cdot)$ is the time derivative of the tangential gap function [51], γ represents, in most cases³, an approximation to the magnitude of the relative contact velocity, matrix $E := \text{BlockDiag}(\mathbf{1}, \dots, \mathbf{1}) \in \mathbb{R}^{(dc) \times c}$, with $\mathbf{1} \in \mathbb{R}^d$, $\mu \geq 0$ is the coefficient of friction, and $H := \text{BlockDiag}(H^{(1)}, \dots, H^{(c)})$, where the $H_{lm}^{(i)} = t_{i,l}^\top t_{i,m}$ ($l, m \in \{1, \dots, d\}$) is the metric form [12, Sec. 2-5] of the basis $t_{i,l}$ that positively spans the tangent plane at contact i . Eqs. (9a) state that bodies cannot interpenetrate ($g_N(q_{k+1}) \geq 0$), normal impulses can only push objects away ($\lambda_{N_{k+1}} \geq 0$), and that, in order for the impulse to be non-zero in the interval $[t_k, t_{k+1}]$, the normal gap must be closed at t_{k+1} . This condition also implies that collisions are approximated here as inelastic ones, and interacting bodies may end up sticking together. Eqs. (9b) require tangential impulses to be directed along the positive tangential directions ($\lambda_{T_{k+1}} \geq 0$). The complementarity condition in (9b) selects, for sliding contacts, the tangential impulse that opposes the sliding velocity. This constraint is tightly coupled with the complementarity condition in eqs. (9c), and it ensures that, if a contact is sliding, the tangential force will lie on the boundary of the friction cone. It is worth noting that the bracketed term in eq. (9c) allows one to correctly define the Coulomb friction constraints even in sticking conditions, as it is robust to the physiological failure of eq. (9b) in selecting only one non-zero component in each $\gamma_{k+1}^{(i)}$ for adhesive contacts⁴.

The choice of fully implicit integration schemes and nonlinear complementarity formulations, as described in Eqs. (8) and (9), can be justified in view of the increased numerical stability and modelling accuracy they bring about, while not hindering the general structure of the problem⁵.

² The positive/negative sign must be chosen if, considering equilibrium of body ℓ , the unit normal vector n_i is facing into/away from body ℓ .

³ In situations where the relative contact velocity and the friction vector are both zero, $\gamma \geq 0$ can be arbitrary and has no physical meaning.

⁴ Replacing the bracketed term in (9c) with $[\mu \lambda_N - E^\top \lambda_T]$, as commonly performed in literature [48], would call for unrealistically strict and physically unmotivated conditions to ensure adhesive friction.

⁵ Embedding contact dynamics into the numerical optimization problem as nonlinear constraints, where many other implicit constraints are already present, does not justify explicit or semi-implicit discretization schemes, which are, instead, legitimate when building fast simulators [20, Sec. 5].

4 TRAJECTORY PLANNING AS AN OPTIMIZATION PROBLEM

4.1 Penalty-based contact model

Within our direct transcription framework, for $k \in \{0, \dots, N-1\}$, eqs. (6), (7), and the discretized versions of eqs. (3) and (4) constitute a set of (equality and inequality) *nonlinear constraints* for the optimal control problem (OCP) we set out to formulate. Additional constraints include the (fixed and known) initial state values $x_0 = x(0)$ as well as a *terminal equality constraint* on (some) components of x_N : the latter provides a direct way to specify the required final state of the manipulated object at the final time $T = t_N$. Generally, no terminal constraints on the manipulation system configuration are imposed. Lower and upper bounds for (x_k, \bar{x}_k, u_k) are also included: they act as operational constraints for actuators and the system's workspace, and they are useful to restrain contact forces within safety limits. Other constraints can be introduced to shape emergent behaviors and to render them intrinsically more robust or desirable for several reasons. As an illustrative example, in order to guarantee that any two fingers make always contact with an object in a three-fingered manipulation task, we add the following set of inequalities to the problem: $f_{N_k}^{(1)} + f_{N_k}^{(2)} \geq \varepsilon$, $f_{N_k}^{(2)} + f_{N_k}^{(3)} \geq \varepsilon$, and $f_{N_k}^{(3)} + f_{N_k}^{(1)} \geq \varepsilon$, with $\varepsilon > 0$.

We introduce the vector of decision variables $\mathbf{v} \in \mathbb{R}^n$, which collects the sequence of unknown (x_k, \bar{x}_k, u_k) (i.e., configurations and velocities in (x_k, \bar{x}_k) , contact forces and actuator accelerations in u_k). All equality and inequality constraints can be written compactly as

$$g_{\min} \leq g(\mathbf{v}) \leq g_{\max}, \quad \mathbf{v}_{\min} \leq \mathbf{v} \leq \mathbf{v}_{\max} \quad (10)$$

The general structure of the cost function takes the form

$$f(\mathbf{v}) = \sum_{k=0}^{N-1} \sum_{i \in \mathcal{I}} w_i \phi_i(x_k, u_k), \quad (11)$$

where each $\phi_i(\cdot)$ represents a peculiar type of cost. These have to be carefully selected according to the character of the manipulation action we desire to perform, along with the corresponding *weights* w_i (also acting as important scaling factors). Multiple cost terms $\phi_i(\cdot)$ can be used to shape different manipulation behaviors. The following terms (specifically, their squared 2-norm) have proved to be decisive in directing the optimization process: contact forces, and their variations from one interval to the next (to minimize jerk); accelerations of actuators; deviations of actual object trajectories from ideal, smooth trajectories (task-specific).

4.2 Velocity-based time stepping scheme

Similarly to the penalty-based contact model scheme, the discrete formulation of the dynamics of systems with contacts expressed by eqs. (8) and (9) can be used as a set of nonlinear constraints in an optimal control problem (OCP), involving the sequence of unknown $(q_k, v_{k+1}, \lambda_{k+1}, \gamma_{k+1})$. Additional equality constraints are introduced: for the manipulated object, both initial and final configurations and velocities are imposed, whereas only the initial conditions are specified for the manipulation system.

Inequality constraints are also introduced with similar intentions as in the penalty-based scheme. It is worth noting that, since in our applications the hand is velocity controlled, the hand dynamics is not included in the optimization constraints, and the hand velocities will play the role of control actions. Therefore, limited control authority is imposed as bounds on hand ve-

locities and accelerations in the form $v_{\min}^{(l)} \leq v^{(l)} \leq v_{\max}^{(l)}$ and $a_{\min}^l h \leq \Delta v^{(l)} \leq a_{\max}^{(l)} h$, respectively, with l belonging to the index set corresponding to the hand.

Defining $\mathbf{v} \in \mathbb{R}^n$ as the multi-stage sequence of configurations, velocities, contact impulses and inputs, $(q_k, v_{k+1}, \lambda_{k+1}, \gamma_{k+1})$, all constraints are still expressed in the form (10), whereas the cost function takes the form

$$f(\mathbf{v}) = \sum_{k=0}^{N-1} \sum_{i \in \mathcal{I}} w_i \phi_i(q_k, v_{k+1}, \lambda_{k+1}, \gamma_{k+1}) \quad (12)$$

4.3 Final optimization problem

From the previous discussion, we now present the nonlinear program (NLP) that has to be solved to generate optimal trajectories. With $\mathbf{v} \in \mathbb{R}^n$ previously defined, we consider the following optimization problem

$$\min_{\mathbf{v}} f(\mathbf{v}), \quad \text{subject to} \quad g_{\min} \leq g(\mathbf{v}) \leq g_{\max} \quad \mathbf{v}_{\min} \leq \mathbf{v} \leq \mathbf{v}_{\max} \quad (13)$$

in which: $f : \mathbb{R}^n \rightarrow \mathbb{R}$ is the objective function, $g : \mathbb{R}^n \rightarrow \mathbb{R}^m$ is the nonlinear constraint function, $g_{\min} \in [-\infty, \infty]^m$ and $g_{\max} \in (-\infty, \infty]^m$ (with $g_{\min} \leq g_{\max}$) are, respectively, lower and upper bound vectors of the nonlinear constraints, $\mathbf{v}_{\min} \in [-\infty, \infty]^n$ and $\mathbf{v}_{\max} \in (-\infty, \infty]^n$ (with $\mathbf{v}_{\min} \leq \mathbf{v}_{\max}$) are, respectively, lower and upper bound vectors of the decision variables. Problem (13) is a *large-scale*, but *sparse* NLP, that should be solved by structure-exploiting solvers. To this end, as detailed in the next section, we resorted to the IPOPT [50] implementation of the interior-point method within the CasADi framework. As initial guess required by the algorithm, we somewhat crudely mapped the initial state x_0 and a rough estimate of the controls to all the $(N-1)$ variable instances. Obviously, better initial guesses should be provided whenever possible. With the penalty-based approach, (partial) solutions of the NLP (13) have also been used as initial guesses for a subsequent optimization according to a *homotopy* strategy [39, Sec. 11.3], thereby maximizing physical realism while facilitating convergence.

5 NONLINEAR PROGRAMMING VIA AN INTERIOR-POINT ALGORITHM

5.1 The barrier problem formulation

Problem (13) is equivalently rewritten as

$$\min_x f(x), \quad \text{subject to} \quad (14a)$$

$$c(x) = 0 \quad (14b)$$

$$x_{\min} \leq x \leq x_{\max} \quad (14c)$$

in which x is formed by augmenting the decision variable vector \mathbf{v} with suitable slack variables that transform inequality constraints in (13) into equality constraints.⁶

Let $I_{\min} = \{i : x_{\min}^{(i)} \neq -\infty\}$, and $I_{\max} = \{i : x_{\max}^{(i)} \neq \infty\}$. We consider the barrier function

⁶ With a slight abuse of notation, we still use n and m to denote the dimension of x and $c(x)$, respectively, and $f(x)$ to denote $f(\mathbf{v})$.

$$\varphi_\mu(x) = f(x) - \mu \left(\sum_{i \in I_{\min}} \ln(x^{(i)} - x_{\min}^{(i)}) + \sum_{i \in I_{\max}} \ln(x_{\max}^{(i)} - x^{(i)}) \right)$$

in which $\mu > 0$ is a (small) barrier parameter. Instead of solving (14), IPOPT performs iterations to achieve an approximate solution of the equality constrained NLP

$$\min_x \varphi_\mu(x), \quad \text{subject to: } c(x) = 0 \quad (15)$$

Note that $\varphi_\mu(x)$ is well defined if and only if $x_{\min} < x < x_{\max}$, i.e. if x is in the *interior* of its admissible region. The value of μ is progressively reduced so that $\varphi_\mu(x) \rightarrow f(x)$, and in this way solving (15), in the limit, becomes equivalent to solving (14). Clearly, as $\mu \rightarrow 0$, any component of x can approach its bound if this is required by optimality.

5.2 Interior-point approach to NLP

Any local minimizer to (15) must satisfy the following Karush-Kuhn-Tucker (KKT) conditions [39, Sec. 12.2]

$$\nabla f(x) + \nabla c(x)\lambda - \underline{z} + \bar{z} = 0 \quad (16a)$$

$$c(x) = 0 \quad (16b)$$

$$\underline{z}^{(i)}(x^{(i)} - x_{\min}^{(i)}) - \mu = 0 \quad \forall i \in I_{\min} \quad (16c)$$

$$\bar{z}^{(i)}(x_{\max}^{(i)} - x^{(i)}) - \mu = 0 \quad \forall i \in I_{\max} \quad (16d)$$

for some vectors $\lambda \in \mathbb{R}^m$, $\underline{z} \in \mathbb{R}^n$, and $\bar{z} \in \mathbb{R}^n$ (for completeness: $\underline{z}^{(i)} = 0 \quad \forall i \notin I_{\min}$, $\bar{z}^{(i)} = 0 \quad \forall i \notin I_{\max}$). Notice that, if $\mu = 0$, then (16) together with $\underline{z} \geq 0$ and $\bar{z} \geq 0$ represent the KKT conditions for NLP (14). The KKT conditions (16) form a nonlinear algebraic system $F(\xi) = 0$ in the unknown $\xi = (x, \lambda, \underline{z}, \bar{z})$, which is solved in interior-point algorithms via Newton-like methods. If we denote by $E_\mu(\xi)$ the maximum absolute error of the KKT equations (16) (appropriately scaled), the basic algorithm implemented in IPOPT is summarized in Table 1 (in which j is the index of the outer loop, k is the index of the inner loop, and $\varepsilon > 0$ is a user-defined convergence tolerance).

Table 1 Basic Algorithm implemented in IPOPT.

-
1. Define $\mu_0 > 0$, x_0 ($x_{\min} \leq x_0 \leq x_{\max}$), λ_0 , $\underline{z}_0 \geq 0$, $\bar{z}_0 \geq 0$, and form ξ_0 accordingly. Set: $j = 0$, $k = 0$.
 2. Given the current iterate ξ_k , compute a Newton step p_k for $F(\xi) = 0$. Compute the new iterate performing a line search: $\xi_{k+1} = \xi_k + \alpha_k p_k$ (for some $\alpha_k > 0$).
 3. If $E_0(\xi_{k+1}) \leq \varepsilon$, exit: ξ_{k+1} is a local solution to NLP (14). Otherwise, proceed to Step 4.
 4. If $E_{\mu_j}(\xi_{k+1}) \leq \kappa \mu_j$ (for some $\kappa > 0$) proceed to Step 5. Otherwise, update $k \leftarrow k + 1$ and go to Step 2.
 5. Set $\mu_{j+1} = \mu_j / \rho$ (for some $\rho > 1$), update $j \leftarrow j + 1$, $k \leftarrow k + 1$ and go to Step 2.
-

5.3 Main computational aspects: calculating derivatives and solving (sparse) linear systems

The most expensive computation step in the basic interior-point algorithm is the computation of the Newton step p_k for the KKT system $F(\xi) = 0$, i.e. Step 2. We first note that evaluation of $F(\xi)$, at each iteration, involves the computation of the cost function gradient $\nabla f(x) \in \mathbb{R}^n$ and of the constraint Jacobian $\nabla c(x) \in \mathbb{R}^{n \times m}$. Then, the Newton step is found from the solution of the following linear system:

$$\begin{bmatrix} W_k & A_k & -I & I \\ A_k^T & 0 & 0 & 0 \\ \underline{Z}_k & 0 & \underline{X}_k & 0 \\ -\bar{Z}_k & 0 & 0 & \bar{X}_k \end{bmatrix} \begin{bmatrix} p_k^x \\ p_k^\lambda \\ p_k^z \\ p_k^{\bar{z}} \end{bmatrix} = - \begin{bmatrix} \nabla \varphi_{\mu_j}(x_k) + A_k \lambda_k \\ c(x_k) \\ \underline{X}_k \underline{Z}_k \mathbf{1} - \mu_j \mathbf{1} \\ \bar{X}_k \bar{Z}_k \mathbf{1} - \mu_j \mathbf{1} \end{bmatrix} \quad (17)$$

in which: $W_k = \nabla_{xx}^2 \mathcal{L}(x_k, \lambda_k, z_k, \bar{z}_k)$, with $\mathcal{L}(x, \lambda, z, \bar{z}) = f(x) + c(x)^T \lambda - (x - x_{\min})^T z - (x_{\max} - x)^T \bar{z}$ the Lagrangian function associated with NLP (14); $A_k = \nabla c(x_k)$ the constraint Jacobian; $\underline{Z}_k = \text{diag}(z_k)$, $\bar{Z}_k = \text{diag}(\bar{z}_k)$, $\underline{X}_k = \text{diag}(x_k - x_{\min})$, and $\bar{X}_k = \text{diag}(x_{\max} - x_k)$ diagonal matrices; $\nabla \varphi_{\mu_j}(x_k) = \nabla f(x_k) - z_k + \bar{z}_k$. In order to generate the entries of system (17), it is necessary to evaluate the cost function gradient, the constraint Jacobian, as well as the Hessian of the Lagrangian (or a suitable approximation to it). Partial derivatives can be computed numerically by finite differentiation or analytically (for simple functions). A third approach is by means of so-called *Automatic Differentiation* (or Algorithmic Differentiation) techniques, which generate a numerical representation of partial derivatives by exploiting the chain rule in a numerical environment. Different approaches exist for AD, which are tailored to the computation of first-order and second-order derivatives. The interested reader is referred to [21]. A final computation observation is reserved to the numerical solution of system (17). First, it is transformed into a symmetric (indefinite) linear system via block elimination. Then, symmetry can be exploited by symmetric LDL factorizations. Furthermore, it should be noted that in trajectory planning problems considered here (and in general in optimal control problems) the Hessian W_k and the constraint Jacobian A_k are significantly sparse and structured. Exploiting these features can reduce the solution time significantly. To this effect, the MA57 multifrontal solver [14] from the Harwell Software Library [23] is used.

5.4 The CasADi framework

The transcribed optimal control problem is coded in a scripting environment using the Python [40] interface to the open-source CasADi framework [2], which provides building blocks to efficiently formulate and solve large-scale optimization problems.

In the CasADi framework, symbolic expressions for objective and constraints are formed by applying overloaded mathematical operators to symbolic primitives. These expressions are represented in memory as computational graphs, in contrast to tree representations common to computer algebra systems. The graph is sorted into an in-memory algorithm which can be evaluated numerically or symbolically with an efficient stack-based virtual machine or be exported to C code. Forward and backward source-code transforming AD can be performed on such algorithm at will, such that derivatives of arbitrary order can be computed. The sparsity pattern of the constraint Jacobian is computed using hierarchical seeding [18] and its unidirectional graph coloring is used to obtain the Jacobian with a reduced number of AD sweeps [17]. Regarding expressions and algorithm inputs and outputs, everything is a sparse matrix in CasADi. Yet the underlying computational graphs may be of either a type with scalar-valued (SX) nodes or a type with matrix-valued (MX) nodes. The combined usage of these two types amounts to a check-

pointing scheme [21]: low-level functions are constructed with the SX type algorithm, which is optimized for speed. These algorithms are in turn embedded into a graph of the MX type, which is optimized for memory usage, to form the expression of objective and constraints.

In the context of optimal control problems, the CasADi framework offers several advantages over other AD tools: it comes bundled with common algorithms that can be embedded into an infinitely differentiable computational graph (e.g. numerical integrators, root-finding and linear solvers), and takes care of constructing and passing sensitivity information to various NLP solvers backends. Since CasADi does not impose an OCP solution strategy and allows fine-grained speed-memory trade-offs, it is suited more than black-box OCP solvers to explore non-standard optimal control problem formulations or efficient solution strategies.

6 APPLICATION EXAMPLES

6.1 Environment-aware manipulation

6.1.1 Penalty-based approach with disk and two independent fingers

Figure 3 shows a first example of EC-exploiting manipulation. In a vertical plane, the two independent fingers H_0 and H_1 , initially away from the circular object, must interact with the object and have it interact with the environment (edges e_0 and e_1) so that it will be in the shown final position, with any orientation but zero velocity, at the end of a prescribed time horizon T . All contact interactions must occur without slippage (static friction). The object’s initial state corresponds to a configuration of static equilibrium. The fingers have limitations on their horizontal workspace: as a result, grasping and lifting of the object is inhibited, and an environment-exploiting policy needs to be discovered in order to accomplish the task. Also, object-passing between fingers needs to emerge. This planning problem has been formulated and solved using the penalty-based approach. The resulting trajectories in terms of normal contact forces are shown in the first two plots of Fig. 4: finger H_0 approaches the object first (whose weight is symmetrically supported by e_0 and e_1), then rolls it on edge e_1 (without slipping) until it reaches its workspace limit and hands it over to finger H_1 , which completes the task. Friction forces (not shown for brevity) satisfy constraint (3), where $\mu_s = 2$ was used. The third plot shows the actual x -component trajectory of the object versus a suggested trajectory, included as a hint in the objective function to facilitate convergence of the algorithm, but with a low weight (to avoid forcing such trajectory against dynamic constraints). With $N = 180$ discretization intervals (time step $h = 45$ ms) and considering the prescribed initial and terminal conditions, the problem size is $n = 8810$ decision variables. To obtain a solution for this example, starting from an initial guess built by repeating the initial condition for all the time steps, IPOPT took 1062 iterations, which correspond to ~ 23 min on a 2.70 GHz Intel(R) Core(TM) i7-4800MQ CPU with 32 GB of RAM. An animation of the obtained results can be found in part A.1 of the accompanying video [16] which also shows the grasping-and-lifting behavior that is discovered if finger workspace limitations are removed and the contact force exerted by edge e_1 is penalized.

6.1.2 Velocity-based time-stepping scheme with capsule and two-fingered underactuated gripper

With reference to Fig. 5, a capsule-shaped object, starting from an equilibrium configuration in contact with segment P_2P_3 (of a six-edged polygonal environment), has to find itself rotated by 180 deg at the end of the planning horizon T . Since the object is passive, a manipulation gait has to emerge for the gripper. Moreover, since we penalize high contact impulses and the gripper has a reduced mobility due to underactuation — it has symmetrically closing jaws — it turns out

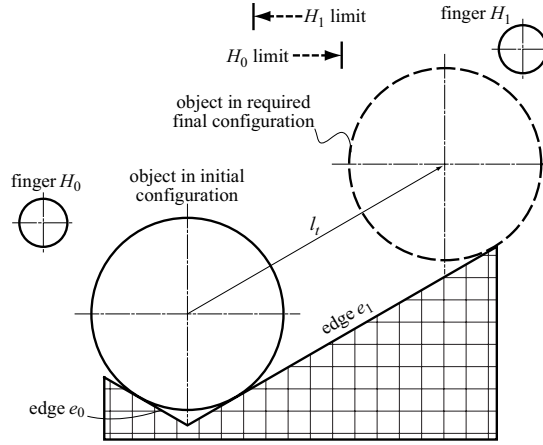


Fig. 3 EC manipulation scenario: the object must reach its final configuration at the prescribed final time $T = 8$ s.

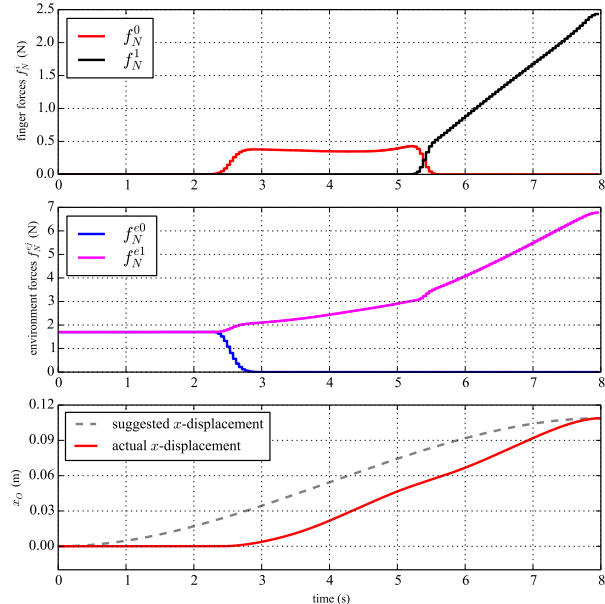


Fig. 4 Trajectories for a circular object manipulated by two independent fingers: normal contact forces f_N^i applied by the fingers; normal contact forces f_N^{ej} applied by the environment (segments e_0, e_1); suggested and actual x -displacement x of the object.

that convenient EC-exploiting behaviors are indeed automatically synthesized by the optimizer. In fact, with reference to Fig. 6, beside finger impulses (first plot), which represent standard grasping/manipulation actions, contact interactions generated by collisions of the object with the environment (second plot) play a role of paramount importance in shaping the object motion. More in detail, with reference to part A.2 of the accompanying video [16], the object is initially grasped and lifted, then it is gently dropped so that it lays on segment P_2P_3 after hitting segment P_3P_4 (see the corresponding bumps in λ_N^{23} and λ_N^{34}). Then, with the circular part of the capsule pushed to corner P_3 , the object is rotated with only one finger by sliding it on edges P_2P_3 and

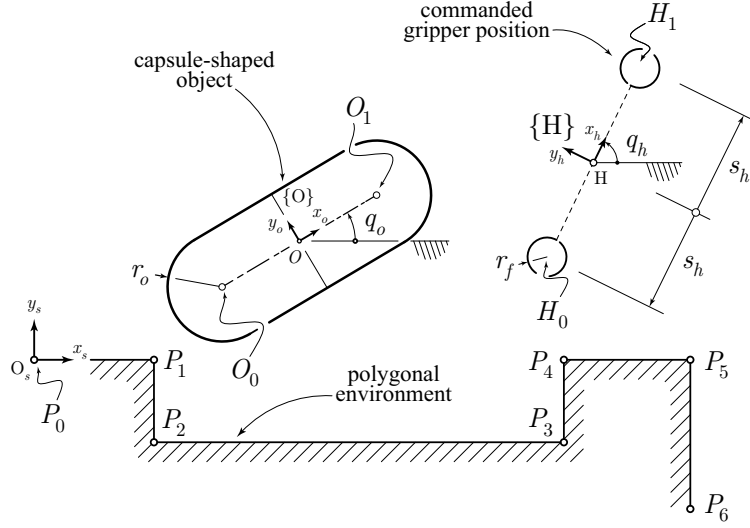


Fig. 5 EC manipulation scenario. Starting at $q_O(0) = \pi/2$, in contact with segment P_2P_3 , the capsule must be placed, at time $T = 5$ s, in the same position but with $q_O(T) = -\pi/2$.

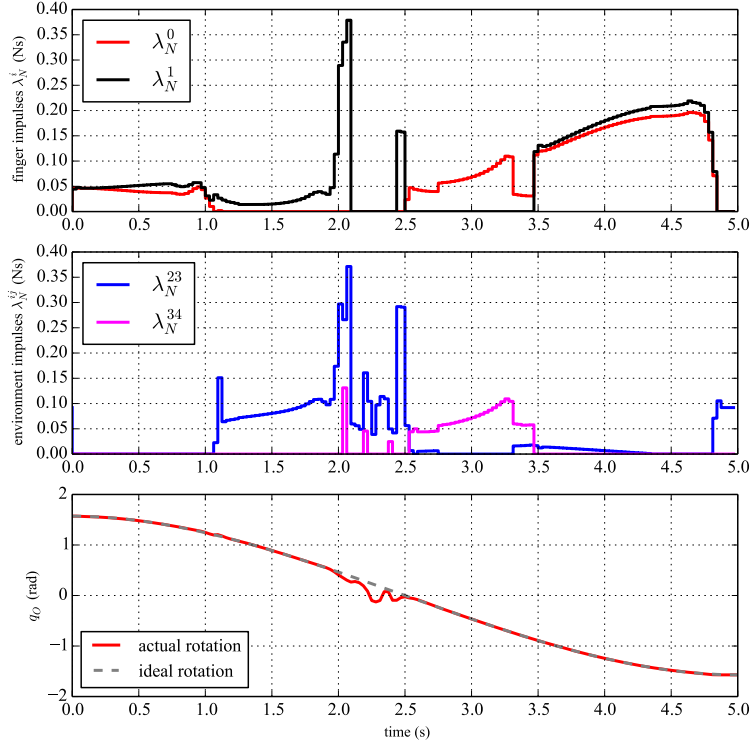


Fig. 6 Motion trajectories of a capsule-shaped object manipulated by an underactuated gripper: contact normal impulses λ_N^0 and λ_N^1 applied by the fingers; contact normal impulses λ_N^{ij} applied by the environment through segment P_iP_j ; ideal and actual rotation q_O of the object-fixed frame.

P_3P_4 . Finally, both fingers grasp the object and, slightly lifting it up, they slide it on edge P_2P_3 to the initial position. It is worth noting that, with a wise exploitation of EC, the actual rotation of the object can closely follow the desired one (third plot). This condition can be violated in general, since the trajectory prescribed from the outset only constitutes a suggested behavior for some components of the system. Regarding the underlying numerical OCP, at each time step $k \in \{0, \dots, N-1\}$, the problem variables have the following dimensions: $q_k \in \mathbb{R}^{4+3}$, $v_{k+1} \in \mathbb{R}^{4+3}$, $\lambda_{N_{k+1}} \in \mathbb{R}^{6+2}$, $\lambda_{T_{k+1}} \in \mathbb{R}^{12+4}$, $\gamma_{k+1} \in \mathbb{R}^{6+2}$. With $N = 160$ discretization intervals ($h = 30$ ms) and considering the prescribed boundary conditions on the object/gripper, the problem size is $n = 7375$. To obtain a solution for this example, starting from an initial guess built by repeating the initial condition for all the time steps, IPOPT took 920 iterations, which correspond to ~ 25 min on a 2.70 GHz Intel(R) Core(TM) i7-4800MQ CPU with 32 GB of RAM. An animation of the results can be found in part A.2 of the accompanying video [16].

6.2 Dexterous manipulation

With reference to Fig. 7, a circular object, starting from a configuration where it is held in equilibrium by three independent fingers in a force-closure grasp, has to find itself rotated by 360 deg at the end of the planning horizon T , with zero velocity. Since, again, the object itself is passive and each finger has workspace limitations (see Fig. 7), a relatively complex (dexterous) manipulation gait has to be discovered for the fingers. To obtain an in-place manipulation, a box constraint has also been assigned on the position of the object center. In order to obtain a relatively robust manipulation, the constraint described in section 4.1 has been included to guarantee that any two fingers are always in contact. As we want no slipping between the fingers and the object during manipulation, the penalty-based approach has been used (with a coefficient of friction $\mu_s = 1.5$). The resulting optimal trajectories in terms of finger forces are shown in the first two plots of Fig. 8: intermittent contacts due to the discovered manipulation gait can be clearly seen. The third plot shows the object's actual rotation versus a smooth (third-order), suggested rotation trajectory. With $N = 200$ discretization intervals ($h = 30$ ms) and accounting for the fixed initial and terminal conditions, the problem size is $n = 12585$. To obtain a solution for this example, starting from an initial guess built by repeating the initial condition for all the time steps, IPOPT took 1661 iterations, which correspond to ~ 81 min on a 2.70 GHz Intel(R) Core(TM) i7-4800MQ CPU with 32 GB of RAM. An animation is provided in part B.1 of the accompanying video [16], while part B.2 shows the results obtained by solving the same problem with the velocity-based time-stepping scheme, where sliding between fingers and object is allowed and exploited.

7 CONCLUSIONS AND FUTURE WORK

This paper proposed a computational framework to plan environment-aware manipulation behaviors that do not rely on an a-priori defined sequences of contacts. To this end, we framed the problem as a numerical optimal control one, including contact forces among the optimization variables as a key factor, and we sharpened the algorithmic pipeline by exploiting structural sparsity and leveraging Automatic Differentiation. Two contact models were proposed that best fit manipulation scenarios where sliding primitives need to be avoided or sought, respectively. These proved effective in solving manipulation planning problems where essential interactions with the environment had to be synthesized to accomplish a task (sub-section 6.1). The results presented in sub-section 6.2 demonstrated that the very same method is able to perform successfully in discovering non-trivial gaits also in dexterous manipulation tasks. Current research is devoted to extending the method to 3D scenarios, the major thrust being the synthesis of EC-exploiting, whole-body manipulation strategies for humanoid platforms. Injection of motion

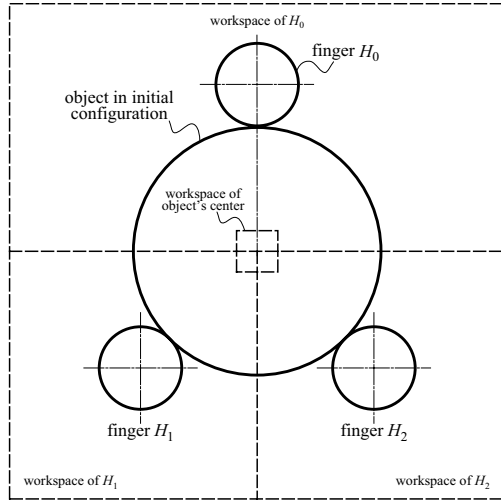


Fig. 7 Dexterous manipulation scenario: the object must find itself rotated by 360 deg at the final time $T = 6$ s.

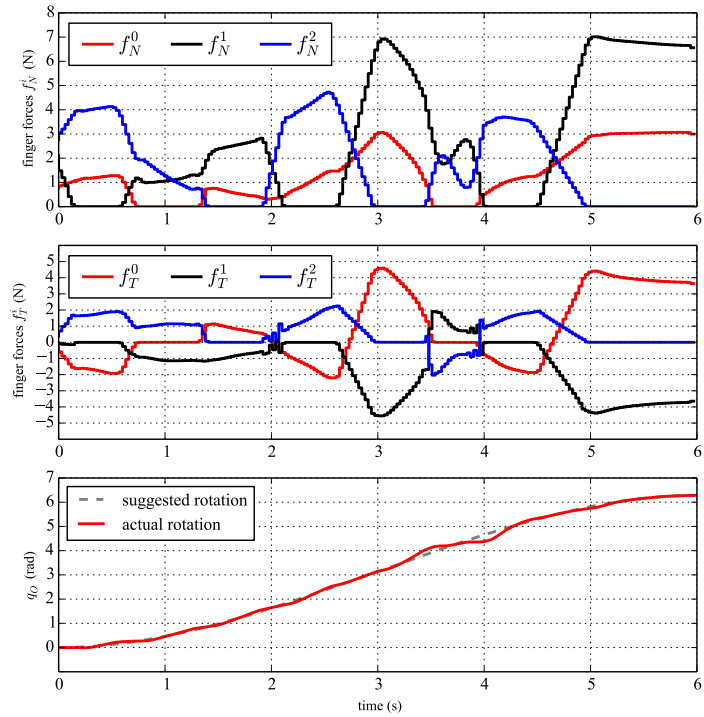


Fig. 8 Trajectories for a circular object manipulated by three independent fingers. Shown are: normal contact forces f_N^i and tangential contact forces f_T^i applied by the fingers; suggested and actual rotation q_O of the object.

primitives/synergies into the model are also being considered, and proper model scaling and tuning of IPOPT convergence parameters are under way to maximize computational efficiency.

8 ACKNOWLEDGEMENT

This work is supported by the grant no. 600918 “PACMAN” - Probabilistic and Compositional Representations of Object for Robotic Manipulation - within the FP7-ICT-2011-9 program “Cognitive Systems”. European Research Council and under the ERC Advanced Grant no. 291166 SoftHands (A Theory of Soft Synergies for a New Generation of Artificial Hands).

References

1. A. P. Ambler and R. J. Popplestone. Inferring the positions of bodies from specified spatial relationships. *Artificial Intelligence*, 6:157–174, 1975.
2. Joel Andersson. *A General-Purpose Software Framework for Dynamic Optimization*. PhD thesis, Arenberg Doctoral School, KU Leuven, Department of Electrical Engineering (ESAT/SCD) and Optimization in Engineering Center, Kasteelpark Arenberg 10, 3001-Heverlee, Belgium, October 2013.
3. J. T. Betts. *Practical Methods for Optimal Control Using Nonlinear Programming*. SIAM, 2001.
4. L. T. Biegler and V. M. Zavala. Large-scale nonlinear programming using IPOPT: An integrating framework for enterprise-wide dynamic optimization. *Computers & Chemical Engineering*, 33(3):575 – 582, 2009.
5. M. Bonilla, E. Farnoli, C. Piazza, M. Catalano, G. Grioli, M. Garabini, M. Gabiccini, and A. Bicchi. Grasping with soft hands. In *IEEE-RAS Int. Conf. on Humanoid Robots (Humanoids)*, 2014.
6. G. Boothroyd, C. Poli, and L.E. Murch. Handbook of feeding and orienting techniques for small parts. University of Massachusetts at Amherst, Dept. of Mechanical Engineering, Automation Project, 1981.
7. Iain Boyle, Yiming Rong, and David C. Brown. A review and analysis of current computer-aided fixture design approaches. *Robotics and Computer-Integrated Manufacturing*, 27(1):1–12, February 2011.
8. B. Cohen, M. Phillips, and M. Likhachev. Planning single-arm manipulations with n-arm robots. In *Robotics: Science and Systems (RSS)*, 2014.
9. N.C. Dafle, A. Rodriguez, R. Paolini, Bowei Tang, S.S. Srinivasa, M. Erdmann, M.T. Mason, I. Lundberg, H. Staab, and T. Fuhlbrigge. Regrasping objects using extrinsic dexterity. In *IEEE Int. Conf. on Robotics and Automation (ICRA)*, pages 2560–2560, May 2014.
10. G.E. Deacon. An attempt to raise the level of software abstraction in assembly robotics through an apposite choice of underlying mechatronics. *Journal of Intelligent and Robotic Systems*, 28(4):343–399, 2000.
11. R. Diankov. *Automated Construction of Robotic Manipulation Programs*. Phd thesis, Carnegie Mellon University, Robotics Institute, August 2010.
12. Manfredo Perdigao Do Carmo. *Differential Geometry of Curves and Surfaces*. Prentice Hall, Englewood Cliffs, 1976.
13. Mehmet R. Dogar and Siddhartha S. Srinivasa. A planning framework for non-prehensile manipulation under clutter and uncertainty. *Autonomous Robots*, 33(3):217–236, June 2012.
14. Iain S Duff. Ma57 – a code for the solution of sparse symmetric definite and indefinite systems. *ACM Transactions on Mathematical Software (TOMS)*, 30(2):118–144, 2004.
15. Clemens Eppner and Oliver Brock. Planning grasp strategies that exploit environmental constraints. In *IEEE Int. Conf. on Robotics and Automation (ICRA)*, May 2015.
16. M. Gabiccini, A. Artoni, G. Pannocchia, and J. Gillis. ISRR 2015 submission accompanying video. <http://youtu.be/ozDwPnS00fI>, April 2015.
17. Assefaw Hadish Gebremedhin, Fredrik Manne, and Alex Pothen. What color is your Jacobian? Graph coloring for computing derivatives. *SIAM Review*, 47:629–705, 2005.
18. J. Gillis and M. Diehl. Hierarchical seeding for efficient sparsity pattern recovery in automatic differentiation. In *CSC14: The Sixth SIAM Workshop on Combinatorial Scientific Computing*, 2014.
19. E. Glassman and R. Tedrake. A quadratic regulator-based heuristic for rapidly exploring state space. In *IEEE Int. Conf. on Robotics and Automation (ICRA)*, pages 5021–5028, Anchorage, Alaska, USA, 5 2010.
20. C. Glocker and C. Studer. Formulation and preparation for numerical evaluation of linear complementarity systems in dynamics. *Multibody System Dynamics*, 13:447–463, 2005.
21. A. Griewank and A. Walther. *Evaluating Derivatives*. SIAM, 2 edition, 2008.
22. Andreas Griewank. *Evaluating Derivatives: Principles and Techniques of Algorithmic Differentiation*. Number 19 in Frontiers in Appl. Math. SIAM, Philadelphia, PA, 2000.
23. HSL. A collection of fortran codes for large scale scientific computation, 2014.

24. A. Ijspeert, J. Nakanishi, and S. Schaal. Learning attractor landscapes for learning motor primitives. 2003.
25. Rico Jonschkowski and Oliver Brock. State representation learning in robotics: Using prior knowledge about physical interaction. In *Proceedings of Robotics: Science and Systems*, Berkeley, USA, July 2014.
26. S. Karaman and E. Frazzoli. Sampling-based algorithms for optimal motion planning. *International Journal of Robotics Research*, 30(7):846–894, June 2011.
27. Moslem Kazemi, Jean-Sebastien Valois, J. Andrew Bagnell, and Nancy Pollard. Human-inspired force compliant grasping primitives. *Autonomous Robots*, pages 1–17, 2014.
28. J. Kober, J. A. Bagnell, and J. Peters. Reinforcement learning in robotics: A survey. *Int. Journal of Robotics Research (IJRR)*, 32(11):1238–1274, 2013.
29. Y. Koga and J.-C. Latombe. On multi-arm manipulation planning. In *IEEE Int. Conf. on Robotics and Automation (ICRA)*, 1994.
30. N. Kohl and P. Stone. Policy gradient reinforcement learning for fast quadrupedal locomotion. In *IEEE Int. Conf. on Intelligent Robots and Systems (IROS)*, 2004.
31. Sergey Levine and Pieter Abbeel. Learning neural network policies with guided policy search under unknown dynamics. In *Neural Information Processing Systems (NIPS)*, 2014.
32. Sergey Levine, Nolan Wagener, and Pieter Abbeel. Learning contact-rich manipulation skills with guided policy search. In *IEEE Int. Conf. on Robotics and Automation (ICRA)*, 2015.
33. Tomás Lozano-Pérez, Matthew T. Mason, and Russell H. Taylor. Automatic synthesis of fine-motion strategies for robots. *Int. Journal of Robotics Research (IJRR)*, 3(1):3–24, March 1984.
34. Matthew T. Mason. The mechanics of manipulation. In *IEEE Int. Conf. on Robotics and Automation (ICRA)*, volume 2, pages 544–548, 1985.
35. A.T. Miller and P.K. Allen. Graspit! a versatile simulator for robotic grasping. *IEEE Robotics and Automation Magazine*, 11(4):110–122, 2004.
36. I. Mordatch, Z. Popović, and E. Todorov. Contact-invariant optimization for hand manipulation. In *Eurographics/ACM Symposium on Computer Animation*, 2012.
37. I. Mordatch, E. Todorov, and Z. Popović. Discovery of complex behaviors through contact-invariant optimization. In *ACM Transactions on Graphics*, 2012.
38. Igor Mordatch and Emo Todorov. Combining the benefits of function approximation and trajectory optimization. In *Proceedings of Robotics: Science and Systems*, Berkeley, USA, July 2014.
39. J. Nocedal and S. J. Wright. *Numerical Optimization*. Springer Verlag, New York, 2006.
40. Travis E Oliphant. Python for scientific computing. *Computing in Science & Engineering*, 9(3):10–20, 2007.
41. A. Perez, R. Platt, G. Konidaris, L. Kaelbling, and T. Lozano-Perez. LQR-RRT*: Optimal sampling-based motion planning with automatically derived extension heuristics. In *Robotics and Automation (ICRA), 2012 IEEE International Conference on*, 2012.
42. J. Peters and S. Schaal. Reinforcement learning of motor skills with policy gradients. *Neural Networks*, 21(4):682–697, 2008.
43. M. Posa, C. Cantu, and R. Tedrake. A direct method for trajectory optimization of rigid bodies through contact. *Int. Journal of Robotics Research (IJRR)*, 33(1):69–81, 2014.
44. C. Samson, M. Le Borgne, and B. Espiau. *Robot Control, the Task Function Approach*. Clarendon Press, Oxford, England, 1991.
45. G. Schultz and K. Mombaur. Modeling and optimal control of human-like running. *IEEE/ASME Transactions on Mechatronics*, 15(5):783–792, 2010.
46. Joris De Schutter, Tinne De Laet, Johan Rutgeerts, Wilm Decré, Ruben Smits, Erwin Aertbeljén, Kasper Claes, and Herman Bruyninckx. Constraint-based task specification and estimation for sensor-based robot systems in the presence of geometric uncertainty. *International Journal of Robotics Research*, 26(5):433–455, 2007.
47. D. E. Stewart and J. C. Trinkle. An implicit time-stepping scheme for rigid body dynamics with inelastic collisions and coulomb friction. *Int. Journal for Numerical Methods in Engineering*, 39:2673–2691, 1996.
48. David Stewart and Jeffrey C Trinkle. An implicit time-stepping scheme for rigid body dynamics with coulomb friction. In *IEEE Int. Conf. on Robotics and Automation (ICRA)*, volume 1, pages 162–169. IEEE, 2000.
49. R. Tedrake, T. Zhang, and H. Seung. Stochastic policy gradient reinforcement learning on a simple 3d biped. In *IEEE Int. Conf. on Intelligent Robots and Systems (IROS)*, 2004.
50. A. Wächter and L. T. Biegler. On the implementation of a primal-dual interior point filter line search algorithm for large-scale nonlinear programming. *Mathematical Programming*, 106:25–57, 2006.
51. Peter Wriggers. *Computational contact mechanics*. Springer, Berlin, New York, 2006.
52. W. Xi and C.D. Remy. Optimal gaits and motions for legged robots. In *IEEE Int. Conf. on Intelligent Robots and Systems (IROS)*, pages 3259–3265, 2014.

A.6 Article: Offset-free MPC explained: novelties, subtleties, and applications

Authors G. Pannocchia, M. Gabiccini, and A. Artoni

Info Published in: 5th IFAC Conference on Nonlinear Model Predictive Control, Seville, Spain, September 17-20, 2015

Abstract This paper presents an updated and comprehensive description of offset-free MPC algorithms for nonlinear (and linear) discrete-time systems, with the intended objectives of clarifying the main concepts, showing new results, highlighting subtleties by means of challenging applications. First, the offset-free tracking problem for nonlinear systems is presented, putting a strong accent on the role of the disturbance model and observer, and then novel and stronger offset-free estimation results are presented. Next, recent advances in linear offset-free MPC are described, which show the equivalence of the velocity form algorithm (so far considered an alternative method) to a particular disturbance model and observer. Then, the concepts of offset-free estimation are exploited to design an offset-free economic MPC algorithm, which can asymptotically achieve the highest economic performance despite persistent model errors and disturbances. Extensive application results are presented to show the benefits of offset-free MPC algorithms over standard ones, and to clarify misconceptions and design errors that can prevent constraint satisfaction, closed-loop stability, and offset-free performance.

Relation with the deliverable this work is concerned with providing the necessary theoretical background to design offset-free MPC algorithms, which are fundamental to turn direct trajectory optimization-based manipulation planners (presented in Sec. 1.5.1) into controllers able to asymptotically achieve economic performances despite model errors and disturbances.

Attachment (following pages until next annex)

Offset-free MPC explained: novelties, subtleties, and applications

Gabriele Pannocchia ^{*,**} Marco Gabicci ^{*} Alessio Artoni ^{*}

^{*}Department of Civil and Industrial Engineering, University of Pisa, Italy

^{**}Corresponding author, e-mail: gabriele.pannocchia@unipi.it

Abstract: This paper presents an updated and comprehensive description of offset-free MPC algorithms for nonlinear (and linear) discrete-time systems, with the intended objectives of clarifying the main concepts, showing new results, highlighting subtleties by means of challenging applications. First, the offset-free tracking problem for nonlinear systems is presented, putting a strong accent on the role of the disturbance model and observer, and then novel and stronger offset-free estimation results are presented. Next, recent advances in linear offset-free MPC are described, which show the equivalence of the velocity form algorithm (so far considered an alternative method) to a particular disturbance model and observer. Then, the concepts of offset-free estimation are exploited to design an offset-free economic MPC algorithm, which can asymptotically achieve the highest economic performance despite persistent model errors and disturbances. Extensive application results are presented to show the benefits of offset-free MPC algorithms over standard ones, and to clarify misconceptions and design errors that can prevent constraint satisfaction, closed-loop stability, and offset-free performance.

Keywords: Nonlinear discrete-time systems, linear discrete-time systems, model predictive control, state and disturbance estimation.

1. INTRODUCTION

The role of feedback in the design of effective control systems is central. In traditional PID control, for instance, the error between reference and actual *measured* output is the *sole* variable that determines the computed control action. In Model Predictive Control (MPC), an optimal control problem is solved at each decision time (mainly) because a new state *measurement* (or estimate) becomes available. Feedback is necessary to reduce the effect of disturbances and to cope with unavoidable modeling errors. Nonetheless, the way in which feedback is used to achieve offset-free tracking in the presence of persistent errors or disturbances appears to be often a question of personal preference among possible different methods.

In conventional linear (PID) control design, the offset-free goal is achieved by integrating the tracking error. In the linear quadratic regulation (LQR) framework, the use of *disturbance observers* was proposed and discussed in (Davison and Smith, 1971; Kwakernaak and Sivan, 1972). In the context of MPC, several methods have been proposed. In the first industrial implementations, such as Dynamic Matrix Control [see e.g. (Prett and Garcia, 1988, Sec. 5.2)], an output correction term defined as the difference between the measured and the predicted output was adopted. This method is probably the simplest disturbance model, usually referred to as *output disturbance model* (Rawlings, 2000), and it is known to be applicable only to open-loop stable systems. In the context of state-space linear systems, a wider range of approaches are known and applied. General formulations based on disturbance models and observers have been extensively discussed (Muske and Badgwell, 2002; Pannocchia and Rawlings, 2003; Maeder et al., 2009), although an important issue on which disturbance model is more effective was matter of investigation until Rajamani et al. (2009) presented an important result on the equivalence of different dis-

turbance models. Alternative offset-free approaches are based on a *velocity form* linear model, in which the input (and usually also the state) are replaced by their variation between two time steps [see e.g. (Pannocchia and Rawlings, 2001; Wang, 2004; González et al., 2008; Betti et al., 2012, 2013) and references therein]. The concepts of linear offset-free MPC have been extended to nonlinear MPC in (Morari and Maeder, 2012).

The general goal of this paper is to shed some light on this aspect of MPC theory and design, which is often overlooked in academic papers but is fundamental for actual implementation. The rest of the paper is organized as follows. In Section 2, we present a comprehensive description of the available results on offset-free nonlinear MPC, and then we show new results on the asymptotic convergence of the estimator. In Section 3, the offset-free linear MPC design is discussed to show that the velocity-form model is a special case of disturbance model/observer, and not an alternative method as commonly believed. In Section 4, we extend the concepts of offset-free nonlinear MPC to design an economic MPC algorithm that is able to cope with persistent errors while still achieving the optimal ultimate economic performance. Three application examples are extensively presented in Section 5 to emphasize the results of the previous sections, and to highlight possible pitfalls of the offset design. Finally, we summarize the main achievements and sketch possible research directions in Section 6.

Notation. The fields of real (nonnegative real), integer (non-negative integer), and complex numbers are denoted by \mathbb{R} ($\mathbb{R}_{\geq 0}$), \mathbb{I} ($\mathbb{I}_{\geq 0}$) and \mathbb{C} , respectively. The n -dimensional vector space with components in \mathbb{R} is denoted by \mathbb{R}^n . For any $x \in \mathbb{R}^n$, the Euclidean norm is denoted by $|x|$. A matrix $A \in \mathbb{R}^{n \times n}$ is said to be Hurwitz if all its eigenvalues lie strictly inside the unit circle. Given a sequence $\mathbf{x} = \{x(0) \ x(1) \ \dots\}$ and $a, b \in \mathbb{I}_{\geq 0}$, $a < b$, we define: $\|\mathbf{x}\|_{a:b} = \max_{k \in \mathbb{I}, a \leq k \leq b} |x(k)|$. A time-invariant

discrete-time system is written as $x(k+1) = f(x(k), u(k))$ or simply $x^+ = f(x, u)$ when it is not necessary to specify the current time k . A function $\sigma : \mathbb{R}_{\geq 0} \rightarrow \mathbb{R}_{\geq 0}$ belongs to the class \mathcal{K} if it is continuous, zero at zero, and strictly increasing. A function $\beta : \mathbb{R}_{\geq 0} \times \mathbb{I}_{\geq 0} \rightarrow \mathbb{R}_{\geq 0}$ belongs to the class \mathcal{KL} if for each $k \geq 0$ the function $\beta(\cdot, k) \in \mathcal{K}$, and for each $s \in \mathbb{R}_{\geq 0}$ there holds $\lim_{k \rightarrow \infty} \beta(s, k) = 0$.

2. OFFSET-FREE NONLINEAR MPC: DEFINITIONS, KNOWN AND NOVEL RESULTS

2.1 Plant, nominal model and constraints

In the paper we are concerned with the control of time-invariant dynamical systems in the form:

$$\begin{aligned} x_p^+ &= f_p(x_p, u, w_p) \\ y &= h_p(x_p, v_p) \end{aligned} \quad (1)$$

in which $x_p, x_p^+ \in \mathbb{R}^n$ denote the current and successor *plant* states, $u \in \mathbb{R}^m$ is the control input, $y \in \mathbb{R}^p$ is the output, $w_p \in \mathbb{R}^{n_w}$ and $v_p \in \mathbb{R}^{n_v}$ denote plant state and output disturbances. The plant output is measured at each time $k \in \mathbb{I}$.

Functions $f_p : \mathbb{R}^n \times \mathbb{R}^m \times \mathbb{R}^{n_w} \rightarrow \mathbb{R}^n$ and $h_p : \mathbb{R}^n \times \mathbb{R}^{n_v} \rightarrow \mathbb{R}^p$ are not known precisely but are assumed to be continuous. However, in order to design a Model Predictive Control algorithm for (1), a time-invariant dynamical system *model* is known:

$$\begin{aligned} x^+ &= f(x, u) \\ y &= h(x) \end{aligned} \quad (2)$$

in which $x, x^+ \in \mathbb{R}^n$ denote the current and successor *model* states. The functions $f : \mathbb{R}^n \times \mathbb{R}^m \rightarrow \mathbb{R}^n$ and $h : \mathbb{R}^n \rightarrow \mathbb{R}^p$ are assumed to be continuous.

Let $w \in \mathbb{R}^n$ and $v \in \mathbb{R}^p$ be defined as:

$$w := f_p(x_p, u, w_p) - f(x, u), \quad v := h_p(x_p, v_p) - h(x) \quad (3)$$

The next assumption is considered throughout the paper.

Assumption 1. (General). Disturbances are bounded in compact sets: $w \in \mathbb{W}, v \in \mathbb{V}$.

Input and output are required to satisfy the following constraints at all times:

$$g_u(u) \leq 0, \quad g_y(y) \leq 0 \quad (4)$$

in which $g_u : \mathbb{R}^m \rightarrow \mathbb{R}^{q_u}$ and $g_y : \mathbb{R}^p \rightarrow \mathbb{R}^{q_y}$ are convex functions defining the following compact convex sets:

$$\mathbb{U} := \{u \in \mathbb{R}^m \mid g_u(u) \leq 0\}, \quad \mathbb{Y} := \{y \in \mathbb{R}^p \mid g_y(y) \leq 0\} \quad (5)$$

Moreover, induced by the model (2) and the output constraint set, the following state constraint set is defined:

$$\mathbb{X} := \{x \in \mathbb{R}^n \mid g_y(h(x)) \leq 0\} \quad (6)$$

Remark 2. If the state is measurable, it follows that $h_p(x_p, v_p) = x_p$ and $v_p = 0$ at all times. Clearly, in such cases, the model output function is chosen as $h(x) = x$ and \mathbb{Y} also represents the constraint set for the state.

Given a sequence of inputs $\mathbf{u} = \{u(0), u(1), \dots\}$ and an initial state z , we define $\mathbf{y}_{z, \mathbf{u}} = \{y(0), y(1), \dots\}$ as the corresponding sequence of outputs generated by system (2). We also denote by $x(k; z, \mathbf{u})$ the solution at time k of system (2). Next, we recall the following definitions (Rawlings and Mayne, 2009, Sec.4.2).

Definition 3. (Observability). System (2) is observable if there exists a finite $N_o \in \mathbb{I}$ and $\gamma(\cdot) \in \mathcal{K}$ such that for any two initial states z_1 and z_2 and control sequence \mathbf{u} , and all $k \geq N_o$

$$|z_1 - z_2| \leq \gamma(\|\mathbf{y}_{z_1, \mathbf{u}} - \mathbf{y}_{z_2, \mathbf{u}}\|_{0:k}) \quad (7)$$

Definition 4. (Asymptotic stability of the estimate). Let $\hat{x}(k)$ be an estimate of $x(k; x_0, \mathbf{u})$ obtained for system (2), given a sequence of output measurements $\mathbf{y}_{x_0, \mathbf{u}} = \{y(0), \dots, y(k)\}$ and a (prior) estimate of the initial state \bar{x}_0 . The estimate is asymptotically stable if there exists $\beta \in \mathcal{KL}$ such that for all initial state x_0 and prior estimate \bar{x}_0 and $k \in \mathbb{I}_{\geq 0}$ there holds:

$$|x(k; x_0, \mathbf{u}) - \hat{x}(k)| \leq \beta(\|x_0 - \bar{x}_0\|, k) \quad (8)$$

2.2 Offset-free tracking problem definition

The controlled output $y_c \in \mathbb{R}^{p_c}$ is defined as function of the measured output:

$$y_c = r(y) \quad (9)$$

and $\bar{y}_c \in \mathbb{Y}$ denotes its desired setpoint. The offset-free problem is to design an output feedback MPC law $u = \kappa(y)$ such that:

G1: Input and output constraints are satisfied at all times.

G2: The closed-loop system reaches an equilibrium.

G3: The following condition holds true:

$$\lim_{k \rightarrow \infty} y_c(k) = \bar{y}_c \quad (10)$$

For these goals (in particular G2 and G3) to be attainable the following additional assumption is necessary.

Assumption 5. Disturbances are asymptotically constant, i.e. there exist $\bar{w} \in \mathbb{W}$ and $\bar{v} \in \mathbb{V}$ such that:

$$\lim_{k \rightarrow \infty} w(k) = \bar{w}, \quad \lim_{k \rightarrow \infty} v(k) = \bar{v} \quad (11)$$

2.3 State augmentation and estimation

Offset-free MPC algorithms are generally based on an *augmented model* (Muske and Badgwell, 2002; Pannocchia and Rawlings, 2003; Maeder et al., 2009; Maeder and Morari, 2010). The general augmented model can be written as:

$$\begin{aligned} x^+ &= F(x, d, u) \\ d^+ &= d \\ y &= H(x, d) \end{aligned} \quad (12)$$

in which $d \in \mathbb{R}^{n_d}$ is the so-called *disturbance state* or simply disturbance. Functions $F : \mathbb{R}^n \times \mathbb{R}^{n_d} \times \mathbb{R}^m \rightarrow \mathbb{R}^n$ and $H : \mathbb{R}^n \times \mathbb{R}^{n_d} \rightarrow \mathbb{R}^p$ are assumed to be continuous, and *consistent* with the nominal model, i.e. for all $x \in \mathbb{R}^n$ and $u \in \mathbb{R}^m$ there holds:

$$F(x, 0, u) = f(x, u), \quad H(x, 0) = h(x) \quad (13)$$

Remark 6. The disturbance d follows an integral dynamics.

We make the following assumption on the augmented system.

Assumption 7. The augmented model (12) is observable.

Remark 8. The augmented model (12) is observable only if the nominal model (2) is observable. Conversely, given an observable model (2), it is in general possible to define an augmented model (12), with $n_d \leq p$ disturbance states, that is observable.

At each time k , given the measurement of the output $y(k)$, an observer for (12) is used to estimate the augmented state $(x(k), d(k))$. For simplicity of exposition, we focus on a ‘steady-state Kalman filter like’ estimator, in which only the current measurement of $y(k)$ is used to update the prediction of $(x(k), d(k))$ made at the previous decision time. Alternative methods based on Moving Horizon Estimation (MHE) use instead a sequence of previous output measurements, and can be applied in a similar manner.

Without introducing the double-index notation, we define $\hat{x}(k)$ and $\hat{d}(k)$ as the *filtered* estimate of $x(k)$ and $d(k)$ obtained using the output measurement at time k . We instead use the symbols $\hat{x}^*(k)$, $\hat{d}^*(k)$ and $\hat{y}^*(k)$ to denote the *predicted* estimate of $x(k)$, $d(k)$ and $y(k)$, respectively, obtained at time $k-1$ using the augmented model (12), i.e.:

$$\begin{aligned}\hat{x}^*(k) &= F(\hat{x}(k-1), \hat{d}(k-1), u(k-1)) \\ \hat{d}^*(k) &= \hat{d}(k-1) \\ \hat{y}^*(k) &= H(\hat{x}^*(k), \hat{d}^*(k))\end{aligned}\quad (14)$$

Having defined the output prediction error as:

$$e(k) = y(k) - \hat{y}^*(k) \quad (15)$$

the filtering relations can be written as follows:

$$\begin{aligned}\hat{x}(k) &= \hat{x}^*(k) + \kappa_x(e(k)) \\ \hat{d}(k) &= \hat{d}^*(k) + \kappa_d(e(k))\end{aligned}\quad (16)$$

We make the following assumption on the observer.

Assumption 9. (Nominal observer). The functions $\kappa_x : \mathbb{R}^p \rightarrow \mathbb{R}^n$ and $\kappa_d : \mathbb{R}^p \rightarrow \mathbb{R}^{nd}$ are continuous and satisfy:

$$\kappa_x(0) = 0, \quad \kappa_d(e) = 0 \Leftrightarrow e = 0 \quad (17)$$

Moreover, relations (14)–(16) form an asymptotically stable observer for the augmented system (12).

Remark 10. From condition (17) in Assumption 9, it follows in general that $n_d \geq p$. This observation and Remark 8 lead to the choice $n_d = p$.

The issues associated with the use of $n_d < p$ are highlighted later in Section 5.

2.4 Target calculation, optimal control problem and receding horizon implementation

Given the current estimate of the augmented state $(\hat{x}(k), \hat{d}(k))$, an offset-free MPC algorithm needs to compute the equilibrium target that ensures exact tracking of the controlled variable. Depending on input/output dimensions and on the system dynamics, such a target may not be unique. Hence, in the general case we solve the following target problem denoted by $\mathbb{P}_s(\bar{y}_c, \hat{d}(k))$:

$$\min_{x,u,y} \ell_s(y, u) \quad (18a)$$

subject to:

$$x = F(x, \hat{d}(k), u) \quad (18b)$$

$$y = H(x, \hat{d}(k)) \quad (18c)$$

$$r(y) = \bar{y}_c \quad (18d)$$

$$y \in \mathbb{Y}, \quad u \in \mathbb{U} \quad (18e)$$

in which $\ell_s : \mathbb{R}^p \times \mathbb{R}^m \rightarrow \mathbb{R}$ is the *steady-state cost function*. We assume that (18) is feasible and we denote its (unique) solution as $(x_s(k), u_s(k), y_s(k))$.

Remark 11. Problem $\mathbb{P}_s(\bar{y}_c, \hat{d}(k))$ is parametric in the controlled variable setpoint and in the current disturbance estimate. It needs therefore to be solved at each decision time, and not only when the setpoint changes.

Let $\mathbf{x} = \{x_0 \ x_1 \ \dots \ x_N\}$ and $\mathbf{u} = \{u_0 \ u_1 \ \dots \ u_{N-1}\}$ be, respectively, a state sequence and an input sequence. For $i = 0, \dots, N-1$, let $y_i = H(x_i, \hat{d}(k))$ be the model output corresponding to a state x_i and disturbance estimate $\hat{d}(k)$. Furthermore, let $\tilde{x}_i := x_i - x_s(k)$ for $i = 0, \dots, N$, and $\tilde{u}_i := u_i - u_s(k)$ for

$i = 0, \dots, N-1$. The following finite-horizon optimal control problem, denoted by $\mathbb{P}(\hat{x}(k), \hat{d}(k), x_s(k), u_s(k), y_s(k))$, is posed:

$$\min_{\mathbf{x}, \mathbf{u}} \sum_{i=0}^{N-1} \ell(\tilde{x}_i, \tilde{u}_i) + V_f(\tilde{x}_N) \quad (19a)$$

subject to:

$$x_0 = \hat{x}(k) \quad (19b)$$

$$x_{i+1} = F(x_i, \hat{d}(k), u_i) \quad (19c)$$

$$H(x_i, \hat{d}(k)) \in \mathbb{Y}, \quad u_i \in \mathbb{U} \quad (19d)$$

$$\tilde{x}_N \in \mathbb{X}_f \quad (19e)$$

in which $\ell : \mathbb{R}^n \times \mathbb{R}^m \rightarrow \mathbb{R}_{\geq 0}$ is a strictly positive definite convex function. $V_f : \mathbb{R}^n \rightarrow \mathbb{R}_{\geq 0}$ and \mathbb{X}_f are, respectively, a terminal cost function and a terminal set, designed according to the usual stabilizing conditions (Rawlings and Mayne, 2009, Sec. 2.5).

Assuming that problem (19) is feasible, its solution is denoted by $(\mathbf{x}^0(k), \mathbf{u}^0(k))$ and the associated receding horizon implementation is given by:

$$u(k) = u_0^0(k) \quad (20)$$

Remark 12. In problem $\mathbb{P}(\cdot)$, the disturbance estimate $\hat{d}(k)$ is a fixed parameter. Consequently, $\mathbb{P}(\cdot)$ can be rewritten as a regulation problem in the deviation variables $\{\tilde{x}_i, \tilde{u}_i\}$.

Remark 13. Following the ideas of (Limon et al., 2008), the target problem $\mathbb{P}_s(\cdot)$ and the dynamic optimization problem $\mathbb{P}(\cdot)$ could be merged together in a single optimization problem (Betti et al., 2013).

2.5 Asymptotic stability and offset-free tracking

In order to establish offset-free tracking, it is necessary that the closed-loop system reaches an asymptotically stable equilibrium. Establishing conditions under which this occurs is very hard because of the combined presence of state estimator, target calculation and dynamic optimization. Indeed, almost all available methods for offset-free MPC assume that an asymptotically stable equilibrium has been reached, and then show that offset-free control is attained at such an equilibrium. One noticeable exception is the robust offset-free linear MPC algorithm proposed in (Betti et al., 2013), which is designed under the assumption that the full state is measurable at each time. Such an algorithm uses the so-called velocity form model (Pannocchia and Rawlings, 2001), which is reviewed later in Section 3 and for which equivalence to a particular disturbance model and observer has been recently established in (Pannocchia, 2015).

We next present the main offset-free result and a streamlined proof. Similar results and arguments have been shown in (Muske and Badgwell, 2002; Pannocchia and Rawlings, 2003; Maeder et al., 2009; Morari and Maeder, 2012).

Theorem 14. Assume that the target calculation problem (18) and the regulation problem (19) are feasible at all times, and that the closed-loop system reaches an equilibrium with input u_∞ and output y_∞ . It follows that:

$$r(y_\infty) = \bar{y}_c \quad (21)$$

Proof. If the closed loop reaches a steady state, stability of the observer implies that the augmented state estimate also reaches a steady state. Let $(\hat{x}_\infty, \hat{d}_\infty)$ be such a steady state, and let $\hat{y}_\infty := H(\hat{x}_\infty, \hat{d}_\infty)$. From (14) and (16), we can write

$\hat{d}_\infty^* = \hat{d}_\infty = \hat{d}_\infty^* + \kappa_d(y_\infty - \hat{y}_\infty^*)$, which implies $\kappa_d(y_\infty - \hat{y}_\infty^*) = 0$. From (17), it then follows $y_\infty = \hat{y}_\infty^* = \hat{y}_\infty$.

We now turn our attention to the target calculation problem $\mathbb{P}_s(\bar{y}_c, \hat{d}_\infty)$, and denote its solution as $(x_{s,\infty}, u_{s,\infty}, y_{s,\infty})$. At steady state, the first element of the optimal control sequence is given by u_∞ , and the corresponding first element of the optimal state sequence is \hat{x}_∞ . Closed-loop stability of the equilibrium and positive definiteness of the cost function $\ell(\cdot)$ imply that $(\hat{x}_\infty, u_\infty) = (x_{s,\infty}, u_{s,\infty})$, which, coupled with (18c)–(18d) and the previous relations, imply that $r(y_\infty) = r(\hat{y}_\infty) = r(y_{s,\infty}) = \bar{y}_c$. \square

We next present a novel result on the asymptotic stability and offset-free estimation under state feedback.

Theorem 15. Assume that the state is measurable (i.e. $y = x$), and that the augmented model and observer functions are:

$$F(x, u, d) := f(x, u) + B_d d, \quad H(x, d) := x, \\ \kappa_x(e) = e, \quad \kappa_d(e) = K_d e \quad (22)$$

with $B_d \in \mathbb{R}^{n \times n}$ invertible, and $B_d K_d = I$.

- (1) The observer is nominally asymptotically stable.
- (2) For any w respecting Assumption 5, there holds:

$$\lim_{k \rightarrow \infty} x(k) - \hat{x}^*(k) = 0, \quad \lim_{k \rightarrow \infty} \hat{d}^*(k) = B_d^{-1} \bar{w} \quad (23)$$

Proof. (Observability and stability of the observer) To prove this result, we consider that the “actual” augmented state evolves as:

$$\begin{aligned} x(k+1) &= f(x(k), u(k)) + B_d d(k) \\ d(k+1) &= d(k) \end{aligned} \quad (24)$$

Recall that in this case the prediction error is $e(k) = x(k) - \hat{x}^*(k)$. Since $\kappa_x(e) = e$, it follows that $\hat{x}(k) = x(k)$ for all $k \in \mathbb{I}$. Therefore, the “predicted” augmented state is given by:

$$\begin{aligned} \hat{x}^*(k+1) &= f(x(k), u(k)) + B_d \hat{d}(k) \\ \hat{d}^*(k+1) &= \hat{d}(k) \end{aligned} \quad (25)$$

whereas the filtered disturbance estimate, $\hat{d}(k)$, is given by:

$$\hat{d}(k) = \hat{d}^*(k) + K_d e(k) = \hat{d}^*(k) + K_d(x(k) - \hat{x}^*(k)) \quad (26)$$

By combining (24), (25) and (26), and defining $e_d(k) := d(k) - \hat{d}^*(k)$, we obtain:

$$\begin{bmatrix} e^+ \\ e_d^+ \end{bmatrix} = \begin{bmatrix} -B_d K_d & B_d \\ -K_d & I \end{bmatrix} \begin{bmatrix} e \\ e_d \end{bmatrix} = \begin{bmatrix} -I & B_d \\ -K_d & I \end{bmatrix} \begin{bmatrix} e \\ e_d \end{bmatrix} = \mathcal{M}_1 \begin{bmatrix} e \\ e_d \end{bmatrix} \quad (27)$$

It is easy to see that the matrix \mathcal{M}_1 in (27) is nilpotent of degree 2, i.e. $\mathcal{M}_1^2 = 0$, which proves the nominal asymptotic stability of the observer of the augmented system.

(Asymptotic zero estimation offset) We study the estimation error with respect to the process state, which evolves as:

$$x(k+1) = f(x(k), u(k)) + w(k) \quad (28)$$

We again have that $\hat{x}(k) = x(k)$ for all $k \in \mathbb{I}$. Combining (28), (25), (26) and $B_d K_d = I$, we obtain:

$$\begin{aligned} \begin{bmatrix} e(k+1) \\ \hat{d}^*(k+1) \end{bmatrix} &= \begin{bmatrix} -I & -B_d \\ K_d & I \end{bmatrix} \begin{bmatrix} e(k) \\ \hat{d}^*(k) \end{bmatrix} + \begin{bmatrix} w(k) \\ 0 \end{bmatrix} \\ &= \mathcal{M}_2 \begin{bmatrix} e(k) \\ \hat{d}^*(k) \end{bmatrix} + \begin{bmatrix} w(k) \\ 0 \end{bmatrix} \end{aligned} \quad (29)$$

The matrix \mathcal{M}_2 is also nilpotent of degree 2, so that $\begin{bmatrix} e(k) \\ \hat{d}^*(k) \end{bmatrix} \rightarrow \begin{bmatrix} e_\infty \\ \hat{d}_\infty^* \end{bmatrix}$ as $k \rightarrow \infty$. Since K_d is invertible, the limit values are:

$$e_\infty = 0, \quad \hat{d}_\infty^* = B_d^{-1} \bar{w} \quad (30)$$

which completes the proof. \square

3. OFFSET-FREE LINEAR MPC: DISTURBANCE MODELS, WHAT ELSE?

In this section we restrict our attention to the case in which the nominal model (2) is linear and the controlled variable is a linear combination of the output, i.e.

$$f(x, u) := Ax + Bu, \quad h(x) := Cx, \quad r(y) := Dy \quad (31)$$

It is assumed that the following condition holds true:

$$\text{rank} \begin{bmatrix} A - I & B \\ DC & 0 \end{bmatrix} = n + p_c \quad (32)$$

which ensures that problem (18) can admit a solution.

We present the general disturbance model and the velocity form model. Then, we show that the latter method is equivalent to the use of a particular case of disturbance model/observer, covering and strengthening the results recently reported in (Pannocchia, 2015), which also showed that the method proposed in (Tatjewski, 2014) is a particular case of disturbance model/observer.

3.1 Disturbance model and observer

The augmented model functions in (12) read as follows:

$$F(x, u, d) := Ax + Bu + B_d d, \quad H(x, d) := Cx + C_d d \quad (33)$$

and the observer functions are linear, in the form:

$$\kappa_x(e) := K_x e, \quad \kappa_d(e) := K_d e, \quad (34)$$

in which $K_x \in \mathbb{R}^{n \times p}$, $K_d \in \mathbb{R}^{n_d \times p}$ and $\text{rank}(K_d) = n_d$.

Compactly, we define the augmented state $\xi := \begin{bmatrix} x \\ d \end{bmatrix}$, the augmented model matrices:

$$A_a := \begin{bmatrix} A & B_d \\ 0 & I \end{bmatrix}, \quad B_a := \begin{bmatrix} B \\ 0 \end{bmatrix}, \quad C_a := [C \ C_d] \quad (35)$$

and write the augmented model dynamics as:

$$\begin{aligned} \xi^+ &= A_a \xi + B_a u \\ y &= C_a \xi \end{aligned} \quad (36)$$

Similarly, let $K_a := \begin{bmatrix} K_x \\ K_d \end{bmatrix}$ be the augmented observer gain matrix, and let the filtered estimate of the augmented state be denoted as $\hat{\xi} := \begin{bmatrix} \hat{x} \\ \hat{d} \end{bmatrix}$. For the linear augmented model (36), the general observer relations (14)–(16) can be written as:

$$\hat{\xi}(k) = A_a \hat{\xi}(k-1) + B_a u(k-1) + K_a e(k) \quad (37)$$

Remark 16. Asymptotic stability of the augmented observer requires that the characteristic matrix $(A_a - K_a C_a A_a)$ is Hurwitz.

The next proposition summarizes the main results regarding the design of offset-free linear MPC algorithms based on a disturbance model (Pannocchia and Rawlings, 2003).

Proposition 17. Consider the augmented matrices given in (35). The following results hold true:

- (1) The pair (C_a, A_a) is detectable (observable) if and only if (C, A) is detectable (observable) and

$$\text{rank} \begin{bmatrix} A - I & B_d \\ C & C_d \end{bmatrix} = n + n_d \quad (38)$$

- (2) There exist matrices (B_d, C_d) such that condition (38) holds if and only if $n_d \leq p$.

- (3) If $n_d = p$, it follows that any asymptotically stable observer gain matrix is such that K_d is invertible and the offset-free Assumption 9 holds true.

3.2 Velocity form

Another known method to design a linear offset-free MPC algorithm is to use the so-called velocity form model (Pannocchia and Rawlings, 2001; Wang, 2004; González et al., 2008; Betti et al., 2012, 2013), which is obtained from the nominal model (31) by defining the state increment $\delta x(k) := x(k) - x(k-1)$, the input increment as $\delta u(k) := u(k) - u(k-1)$, and rewriting the nominal model as follows:

$$\begin{aligned}\delta x^+ &= A\delta x + B\delta u \\ y^+ &= y + C\delta x^+ = y + CA\delta x + CB\delta u\end{aligned}\quad (39)$$

If we define the augmented state of the velocity form model as

$$\xi_\delta := \begin{bmatrix} \delta x \\ y \end{bmatrix}$$

$$A_\delta := \begin{bmatrix} A & 0 \\ CA & I \end{bmatrix}, \quad B_\delta := \begin{bmatrix} B \\ CB \end{bmatrix}, \quad C_\delta := [0 \ I] \quad (40)$$

the velocity form model can be written as:

$$\begin{aligned}\xi_\delta^+ &= A_\delta \xi_\delta + B_\delta \delta u \\ y &= C_\delta \xi_\delta\end{aligned}\quad (41)$$

Remark 18. The second block component (y) of the velocity form state is measurable, but the first block component (δx) may not be measurable. So, in general, an observer is also needed for this model form to estimate δx .

Let $K_\delta := \begin{bmatrix} K_{\delta x} \\ K_y \end{bmatrix}$ be the associated observer gain matrix for the velocity form model. The general observer relations (14)–(16) for the velocity form model can be written compactly as:

$$\hat{\xi}_\delta(k) = A_\delta \hat{\xi}_\delta(k-1) + B_\delta \delta u(k-1) + K_\delta e(k) \quad (42)$$

We remark that K_δ should be chosen such that $(A_\delta - K_\delta C_\delta A_\delta)$ is Hurwitz.

The next proposition (easily proved) summarizes the main properties of the velocity form model.

Proposition 19. Consider the velocity form model matrices in (40). The following results hold true:

- (1) The pair (C_δ, A_δ) is detectable if and only if (C, A) is detectable.
- (2) The pair (A_δ, B_δ) is stabilizable if and only if (A, B) is stabilizable and condition (32) holds true.

Since y is measured, it is customary to use a deadbeat observer for this second component of the state ξ_δ , i.e. $K_y = I$, so that from (42) it follows $\hat{y}(k) = y(k)$. In this case, the only matrix to choose is $K_{\delta x}$, and the following result holds true. The next result (easily proved) explains the conditions that $K_{\delta x}$ should satisfy to ensure stability of the observer.

Proposition 20. Let $K_y = I$. The velocity form observer characteristic matrix $(A_\delta - K_\delta C_\delta A_\delta)$ is Hurwitz if and only if $K_{\delta x}$ is chosen such that $(A - K_{\delta x} C A)$ is Hurwitz.

Remark 21. We notice by inspection that the observer characteristic matrix $(A_\delta - K_\delta C_\delta A_\delta)$ has p eigenvalues at the origin.

3.3 Velocity form equivalent disturbance model

We now show that the velocity form model, with deadbeat observer gain $K_y = I$, is equivalent to a particular disturbance

model/observer. This new result, first shown in (Pannocchia, 2015), is here reported and proved in a slightly different form. *Theorem 22.* Consider the velocity form model (41) and observer (42), with a stable output deadbeat observer gain $K_\delta = \begin{bmatrix} K_{\delta x} \\ I \end{bmatrix}$. This is equivalent to using the following disturbance model and observer gains:

$$B_d = K_{\delta x}, \quad C_d = I - CK_{\delta x}, \quad K_x = K_{\delta x}, \quad K_d = I \quad (43)$$

Proof. By expanding and rearranging the various terms in (42), and recalling (40), we obtain:

$$\begin{aligned}\delta \hat{x}(k) &= (A - K_{\delta x} C A) \delta \hat{x}(k-1) + (B - K_{\delta x} C B) \delta u(k-1) \\ &\quad + K_{\delta x} (y(k) - \hat{y}(k-1)) \\ \hat{y}(k) &= y(k)\end{aligned}$$

which can also be rewritten as:

$$\begin{aligned}\delta \hat{x}(k) &= (A - K_{\delta x} C A) \delta \hat{x}(k-1) + \\ &\quad (B - K_{\delta x} C B) \delta u(k-1) + K_{\delta x} (y(k) - y(k-1))\end{aligned}\quad (44)$$

Now consider the evolution of the augmented system with matrices given in (43), which can be written:

$$\begin{aligned}\hat{x}(k) &= A \hat{x}(k-1) + B u(k-1) \\ &\quad + K_{\delta x} (y(k) - C(A \hat{x}(k-1) + B u(k-1)))\end{aligned}\quad (45)$$

By rewriting (45) at time $k-1$ and taking the difference of both sides, we obtain:

$$\begin{aligned}\delta \hat{x}(k) &= A \delta \hat{x}(k-1) + B \delta u(k-1) + K_{\delta x} (y(k) - y(k-1)) \\ &\quad - K_{\delta x} C (A \delta \hat{x}(k-1) + B \delta u(k-1))\end{aligned}\quad (46)$$

which can be rewritten as

$$\begin{aligned}\delta \hat{x}(k) &= (A - K_{\delta x} C A) \delta \hat{x}(k-1) + \\ &\quad (B - K_{\delta x} C B) \delta u(k-1) + K_{\delta x} (y(k) - y(k-1))\end{aligned}\quad (47)$$

The proof is completed by comparing (47) with (44). \square

3.4 Equivalence in the state feedback case

If the state is measurable, the previous relations between the velocity form and disturbance model methods become even stronger. Since the state is measurable, it may be desirable/possible to use a deadbeat observer for the state, i.e. such that $\hat{x}(k) = x(k)$.

When the state is measurable, the augmented matrices of the disturbance model method read as follows:

$$A_a = \begin{bmatrix} A & B_d \\ 0 & I \end{bmatrix}, \quad B_a = \begin{bmatrix} B \\ 0 \end{bmatrix}, \quad C_a = [I \ C_d] \quad (48)$$

with $B_d \in \mathbb{R}^{n \times n}$, $C_d \in \mathbb{R}^{n \times n}$ (i.e. $n_d = n$), and K_a is chosen such that $(A_a - K_a C_a A_a)$ is Hurwitz. The general detectability condition (38) is consequently replaced by:

$$\text{rank} \begin{bmatrix} A - I & B_d \\ I & C_d \end{bmatrix} = 2n \quad (49)$$

A state/disturbance deadbeat observer is then designed by satisfying the following restrictions:

$$\text{rank}(B_d) = n, \quad C_d = 0, \quad K_x = I, \quad K_d = B_d^{-1} \quad (50)$$

Remark 23. Using (50), it is straightforward to see that $A_a - K_a C_a A_a = \begin{bmatrix} 0 & 0 \\ -B_d^{-1} A & 0 \end{bmatrix}$, i.e. the observer characteristic matrix has all its eigenvalues at zero.

In the velocity form model, the augmented matrices are still defined in (40), and K_δ should be chosen such that $(A_\delta - K_\delta C_\delta A_\delta)$ is Hurwitz. In the state feedback case, the state/output

deadbeat observer is obtained by choosing $K_{\delta x} = I$ and $K_y = I$. With such a choice, we see $A_\delta - K_\delta C_\delta A_\delta = \begin{bmatrix} 0 & -I \\ 0 & 0 \end{bmatrix}$, i.e. the observer characteristic matrix has all its eigenvalues at zero.

We now present the equivalence results.

Theorem 24. Assume the state is measurable, and consider the velocity form model (41) and observer (42), with a state/output deadbeat observer gain $K_\delta = \begin{bmatrix} I \\ I \end{bmatrix}$. This model is a particular case of disturbance model with:

$$B_d = I, \quad C_d = 0, \quad K_x = I, \quad K_d = I \quad (51)$$

Proof. The result is a direct consequence of the equivalence relations (43), with $K_{\delta x} = I$ and $C = I$. \square

4. OFFSET-FREE ECONOMIC MPC

We discuss in this section how the fundamentals of offset-free design can be embedded into an economic MPC framework, in order to ensure that the best economic performance can be achieved despite the presence of persistent discrepancies between the actual process and the MPC model.

4.1 A brief overview of economic MPC

To set up a framework that is consistent with the previous results on output feedback offset-free MPC, we consider an economic stage cost function defined in terms of measurable quantities, namely input and output. We denote such a cost function as $\ell_e(y, u)$, with $\ell_e : \mathbb{R}^P \times \mathbb{R}^m \rightarrow \mathbb{R}$. At each decision time, let $\hat{x}(k)$ be the estimate of the current state. Let $\mathbf{x} = \{x_0 \ x_1 \ \dots \ x_N\}$ and $\mathbf{u} = \{u_0 \ u_1 \ \dots \ u_{N-1}\}$ be, respectively, a state sequence and an input sequence. Then, the economic MPC solves the following optimization problem, denoted by $\mathbb{P}_e(\hat{x}(k), x_s)$:

$$\min_{\mathbf{x}, \mathbf{u}} \sum_{i=0}^{N-1} \ell_e(h(x_i), u_i) \quad (52a)$$

subject to:

$$x_0 = \hat{x}(k) \quad (52b)$$

$$x_{i+1} = F(x_i, u_i) \quad (52c)$$

$$g_u(u_i) \leq 0, \quad g_y(h(x_i)) \leq 0 \quad (52d)$$

$$x_N = x_s \quad (52e)$$

in which x_s represents the feasible equilibrium state such that $\ell_e(\cdot)$ is minimized. As usual, only the first input of the optimal solution to (52) is sent to the plant, i.e. $u(k) = u_0^0(k)$, and at the next decision time a new problem $\mathbb{P}_e(\cdot)$ is solved for the new current state estimate.

4.2 An offset-free economic MPC algorithm

If the actual plant equals model (2) and the state is measured, under mild conditions, it can be shown that the closed-loop system state converges asymptotically to the equilibrium x_s (Diehl et al., 2011; Rawlings et al., 2012). On the other hand, if the actual plant (1) differs from the nominal model (2), besides the issues of robust stability and constraint satisfaction, the closed-loop system may converge to an equilibrium that is not optimal, i.e. in which $\ell_e(\cdot)$ is not minimized. For instance, under Assumption 5, the best plant equilibrium is:

$$\min_{\bar{x}_p, \bar{u}, \bar{y}} \ell_e(\bar{y}, \bar{u}) \quad (53a)$$

subject to:

$$\bar{x}_p = f(\bar{x}_p, \bar{u}) + \bar{w} \quad (53b)$$

$$\bar{y} = h(\bar{x}_p) + \bar{v} \quad (53c)$$

$$\bar{u} \in \mathbb{U}, \quad \bar{y} \in \mathbb{Y} \quad (53d)$$

Clearly, it would be desirable to achieve this same equilibrium input/output even if the actual plant (1) is not known precisely. To this aim, we augment the nominal system (2) and define the augmented model (12), whose current state (\hat{x}, \hat{d}) is estimated from the output measurement by the observer (14)–(16).

Then, the (current) best equilibrium steady state is given by:

$$(x_s(k), u_s(k), y_s(k)) := \arg \min_{x, u, y} \ell_e(y, u) \quad (54a)$$

subject to:

$$x = F(x, \hat{d}(k), u), \quad y = H(x, \hat{d}(k)) \quad (54b)$$

$$g_u(u) \leq 0, \quad g_y(y) \leq 0 \quad (54c)$$

Remark 25. Since $\hat{d}(k)$ is not necessarily constant, the equilibrium problem (54) needs to be solved at each decision time.

Consequently, we modify problem (52) into an offset-free economic MPC problem:

$$\min_{\mathbf{x}, \mathbf{u}} \sum_{i=0}^{N-1} \ell_e(H(x_i, \hat{d}(k)), u_i) \quad (55a)$$

subject to:

$$x_0 = \hat{x}(k) \quad (55b)$$

$$x_{i+1} = F(x_i, \hat{d}(k), u_i) \quad (55c)$$

$$g_u(u_i) \leq 0, \quad g_y(H(x_i, \hat{d}(k))) \leq 0 \quad (55d)$$

$$x_N = x_s(k) \quad (55e)$$

Finally, the first input of the optimal solution to (55) is sent to the plant, and at the next decision time the whole procedure (augmented state estimation, equilibrium calculation, economic MPC problem) is solved again.

We now present the main result on offset-free economic MPC, which is stated and proved assuming state feedback.

Theorem 26. Under the assumptions of Theorem 15, assume that equilibrium problem (54) and the economic MPC problem (55) are feasible at all times, and that the closed-loop system reaches an equilibrium with input and output (u_∞, y_∞) . The achieved ultimate cost $\ell(y_\infty, u_\infty)$ is the same as that in (53).

Proof. If the closed-loop reaches an equilibrium with input and output (u_∞, y_∞) , stability of the observer implies that the augmented state estimate also reaches a steady state. Let $(\hat{x}_\infty, \hat{d}_\infty)$ be the augmented state estimate at the reached equilibrium, and let $(x_{s,\infty}, u_{s,\infty}, y_{s,\infty})$ be the solution to (54) given the equilibrium disturbance estimate \hat{d}_∞ . It follows that the applied input u_∞ , which is the first element of the optimal control sequence solution to (55), is equal to $u_{s,\infty}$.

Under the assumptions of Theorem 15, we observe that $\bar{w} = \lim_{k \rightarrow \infty} w(k) = \lim_{k \rightarrow \infty} B_d \hat{d}(k) = B_d \hat{d}_\infty$, and therefore: $f(x, u) + \bar{w} = F(x, \hat{d}_\infty, u)$ (and obviously $h(x) = x = H(x, \hat{d}_\infty)$). Hence, problem (54) and problem (53) are identical, and this completes the proof. \square

5. ILLUSTRATIVE EXAMPLES

We present several numerical examples to highlight the concepts and results discussed in this paper. Simulations are performed using the Python interface to the open-source CasADi framework (Andersson, 2013), and the arising NLPs/QPs are solved with IPOPT (Wächter and Biegler, 2006).

5.1 Offset-free nonlinear MPC of a cart-pole system in the presence of obstacles

Problem description and control task. The first system we consider is a mechanical one and its schematic is depicted in Fig. 1. It consists of one prismatic (translational) joint and one revolute joint. This system is usually referred to as cart-pole. The configuration of the system is $q = [q_1 \ q_2]^T$, where $q_1 > 0$ is the horizontal displacement of the cart and q_2 is the rotation angle of the pole around the hinge O , taken with respect to the vertical direction. The state of the system is therefore $x = [x_1 \ x_2 \ x_3 \ x_4]^T = [q_1 \ q_2 \dot{q}_1 \dot{q}_2]^T$. The center of mass G of the pole is at a distance r from O . The cart has mass M , and the pole has mass m and moment of inertia J_G with respect to the center of mass G . The gravitational acceleration $g = 9.81 \text{ m/s}^2$ acts in the $-y$ direction of a world frame. A horizontal force $u > 0$ acts in the $+x$ direction of a world frame on the cart and represents the only control input applied to the system. The goal of the MPC regulator is to apply a proper force u to move the system from the initial state $x_0 = [0 \ 0 \ 0 \ 0]^T$ to the final state $x_N = [q_1^f \ 0 \ 0 \ 0]^T$, where q_1^f represents a position *beyond* the two obstacles jutting downward from the ceiling (Fig. 1). The novelty with respect to the classical cart-pole control problem is represented by the introduction of such obstacles. The requirement that the controller has to steer the pole to its final state while *always* maintaining a minimum clearance from the obstacles represents an additional, non trivial, difficulty, as the joint angle q_2 must belong to $[-\pi/2, \pi/2]$.

The Lagrangian dynamics of the system can be written in the standard form as:

$$B(q)\ddot{q} + n(q, \dot{q}) = Pu \quad (56)$$

where $B(q) \in \mathbb{R}^{2 \times 2}$ is the symmetric, positive definite *inertia matrix*, $n(q, \dot{q}) \in \mathbb{R}^2$ is the vector collecting *Coriolis*, *centrifugal* and *gravitational* terms, $P \in \mathbb{R}^2$ is the actuation vector, and $u \in \mathbb{R}$ is the horizontal force applied to the cart.

For the cart-pole system, the explicit expressions of the above quantities are:

$$B(q) = \begin{bmatrix} M_t & -mlc_2 \\ -mlc_2 & J_O \end{bmatrix}, \quad n(q, \dot{q}) = \begin{bmatrix} ml\dot{q}_2^2 s_2 \\ -mgl s_2 \end{bmatrix}, \quad P = \begin{bmatrix} 1 \\ 0 \end{bmatrix} \quad (57)$$

where $c_2 = \cos q_2 = \cos x_2$ and $s_2 = \sin q_2 = \sin x_2$, and the positions $M_t = M + m$, $J_O = J_G + ml^2$ were made. It is worth noting that the above equations are equivalent to: (i) the translational dynamic equilibrium of the whole system along $+x$, and (ii) the rotational dynamic equilibrium around hinge O .

The explicit nonlinear equations in state space form appear as:

$$\begin{bmatrix} \dot{x}_1 \\ \dot{x}_2 \\ \dot{x}_3 \\ \dot{x}_4 \end{bmatrix} = \begin{bmatrix} x_3 \\ x_4 \\ -a(x_2)m l s_2 (J_O x_4^2 - m g l c_2) \\ -a(x_2)m l s_2 (m l x_4^2 c_2 - M_t g) \end{bmatrix} + a(x_2) \begin{bmatrix} 0 \\ 0 \\ J_O \\ m l c_2 \end{bmatrix} u \quad (58)$$

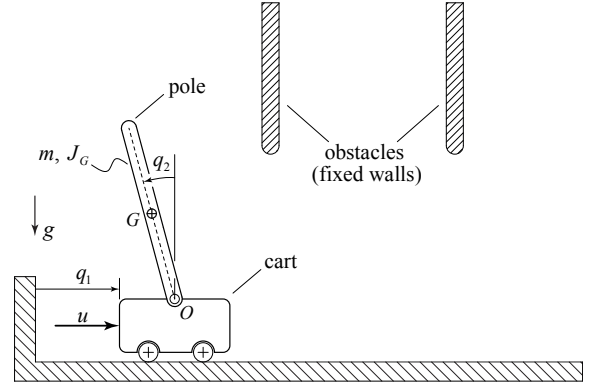


Fig. 1. Schematic of the cart-pole system with obstacles.

where we defined $a(x_2) = [J_O M_t - (ml \cos x_2)^2]^{-1}$.

Results and discussion. We first consider the case in which the full state of the system is measurable, i.e. $h(x) = x$ in (2), and we compare two MPCs:

- NMPC0 uses no disturbance model: $F(x, d, u) = f(x, u)$ and $H(x, d) = h(x) = x$, with a linear deadbeat observer: $\kappa_x(e) = e$.
- NMPC1 uses a state disturbance model: $F(x, d, u) = f(x, u) + d$ and $H(x, d) = h(x) = x$, with a deadbeat augmented linear observer: $\kappa_x(e) = e$ and $\kappa_d(e) = e$.

For both controllers we use a discretization time $T_s = 0.12 \text{ s}$, an MPC horizon with $N = 25$, and a quadratic cost function. The optimal control problem is solved in both state and control sequences, according to a direct multiple shooting scheme in which integration of the model is performed using a fixed step ($T_s/10$) Runge-Kutta algorithm. Control force is constrained in the range $[-100, 100] \text{ N}$, and during the simulation an external unmeasured disturbance force is superimposed to test the disturbance rejection capabilities of the controllers.

Closed-loop simulation results are reported in Fig. 2: the top panel shows the horizontal displacement and rotation angle, along with the system inputs (control force and unmeasured disturbance), vs. time. The bottom panel reports the prediction errors on these two states. An accompanying video showing the cart-pole system behavior is available in (Pannocchia et al., 2015). From these results we see that, due to persistent prediction errors, NMPC0 is not able to stabilize the cart-pole system in the final position. On the other hand, NMPC1 succeeds in this task thanks to the quick suppression of the prediction error.

We next consider the more difficult case in which only two states, cart displacement and pole rotation angle, are measured.

- NMPC2 uses a linear (input) disturbance model with one disturbance state: $F(x, d, u) = f(x, u) + B_d d$ and $H(x, d) = h(x) = x$, in which B_d is chosen as the Jacobian matrix of $f(x, u)$ with respect to the input u at the final equilibrium. A linear observer, $\kappa_x(e) = K_x e$ and $\kappa_d(e) = K_d e$, is designed as a steady-state Kalman filter for the linearized augmented model at the final equilibrium.
- NMPC3 uses a linear (input/output) disturbance model with two disturbance states: $F(x, d, u) = f(x, u) + B_d d$ and $H(x, d) = h(x) + C_d d = x + C_d d$, in which the first column of B_d is chosen as the Jacobian matrix of $f(x, u)$ with respect to the input u at the final equilibrium, whereas the second column of B_d and C_d are chosen so that

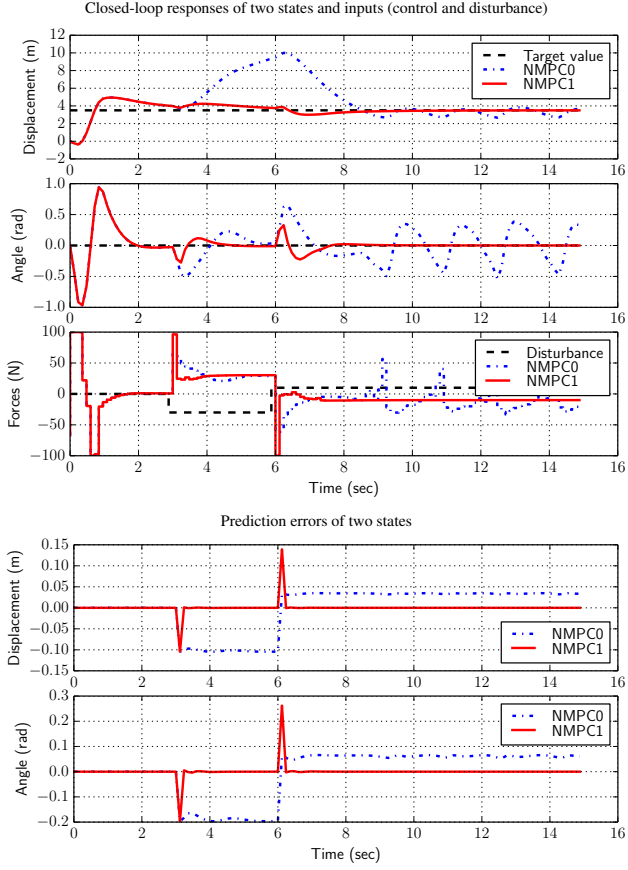


Fig. 2. State feedback control of the cart-pole: comparison of standard vs. offset-free NMPC.

the augmented system is observable. A linear observer, $\kappa_x(e) = K_x e$ and $\kappa_d(e) = K_d e$, is designed as a steady-state Kalman filter for the linearized augmented model at the final equilibrium.

Results are reported in Fig. 3. We notice that both MPCs succeed in the task with rather similar performances. It should be noticed that NMPC2 is using only one disturbance state even if two measurements are available, and hence Assumption 9 does not hold for NMPC2. Nonetheless, it is able to suppress offset because the actual disturbance enters the system with the same dynamics of the input. At any steady state this effect is correctly modeled by the chosen linear (input) disturbance model, but different disturbances may not be rejected by NMPC2. On the other hand, NMPC3 uses two disturbances, and therefore it is capable of ensuring offset-free reconstruction by zeroing the prediction error for any asymptotically constant disturbance. It should be mentioned that the design of an observable augmented system is nontrivial for this example because of the presence of two integrators in the discretized model dynamics (at any equilibrium). For instance, a linear output disturbance model with $B_d = 0$ and $C_d = I$ is not expected to be observable for this case.

5.2 Offset-free linear MPC of a nonisothermal CSTR

Process description and control objectives. The second example is a nonisothermal continuous stirred tank reaction (CSTR) in which an irreversible, exothermic reaction $A \rightarrow B$ occurs in the liquid phase. The process is described by the following set of ODEs, in which the state $x = [c \ T \ h]^T$ (re-

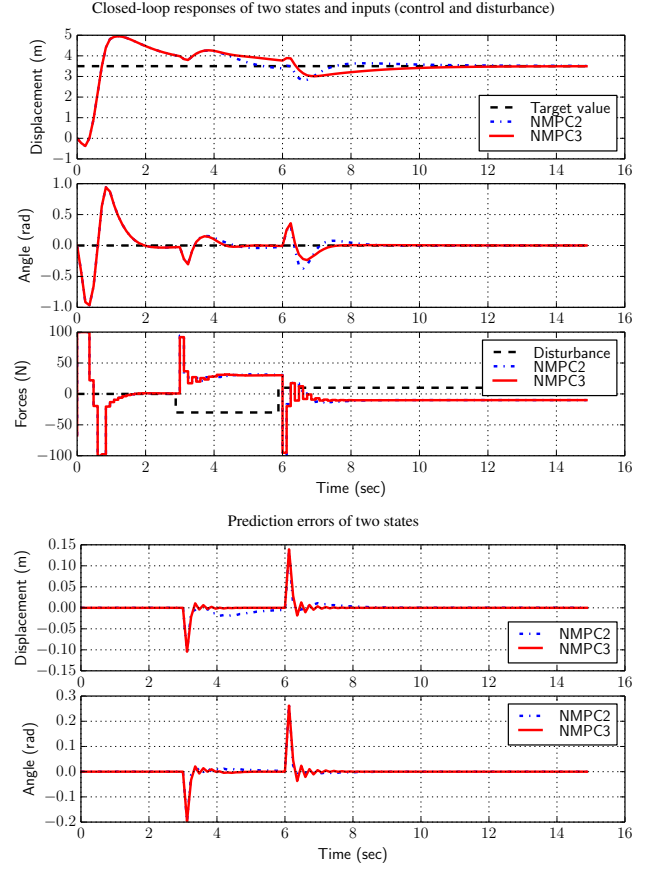


Fig. 3. Output feedback control of the cart-pole: comparison of two offset-free NMPCs.

actant concentration, reactor temperature, liquid level) and $u = [T_c \ F]^T$ (coolant temperature and outlet volumetric flow rate), and the model parameters are taken from (Rawlings and Mayne, 2009, p. 52).

$$\begin{bmatrix} \dot{x}_1 \\ \dot{x}_2 \\ \dot{x}_3 \end{bmatrix} = \begin{bmatrix} \frac{F_0 c_0 - u_2 x_1}{\pi r^2 x_3} - k_0 \exp(-\frac{E}{R x_2}) x_1 \\ \frac{F_0 (T_0 - x_2)}{\pi r^2 x_3} - \frac{\Delta H}{\rho C_p} k_0 \exp(-\frac{E}{R x_2}) x_1 + \frac{2 U_0}{\rho \rho C_p} (u_1 - x_2) \\ \frac{F_0 - u_2}{\pi r^2} \end{bmatrix} \quad (59)$$

The input is constrained $u \in [295, 305] \text{ K} \times [0, 0.25] \text{ m}^3/\text{min}$, and the control task is to regulate the outlet concentration at $\bar{c} = 0.500 \text{ kmol/m}^3$ and the liquid level at $\bar{h} = 0.659 \text{ m}$. This operation is particularly difficult because: (i) this is an open-loop unstable equilibrium, (ii) we use a *linear model* $x^+ = f(x, u)$ in all MPCs, while the controlled process (59) is highly nonlinear because of the exothermic reaction, (iii) from time 5 min to 6 min the inlet flow rate increases linearly acting as unmeasured disturbance. All MPCs use a horizon of $N = 50$, a discretization time of 0.2 min, and a quadratic cost function.

Results and discussion. We consider the state feedback case, i.e. $y = h(x) = x$, and define the controlled variable as $y_c = r(y) = [x_1 \ x_3]^T$. We compare two linear MPCs:

- LMPC0 uses a (partial) state disturbance model:

$$F(x, d, u) = f(x, u) + \begin{bmatrix} d_1 \\ 0 \\ d_2 \end{bmatrix}, \text{ with deadbeat augmented state observer } K_x = I, K_d = \begin{bmatrix} 1 & 0 & 0 \\ 0 & 0 & 1 \end{bmatrix}.$$

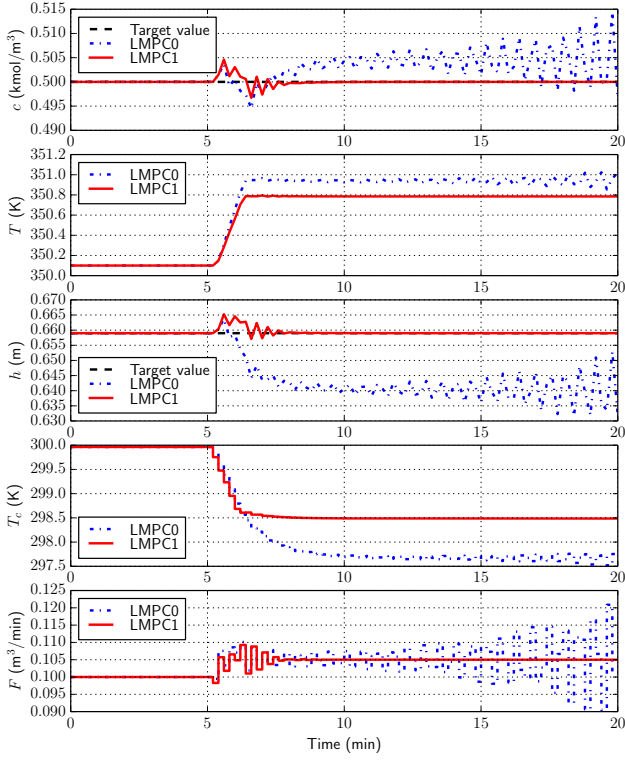


Fig. 4. State feedback control of the CSTR: comparison of states and inputs using linear MPCs.

- LMPC1 uses a (full) state disturbance model: $F(x, d, u) = f(x, u) + d$ with deadbeat augmented state observer $K_x = I$, $K_d = I$.

We remark that both augmented models are observable and the associated deadbeat observers are nominally stable. However, we notice that in LMPC0, disturbances are added only to the two controlled states (x_1 and x_3), but not to the other measured state (x_2), whereas in LMPC1 a disturbance is added to each state. Hence Assumption 9 does not hold for LMPC0.

Closed-loop results (states and inputs) are shown in Fig. 4. From these results, we see that LMPC0 is unable to achieve offset-free control in the two controlled variables when the inlet flow rate disturbance occurs, and indeed the closed-loop system becomes unstable due to the inherent mismatch between the nominal linear model and the nonlinear controlled process (59). Depending on the observer and controller tuning, we could obtain a stable closed-loop behavior with LMPC0, but still there would be offset because of the use of two disturbances in the presence of three measurements. It is also possible to find an augmented observer gain (K_x, K_d) in a way that offset-free control is achieved, but this observer gain would depend on the MPC cost function parameters (Pannocchia and Rawlings, 2003; Maeder et al., 2009). Such a practice is not recommended, in general, because it requires simultaneous retuning of the observer whenever the controller cost function parameters (state and input penalties) change. On the other hand, LMPC1 is perfectly able to achieve offset-free control given that it uses the *correct* number of disturbances in its augmented model. Finally, given the equivalence results discussed in Sections 3.3 and 3.4, an MPC based on the velocity form model would behave identically to LMPC1 because it would (inherently) use three disturbances.

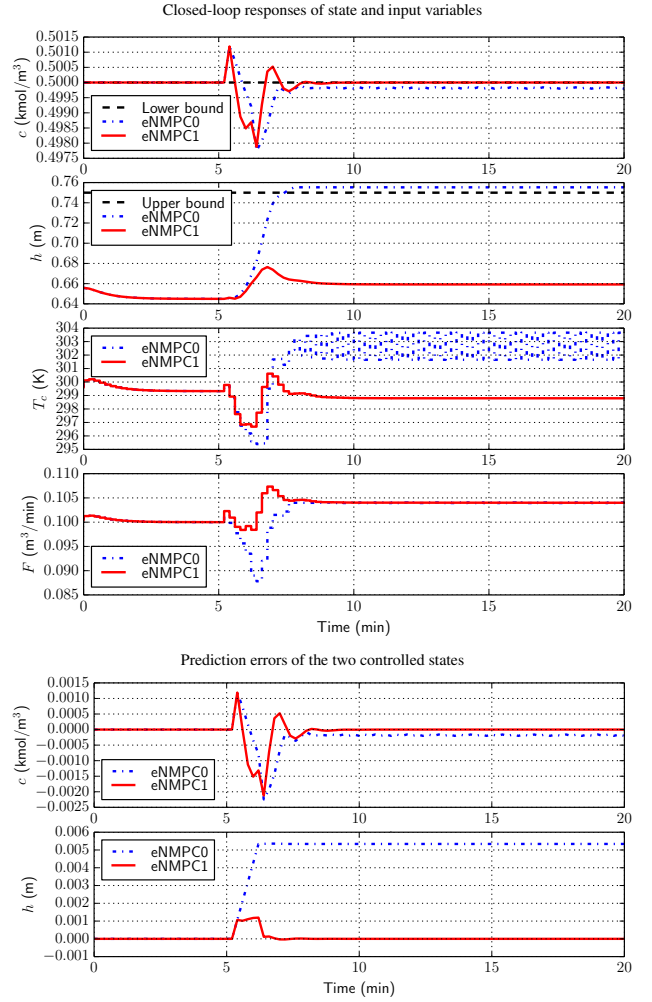


Fig. 5. Output feedback control of the CSTR: comparison of standard economic NMPC vs. offset-free economic NMPC.

5.3 Offset-free economic MPC of a nonisothermal CSTR

The last example that we present concerns the same process of Section 5.2, but in this case the nonlinear nominal model (59) is used in the design of economic nonlinear MPCs, as described in Section 4. We assume to measure only x_1 and x_3 , i.e. $y = [x_1 \ x_3]^T$, and the economic cost function is $\ell_e(y, u) = y_1$, so that the reactant concentration has to be minimized, while the following output constraints are imposed:

$$0.5 \leq y_1 \leq 1.0, \quad 0.5 \leq y_2 := x_3 \leq 0.75 \quad (60)$$

As in the previous section, from time 5 min to 6 min the inlet flow rate increases linearly, acting as an unmeasured disturbance. All MPCs use a horizon of $N = 50$ with a discretization time of 0.2 min.

Two output feedback economic NMPCs are compared:

- eNMPC0 uses no disturbance model: $F(x, d, u) = f(x, u)$ and $H(x, d) = h(x) = x$ and a linear state observer: $\kappa_x(e) = K_x e$, in which K_x is chosen as a steady-state Kalman filter gain at the nominal equilibrium.
- eNMPC1 uses a linear (input) disturbance model: $F(x, d, u) = f(x, u) + B_d d$ and $H(x, d) = h(x) = x$, in which B_d is chosen as the Jacobian matrix of $f(x, u)$ with respect to the input u at the nominal equilibrium. A linear

observer, $\kappa_x(e) = K_x e$ and $\kappa_d(e) = K_d e$, is designed as a steady-state Kalman filter for the linearized augmented model at the nominal equilibrium.

Closed-loop results are reported in Fig. 5: the top panel shows controlled and inputs variables, whereas the bottom panel shows the prediction error on the two controlled variables.

From these results we observe that eNMPC0 makes the closed-loop system unstable due to the fact that output constraints are permanently violated. In fact, both output prediction errors do not vanish at steady state, whereas in eNMPC1 both output prediction errors are quickly eliminated, and consequently the actual output constraints are satisfied. From this example, we can appreciate how offset-free prediction of the outputs is necessary to make sure that an economic controller does not destabilize the closed-loop system in the attempt to recover from a current output that does not satisfy the constraints.

6. CONCLUSIONS

This paper has described the latest advances in the design of offset-free MPC algorithms. We presented a self-contained summary of the available results for nonlinear MPC, based on the use of disturbance models and observers, and we extended the existing asymptotic convergence results. Then we focused on linear MPC and showed that a commonly known method based on the velocity form model is indeed a particular case of disturbance model, and not an alternative route to offset-free tracking. We also extended the concept of offset-free estimation to the design of economic MPC for systems with persistent errors/disturbances. Challenging examples of nonlinear processes (controlled by nonlinear MPC, linear MPC, and economic MPC) have been included to highlight the significance of the presented results, and also to emphasize specific subtleties related to the number of used disturbances and to the process dynamics, which may result in an incorrect design.

A final note is reserved to future directions in this research area. On the one hand, it may be useful to explore the issue of disturbance modeling (i.e. where to put the disturbances) in nonlinear system, coupled with nonlinear observers (MHE, most notably). On the other, robust stability questions for offset-free (linear, nonlinear, economic) MPC are still wide open.

7. ACKNOWLEDGEMENTS

This work is supported by grant no. 600918 “PaCMan” – Probabilistic and Compositional Representations of Objects for Robotic Manipulation within FP7-ICT-2011-9 “Cognitive Systems”.

REFERENCES

- Andersson, J. (2013). *A General-Purpose Software Framework for Dynamic Optimization*. PhD thesis, Arenberg Doctoral School, KU Leuven, Department of Electrical Engineering (ESAT/SCD) and Optimization in Engineering Center, Kas teelpark Arenberg 10, 3001-Heverlee, Belgium.
- Betti, G., Farina, M., and Scattolini, R. (2012). An MPC algorithm for offset-free tracking of constant reference signals. In *Proceedings of 51st IEEE Conference on Decision and Control*, 5182–5187. Maui, Hawaii, USA.
- Betti, G., Farina, M., and Scattolini, R. (2013). A robust MPC algorithm for offset-free tracking of constant reference signals. *IEEE Trans. Auto. Contr.*, 58(9), 2394–2400.
- Davison, E.J. and Smith, H.W. (1971). Pole assignment in linear time-invariant multivariable systems with constant disturbances. *Automatica*, 7, 489–498.
- Diehl, M., Amrit, R., and Rawlings, J.B. (2011). A Lyapunov function for economic optimizing model predictive control. *IEEE Trans. Auto. Contr.*, 56(3), 703–707.
- González, A.H., Adam, E.J., and Marchetti, J.L. (2008). Conditions for offset elimination in state space receding horizon controllers: A tutorial analysis. *Chem. Engng. and Proc.: Process Intensification*, 47(12), 2184–2194.
- Kwakernaak, H. and Sivan, R. (1972). *Linear Optimal Control Systems*. John Wiley & Sons.
- Limon, D., Alvarado, I., Alamo, T., and Camacho, E.F. (2008). MPC for tracking piece-wise constant references for constrained linear systems. *Automatica*, 44, 2382–2387.
- Maeder, U., Borrelli, F., and Morari, M. (2009). Linear offset-free model predictive control. *Automatica*, 45(10), 2214–2222.
- Maeder, U. and Morari, M. (2010). Offset-free reference tracking with model predictive control. *Automatica*, 46(9), 1469–1476.
- Morari, M. and Maeder, U. (2012). Nonlinear offset-free model predictive control. *Automatica*, 48, 2059–2067.
- Muske, K.R. and Badgwell, T.A. (2002). Disturbance modeling for offset-free linear model predictive control. *J. Proc. Cont.*, 12, 617–632.
- Pannocchia, G. (2015). Offset-free tracking MPC: A tutorial review and comparison of different formulations. In *Proceedings of European Control Conference (ECC15)*.
- Pannocchia, G., Gabicci, M., and Artoni, A. (2015). NMPC 2015 submission accompanying video. <https://vimeo.com/132972505>.
- Pannocchia, G. and Rawlings, J.B. (2001). The velocity algorithm LQR: a survey. Technical Report 2001-01, TWMCC, Department of Chemical Engineering, University of Wisconsin-Madison. URL: <http://www.che.wisc.edu/jbr-group/tech-reports/twmcc-2001-01.pdf>.
- Pannocchia, G. and Rawlings, J.B. (2003). Disturbance models for offset-free model predictive control. *AIChE J.*, 49, 426–437.
- Prett, D.M. and Garcia, C.E. (1988). *Fundamental Process Control*. Butterworth Publishers, Boston.
- Rajamani, M.R., Rawlings, J.B., and Qin, S.J. (2009). Achieving state estimation equivalence for misassigned disturbances in offset-free model predictive control. *AIChE J.*, 55, 396–407.
- Rawlings, J.B. (2000). Tutorial overview of model predictive control. *IEEE Control System Magazine*, 20, 38–52.
- Rawlings, J.B., Angeli, D., and Bates, C.N. (2012). Fundamentals of economic model predictive control. In *Proceedings of 51st IEEE Conference on Decision and Control*, 3851–3861.
- Rawlings, J.B. and Mayne, D.Q. (2009). *Model Predictive Control: Theory and Design*. Nob Hill Publishing, Madison, WI.
- Tatjewski, P. (2014). Disturbance modeling and state estimation for offset-free predictive control with state-space process models. *Int. J. Appl. Math. Comput. Sci.*, 24(2), 313–323. doi:10.2478/amcs-2014-0023.
- Wächter, A. and Biegler, L.T. (2006). On the implementation of a primal-dual interior point filter line search algorithm for large-scale nonlinear programming. *Mathematical Programming*, 106, 25–57.

Wang, L. (2004). A tutorial on model predictive control: Using a linear velocity-form model,. *Dev. Chem. Eng. Mineral Process.*, 12(5/6), 573–614.

A.7 Article: Active Touch for Grasping

Authors Claudio Zito, Valerio Ortenzi, Maxime Adjigble, Marek Kopicki and Jeremy L. Wyatt

Info To be submitted to: Autonomous Robots

Abstract

Relation with the deliverable : this paper is central to our work on grasp acquisition under uncertainty. The method we have developed reasons about the uncertainty in the pose of the object, and plans to gather information while reaching the desired grasp state. This places grasp acquisition and active tactile information gathering in a tractable framework.

Attachment (following pages until next annex)